THE ELECTRON-POSITRON DECAY MODE OF THE PHI MESON

By

JOHN PHILIP HORSEY

A Thesis submitted for the Degree of

DOCTOR OF PHILOSOPHY

in the

UNIVERSITY OF LONDON

--- oOo ---

Physics Department,
Imperial College,
London, S.W.7.

November, 1968.

ABSTRACT

An account is presented of an experiment to study the rare electron positron decay mode of the ϕ meson in the reaction

$$\pi^- + p \longrightarrow n + \phi \quad \phi \longrightarrow e^+ + e^-$$

at a beam momentum just above the ϕ threshold.

The neutrons were detected by means of a ring of six large scintillation counters situated four metres downstream of the liquid hydrogen target and their velocities were found by measuring their times of flight over this distance. As a result of kinematic constraints placed on the neutron, the invariant mass of the e^+e^- system was required to be within ~ 8 MeV/c^2 of the ϕ mass at 1020 MeV/c^2.

The secondary electrons were identified by means of their characteristic showers formed in optical spark chamber-lead plate and scintillator arrays on either side of the target. The system supplied sufficient information to permit complete reconstruction of the events for kinematic analysis. About 100,000 photographs were taken above the ϕ threshold and a similar number below. Various shower and kinematic criteria were applied which rejected

all but 27 events. From the excess of events produced in the runs above threshold we were able to show positive evidence for the decay of $\phi \longrightarrow e^+ + e^-$.

An earlier measurement of the ϕ production cross-section is discussed briefly and using the data of this experiment for normalisation the branching ratio of $\phi \longrightarrow e^+ + e^- / \phi$-total was found to be $(7.0 \pm 3.6).10^{-4}$.

CONTENTS

PREFACE

The experiment described in this thesis was performed at the Rutherford Laboratory proton synchrotron 'Nimrod' during 1966-7 by the Imperial College Spark Chamber Group in collaboration with a small team from the Rutherford Laboratory. The experiment naturally involved the work of many people and, although I have tried to present a complete account of the experiment, I have dwelt mainly on those aspects with which I was most concerned. This explains the emphasis laid, in the thesis, on the electron detection system, the design of the criteria and the experimental analysis and, on the other hand, the relatively brief consideration given to the beam, the electronic logic system and related problems.

CHAPTER 1

INTRODUCTION

1.1 The experiment as part of a series

This thesis describes the final experiment of a series of three carried out at the Rutherford Laboratory proton synchrotron, Nimrod, by the Imperial College Spark Chamber Group and its collaborators, during the period 1963-1967. The series consisted primarily of a study of the rare electron-positron decay modes of the isoscalar vector mesons, ω^o and ϕ^o. It comprised:

1. A study of the production of ω^o mesons in the reaction $\pi^- + p \longrightarrow n + \omega^o$ near threshold, and a measurement[1,2] of the Branching Ratio for the decay $\omega \longrightarrow e^+ + e^-$.

2. (a) 'The ϕ search'. A study of the reaction

$$\pi^- + p \longrightarrow n + \phi^o, \quad \phi^o \longrightarrow K^+ + K^-$$

performed to measure the ϕ meson production cross-section near threshold.[3,4]

(b) 'The ϕ decay'. A measurement of the Branching

Ratio for the decay $\phi \longrightarrow e^+ + e^-$ using ϕ^o mesons produced in the reaction $\pi^- + p \longrightarrow n + \phi^o$.

Part 2 (a) was necessary since the ϕ production cross-section in the above reaction was unknown and this information was necessary for normalisation in part 2 (b). The theoretical motivations for studying these leptonic decay modes are discussed below.

1.2 <u>Theoretical interest in the leptonic decay modes of the neutral vector mesons</u>

The theoretical interest in the leptonic decay modes of the neutral vector mesons is threefold: A, to test the ω-ϕ mixing hypothesis; B, to increase our knowledge of the nucleon form factors; C, to test Q.E.D. at small distances.

A) <u>To test the hypothesis of ω-ϕ mixing</u>

One of the major advances in strong interaction physics in recent years has been the observation that, for a particular spin-parity value, the baryons and mesons fall into distinctive patterns of isospin multiplets.[5] Figure 1.1 shows the isospin representation of some of these unitary mutliplets in SU_3. The axes, I_3 and Y, are related by

Fig.1.1 The classification of particles in SU_3

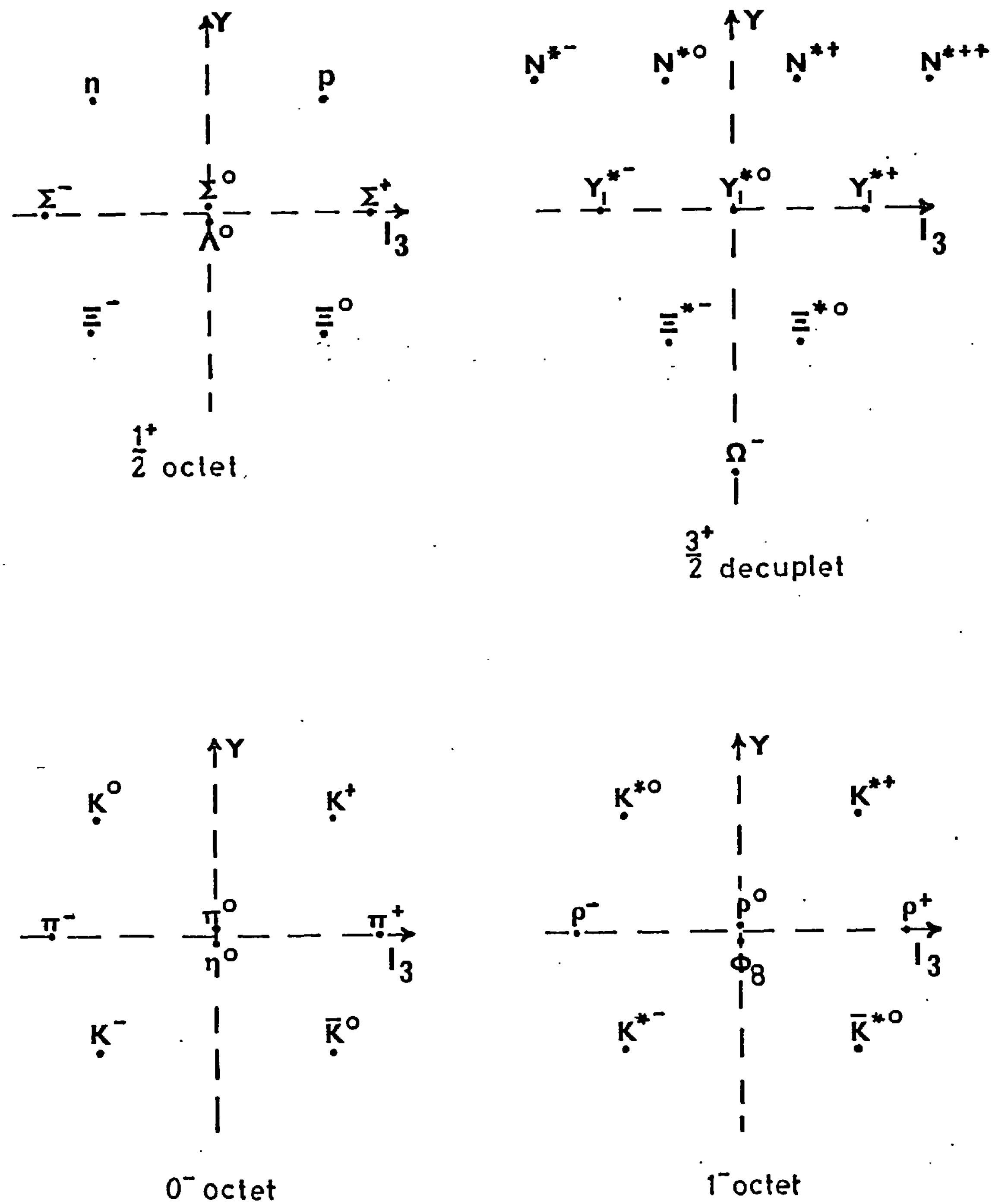

$$Q = I_3 + Y/2 \qquad \ldots\ 1.1$$

where Q, I_3 and Y are the quantum numbers of charge, the third component of isospin and hypercharge, respectively.

If all the interactions were invariant under SU_3, then the masses of all the particles belonging to the same unitary multiplet would be the same. This is not the case and the mass differences between the isospin multiplets within the unitary multiplets can be explained by postulating the existence of medium strong interactions which break SU_3. Assuming the existence of these medium strong interactions, Gell-Mann and Okubo developed their mass formulae.[5,6] For the baryon octet:

$$W_B = W_o \left\{1 + aY + b[I(I+1) - Y^2/4]\right\} \qquad \ldots\ 1.2$$

where W_o, a and b are constants. The corresponding formula for the meson octets employs the squares of the particle masses:

$$W_m^2 = W_o^2 \left\{1 + d[I(I+1) - Y^2/4]\right\} \qquad \ldots\ 1.3$$

In the case of the baryon octet with J^P of $\frac{1}{2}^+$, the mass formula (1.2) fits the experimental values to better than one half percent and the appropriate formula for the decuplet, $\frac{3}{2}^{+}$, is satisfied to a similar accuracy. The agreement is still fairly good for the pseudoscalar meson octet, but in the vector meson, 1^-, octet the predicted mass, m_8, of the Y = 0, I = 0 member is ~930 MeV/c^2 and corresponds to no known particle. The two Y = 0, I = 0 candidates are ω(783) and ∅ (1020), the masses of which are incompatible with m_8. The situation can be explained in terms of symmetry breaking which results in ω-∅ mixing;[7,8] i.e. the physical particles are a mixture of the Y = 0, I = 0 states, $|8\rangle$ and $|1\rangle$, of the 1^- octet and unitary singlet respectively.

Let H be the operator that gives the masses, in I = Y = 0 subspace; i.e. $\langle 1|H|1\rangle = m_1^2$ and $\langle 8|H|8\rangle = m_8^2$. Due to mixing the value of $\langle 1|H|8\rangle = m_{18}^2$ is finite and introduces off-diagonal terms in the mass matrix

$$M = \begin{pmatrix} \langle 8|H|8\rangle & \langle 1|H|8\rangle \\ \langle 8|H|1\rangle & \langle 1|H|1\rangle \end{pmatrix} = \begin{pmatrix} m_8^2 & m_{18}^2 \\ m_{81}^2 & m_1^2 \end{pmatrix} \qquad \ldots 1.4$$

The physical particles, ω and ∅ can be expressed as linear combinations of the octet and singlet states as follows:

$$\begin{aligned} \phi &= |8\rangle \cos\theta - |1\rangle \sin\theta \\ \omega &= |1\rangle \cos\theta + |8\rangle \sin\theta \end{aligned} \qquad \ldots 1.5$$

To obtain the masses of the physical particles the mass matrix has to be diagonalised by means of the transformation

$$S = \begin{pmatrix} \cos\theta & \sin\theta \\ -\sin\theta & \cos\theta \end{pmatrix} \qquad \ldots 1.6$$

To diagonalise the matrix we choose θ such that

$$SMS^{-1} = \begin{pmatrix} m_\phi^2 & 0 \\ 0 & m_\omega^2 \end{pmatrix} \qquad \ldots 1.7$$

Solving equation 1.7 gives the following:

$$m_{18}^2 = m_{81}^2 \qquad \ldots 1.8$$

$$m_\phi^2 + m_\omega^2 = m_8^2 + m_1^2 \qquad \ldots 1.9$$

$$m_{18}^2 = \surd((m_8^2 - m_\omega^2)(m_\phi^2 - m_8^2)) \qquad \ldots 1.10$$

$$\tan 2\theta = \frac{2m_{18}^2}{m_8^2 - m_1^2} \qquad \ldots 1.11$$

Using the value of m_8^2 derived from the Gell-Mann Okubo mass formula (1.3) and the known masses of the physical resonances, ϕ and ω, one gets $\theta = 39.5^\circ$.

The leptonic decay modes of the ω and ϕ vector mesons afford a direct test of the mixing hypothesis since, as the photon can couple only to the octet and not to the unitary singlet state and the $V^o \longrightarrow \ell^+ + \ell^-$ decays proceed via an intermediate virtual photon (Fig. 1.2), the ratio $\Gamma(\omega \longrightarrow \ell^+\ell^-)/\Gamma(\phi \longrightarrow \ell^+\ell^-)$ indicates the relative octet and singlet components of the ω and ϕ. In addition from the partial width, the photon-vector meson coupling constant, γ_V, can be found since the two are related via:[9]

$$\Gamma(V \longrightarrow \ell^+\ell^-) \simeq \frac{\alpha^2}{12}\left(\frac{\gamma_V^{\,2}}{4\pi}\right)^{-1} m_V \qquad \ldots 1.12$$

where α is the fine structure constant.

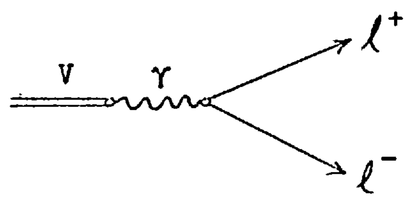

Fig. 1.2 Feynman graph of the leptonic decay of a vector meson which proceeds via a virtual photon.

As well as the mass-mixing model above, other models have been proposed, for example the 'current mixing' model.[10,11,12] In this model the state $|8\rangle$ is assumed coupled to the conserved hypercharge current with a strength f_Y and the state $|1\rangle$ to the conserved baryon current with strength f_B. As emphasised by Kroll Lee and Zumino[11] this leads to two mixing angles θ_Y and θ_B which are related to λ, the generalised mixing angle, by:

$$\tan \lambda = \frac{m_\omega}{m_\phi} \tan \theta_Y = \frac{m_\phi}{m_\omega} \tan \theta_B \qquad ...1.13$$

This is in contradiction to the mass mixing model which requires $\theta_Y = \theta_B \neq 0$, although in the exact SU_3 limit when $m_\omega = m_\phi$ this condition is true for both models.

Experimental values for γ_V can be used to check Weinberg's first sum rule,[13] which is based on the current mixing model and predicts

$$\frac{1}{3}\frac{m_\rho^2}{\gamma_\rho^2} = \frac{m_\omega^2}{\gamma_\omega^2} + \frac{m_\phi^2}{\gamma_\phi^2} \qquad ... 1.14$$

A value for the ω-ϕ mixing angle can also be determined from the quark model[14] in which the mesons are considered as bound states of quark-antiquark pairs $(Q\bar{Q})$. By assuming that the quark Q_3 is heavier than (Q_1, Q_2) by a mass Δ, Dalitz[15] obtains

$$\tan \theta = \frac{2\sqrt{2}}{3} I \Delta \left(\frac{m_8 - m_1}{2} + \frac{\Delta}{3} + \left\{ \left(\frac{m_8 - m_1}{2} - \frac{\Delta}{3} \right)^2 + \frac{8}{9} I^2 \Delta^2 \right\}^{\frac{1}{2}} \right) \qquad ...1.15$$

where θ is defined by equations 1.5 and I is the overlap integral between the octet and singlet radial wave functions.

In the case of 'ideal' mixing, when $m_1 = m_8$ and $I = 1$, equation 1.15 becomes $\tan\theta = \frac{1}{\sqrt{2}}$ corresponding to $\theta = 35.3^\circ$. In this situation the ω would be described by the configuration $(Q_1\overline{Q}_1 + Q_2\overline{Q}_2)/\sqrt{2}$ and the ϕ by $-Q_3\overline{Q}_3$. The decay mode $\phi \longrightarrow \rho + \pi$ is expected to be forbidden since the ϕ state is then composed of Q_3 and $\overline{Q}_3$, whereas the ρ and π are composed of Q_1, Q_2 and $\overline{Q}_1$, $\overline{Q}_2$. Thus the relatively small decay rate of $\phi \longrightarrow \rho\pi$ ($\sim$12%) is consistent with a small departure from this interpretation.

In the above expression (1.15) for the mixing angle, (mass) and not $(\text{mass})^2$ was used as in the derivation of equations (1.8-1.11). At the moment it seems unclear whether the mass terms should be linear or quadratic,[15] or even inversely quadratic as in the current mixing model.[10]

The relation between the photon-vector meson coupling constants

Higher symmetries, such as SU_6, predict the ratio of the coupling strengths of the vector mesons to the photon to be[16]

$$\gamma_\rho^{-2} : \gamma_\omega^{-2} : \gamma_\phi^{-2} = 9:1:2 \qquad \ldots 1.16$$

This same prediction can be obtained from SU_3 using an SU_2 subgroup different from isospin.[17] In this SU_2 subgroup, which is called U-spin, particles belonging to the same multiplet have the same electric charge and different values of hypercharge. Fig. 1.3 shows the isospin and U-spin classification of the 1^- octet. The photon transforms under SU_3 like a member of a unitary octet with U-spin zero, and therefore can couple only to the U-spin singlet, $(\sqrt{3}\rho^\circ + \phi_8)/2$. Now, ϕ_8 is a mixture of ϕ and ω hence, this state can be expressed as:

$$|U = 0, \text{ octet} > = \tfrac{1}{2}\sqrt{3}\ |\rho^\circ> + \tfrac{1}{2}\sin\theta|\omega> + \tfrac{1}{2}\cos\theta|\phi> \quad \ldots\ 1.17$$

where θ is the mixing angle defined by equations 1.5. If strong interactions are invariant under SU_3, only this linear combination can couple to the photon and the three vertices (Fig. 1.3) obey the relation

$$<\gamma|\rho^\circ>:<\gamma|\omega>:<\gamma|\phi> = \sqrt{3} : \sin\theta : \cos\theta \quad \ldots\ 1.18$$

which expressed in terms of the photon-vector meson coupling constants, γ_V, becomes

$$\gamma_\rho^{-2} : \gamma_\omega^{-2} : \gamma_\phi^{-2} = 3 : \sin^2\theta : \cos^2\theta \quad \ldots\ 1.19$$

In the case of ideal mixing when $\tan\theta = 1/\sqrt{2}$, equation

Fig. 1.3 The isospin and U-spin classification of the 1^- octet

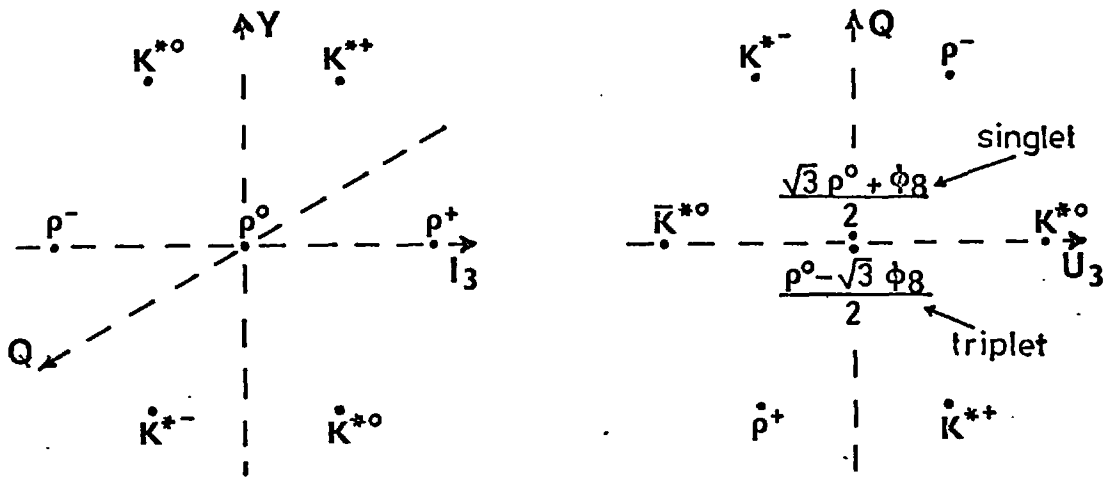

iso spin U-spin

Photon-vector meson vertices

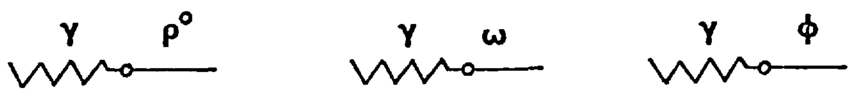

1.19 becomes

$$\gamma_\rho^{-2} : \gamma_\omega^{-2} : \gamma_\phi^{-2} = 9 : 1 : 2 \qquad \ldots 1.20$$

The ratio (1.20) was derived using simple SU_3 and assuming ideal mixing. Other mixing angles modify this ratio, for example, the angle of 39.5^o obtained using mass-mixing and the Gell-Mann Okubo mass formula gives 9:1.2:1.8.

Oakes and Sakurai[10] predict 9:0.65:1.33 using Weinberg's first sum rule[13] (current mixing) and introducing the particle masses as inverse squares. On the other hand, using the Das, Mathur and Okubo model,[18] which also uses the first sum rule but has the mass squared terms in the numerator, the ratio is found to be 9:1.21:1.34.

Experimental determinations of the partial widths $\Gamma(V \longrightarrow \ell^+ + \ell^-)$ will help to point to the correct theoretical concept.

B) <u>To further knowledge of the nucleon form factors</u>

The suggestion by Yukawa in 1935 that mesons could account for nuclear forces implied the existence of a meson cloud around the proton that would extend out to a distance of about a mesonic Compton wavelength. Direct measurement of the meson charge radius by electron-proton scattering studies, however, showed that the charge distributions were too narrow to be explained by the interaction of a single pion. This led to the proposal that the existence of hypothetical mesons whose mass was greater than that of the pion could provide an explanation of the observed structure, and soon afterwards the vector mesons ρ, ω, ϕ were discovered. It has become popular to try to explain the nucleon form factors in terms of the vector mesons with the same quantum numbers as the gamma ray. Since isotopic spin is a good quantum number for the vector mesons, it is assumed that the isovector and isoscalar form factors can be expressed in terms of the isovector and isoscalar vector mesons. Thus it is assumed for example that the isoscalar form factor G_s is of the form:[19,8]

$$G_s = \sum_i \frac{e}{2} \cdot \frac{g_{v_i nn}}{\gamma_{V_i}} \cdot \frac{M_i^2}{M_i^2 - q_i^2} \qquad \ldots 1.21$$

where M_i is the mass of the i-th isoscalar vector meson, $g_{v_i nn}$ is the coupling strength of this meson to the nucleons, and q_i^2 is the squared momentum transfer. In practice the behaviour of G_s can be described using just the known mesons ω and ϕ.[20] The constant γ_{V_i}, which is a measure of the coupling of the vector meson to the gamma ray, can be deduced from the decay rate of the vector mesons into lepton pairs using equation 1.12. A value for γ_{V_i} would make it possible to determine the vector meson-nucleon coupling constants, by fitting equation 1.21 to the form factors known, say from electron-proton scattering experiments. These coupling constants could then be compared with estimates from strong interaction experiments.

C) <u>To test Quantum Electrodynamics at small distances</u>

Investigation of these leptonic decay modes might also give valuable information about the limits of validity of present-day quantum electrodynamics and/or the possible non-electromagnetic structure of the muon.[19,21] Quantum electrodynamics regards the electron and muon as being identical in their interactions, the only difference between them being one of mass. These leptonic decays occur in the region of large time-like momentum transfer, which makes them especially valuable since they test the theory at small distances, where deviations from the theory seem most likely, and where relatively few corroborative experiments have been performed. If the electron and muon are treated as Dirac particles, we get from equation 1.12

$$R_V = \frac{\Gamma(V \longrightarrow \mu^+ + \mu^-)}{\Gamma(V \longrightarrow e^+ + e^-)} \simeq 1 \qquad \ldots 1.22$$

the small difference from unity being due to the additional phase space for the electron decay. This assumes the vertices γee and $\gamma\mu\mu$ have identical properties at c.m.s. lepton energies $\sim m_V$. However, if, for example, the muon were to have some anomalous interaction, the ratio R_V might be very different from unity.[22]

1.3 The ϕ meson

The ϕ meson was discovered in a Bubble chamber experiment by Bertanza et al.[23] using a K^- beam at 2.24 GeV/c. They showed the existence of a resonance in the $K\bar{K}$ system at $\sim$1020 MeV/c^2 with a width < 20 MeV/c^2. The quantum numbers of the ϕ were determined independently.[24] The ϕ was found to decay predominantly into K^+K^- and $K_1^oK_2^o$ but not into $K_1^oK_1^o$. Observation of the $K_1^oK_2^o$ mode demonstrated that the ϕ had odd spin (J) and negative parity (P) and negative C-parity. These assignments follow from:

$$CP\,(K^0\overline{K^0}) = + \qquad CP\,(K_1^0 K_2^0) = (-1)^{J+1}$$

$$C\,(K^+K^-) = P\,(K^+K^-) = (-1)^J$$

Comparison of the three $\Sigma K\overline{K}$ final states showed that the isospin (I) was zero and that G $(= -(-1)^I)$ was odd, since no $\phi^{\pm}$ was seen. Absence of a $\pi^+\pi^-$ decay agrees with this G assignment.

The spin was deduced from the quantity β_J, defined as $\beta_J = \Gamma(\phi \longrightarrow K_1{}^0 K_2{}^0) / \Gamma(\phi \longrightarrow K^+K^-)$. In the absence of a K^+K^0 mass difference, and charge effects, this ratio is independent of J. The spin dependence of β_J arises from different angular momentum and Coulomb barriers appropriate to the $K_1{}^0 K_2{}^0$ and K^+K^- systems. A value of $J = 1$ was found to be favoured over $J = 3$ and the $J = 1$ assignment was consistent with the decay angular distributions.

The quantum numbers of the ϕ are now established[25] as $I^G(J^P)C = 0^-(1^-)-$. The present values[25] of the ϕ mass and width are given as 1019.5 ± 0.6 MeV/c^2 and 3.4 ± 0.8 MeV/c^2 respectively.

The main decays are:

$\phi \rightarrow K^+K^-$	0.48 ± 0.03
$K_1^0 K_2^0$	0.40 ± 0.03
$\pi^+\pi^-\pi^0$ including $(\rho\pi)$	0.12 ± 0.04

As discussed previously, the ϕ meson fits into the $J^P = 1^-$ meson nonet on the SU_3 symmetry scheme, and is considered to be a mixture of the nonet's isoscalar octet and singlet states on the ω-ϕ mixing theory.

1.4 General outline of the ϕ decay experiment

The ϕ decay experiment was similar in principle to the ω experiment,[2] the first of the series. The apparatus employed was designed to be sensitive to the process

$$\pi^- + p \longrightarrow n + Z^0, \quad Z^0 \longrightarrow e^+ + e^- \qquad \ldots 1.23$$

In brief, it consisted of a negative pion beam of known momentum incident upon a liquid hydrogen target. Neutrons were detected by means of a ring of six large scintillation counters four metres downstream of the target (see Fig. 2.1) and their velocities were found by measuring their times of flight over this distance. As a result of kinematic constraints placed on the neutron, the mass of the particle(s) Z^0 was within ~ 8 MeV/c^2 of the ϕ mass at

1020 MeV/c^2. The secondary electrons were identified by means of the typical cascade showers formed in optical spark chamber-lead plate arrays on either side of the target.

Data were taken at two beam momenta, one just above and one just below the ϕ threshold. The presence of the decay $\phi \longrightarrow e^+ + e^-$ was deduced from a significant excess of events, identified as e^+e^- pairs, in the data taken above the ϕ threshold.

A detailed account of the ϕ decay experiment follows.

CHAPTER 2

ϕ PRODUCTION

2.1 Introduction

The process described by the reaction

$$\pi^- + p \longrightarrow n + \phi^0$$
$$\hookrightarrow e^+ + e^- \qquad \ldots\ 2.1$$

can conveniently be separated into its two main parts, namely the production of the ϕ meson and the meson's subsequent decay into an electron-positron pair.

Production of the ϕ meson has already been described fully[3,4] in an account of an experiment, 'the ϕ search', to determine the ϕ cross-section near threshold. To produce the ϕ mesons, the same apparatus was used in both 'ϕ search' and 'ϕ decay' experiments and, in principle, the two differed only in the selection of the decay products, K^+K^- in the 'ϕ search' and e^+e^- in the 'ϕ decay'. The results of the 'ϕ search' which are used for normalisation are discussed later in this chapter. The data used for this normalisation were derived, not from the cross-section but, from the ϕ search data at a stage of the analysis prior to the inclusion of correction factors such as neutron counter efficiency and beam composition. Certain factors are common to both experiments and any uncertainty in their estimation is unimportant.

A short account of the basic apparatus used to detect ϕ mesons in both experiments is presented below, together with a brief discussion of the ϕ search and its relevance to the ϕ decay. The secondary selection of the electron pairs is peculiar to the decay experiment and is considered in detail in Chapter 3.

2.2 Missing Mass Spectroscopy, the neutron counters and time of flight

In both search and decay experiments, the ϕ's were preferentially selected by exploiting the neutron time of flight technique, a form of missing mass spectroscopy.

In the reaction

$$\pi^- + p \longrightarrow n + Z \qquad \ldots\ 2.2$$

the missing mass, m_z of the undetected neutral particle Z (or group of particles of effective mass m_z) is given by

$$m_z{}^2 = (E_\pi + E_p - E_n)^2 - (\underline{p}_\pi + \underline{p}_p - \underline{p}_n)^2 \qquad \ldots\ 2.3$$

where E_i is the total laboratory energy and $\underline{p}_i$ is the 3-momentum of particle i. For the particular case where the target proton is stationary, equation 2.3 becomes

$$m_z^2 = (E_\pi + m_p - E_n)^2 - p_\pi^2 - p_n^2 + 2p_\pi p_n \cos\theta_n \quad \ldots 2.4$$

where θ_n is the angle between the neutron and the incident pion directions in the laboratory system. From equation 2.4 it is evident that a knowledge of the initial pion momentum and the momentum and direction of the neutron is sufficient to determine the missing mass of the Z^o system. In the case of narrow resonances with relatively low cross-sections such as the ω and ϕ, high mass resolution is desirable to enable efficient rejection of background events. The partial derivatives of equation 2.4 give

$$\frac{1}{2}\frac{\partial m_z^2}{\partial p_n} = -\beta_n (E_\pi + m_p) + p_\pi \cos\theta_n \quad \ldots 2.5$$

$$\frac{1}{2}\frac{\partial m_z^2}{\partial \theta_n} = -p_\pi p_n \sin\theta_n \quad \ldots 2.6$$

From these equations the value of m_z^2 is clearly the least sensitive to errors in θ_n and p_n when $\theta_n \sim 0^\circ$ and the velocity of the neutron $\beta_n = \dfrac{p_\pi}{E_\pi + m_p}$, $= \beta_c$

where β_c is the velocity of the c.m.s. in the laboratory.

Good mass resolution is therefore obtained near threshold when the conditions $\theta_n \sim 0^o$ and $\beta_n \sim \beta_c$ are satisfied. A further advantage of working near threshold is that, as the neutrons are kinematically confined to a narrow forward cone in the laboratory, a high neutron collection efficiency can be obtained using a relatively small solid angle coverage in the laboratory. The main disadvantage of working near threshold is that the resonance production cross-sections are likely to be low, but this was compensated in part by the high collection efficiency of the neutron counters.

The neutron detectors consisted of a ring of six large scintillation counters situated 4 metres downstream of the hydrogen target, Fig.2.1. Although a shorter neutron flight path increased the acceptance, a longer one improved the relative time of flight measurement. Four metres was chosen as then the contributions to the error in the missing mass, from the uncertainties in the time of flight measurement, the neutron angle, and the beam momentum, were approximately equal.

Fig.2.1 Basic Apparatus

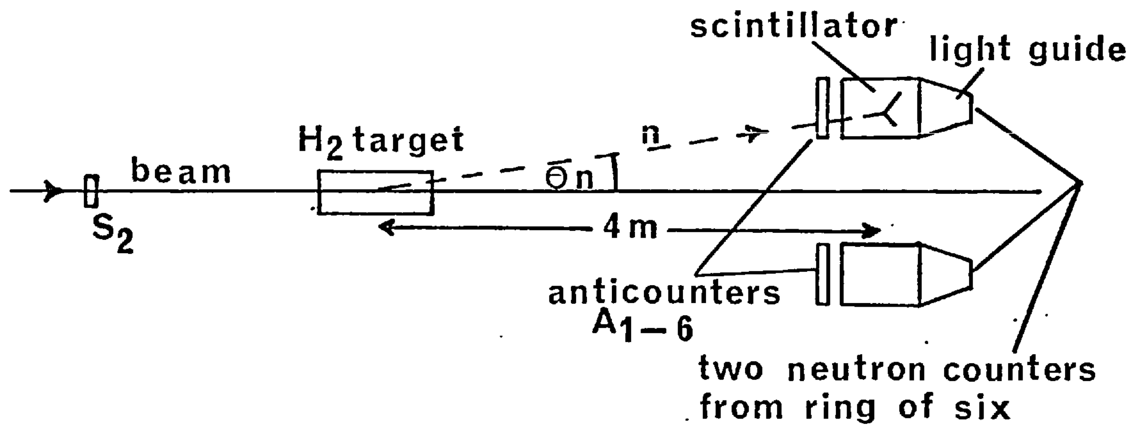

Basic experimental arrangement (not to scale)

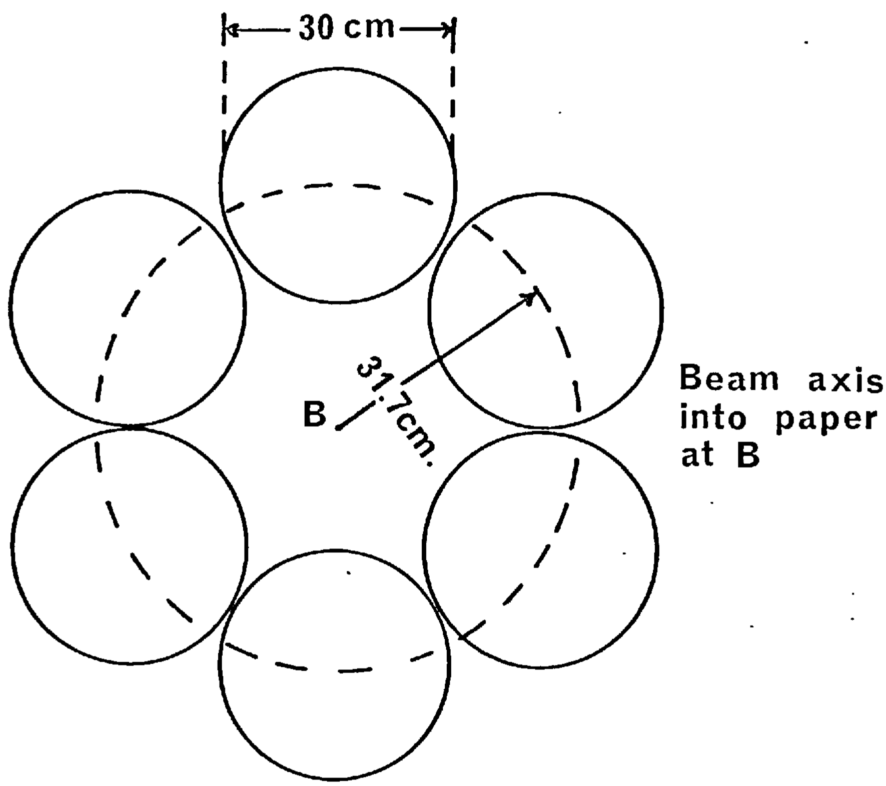

Ring of neutron counters

Each counter was a cylinder, 30 cm long x 30 cm diameter, made of NE 102A plastic scintillator, coupled to a 58 AVP photomultiplier tube by a light-guide. Veto counters, A_{1-6}, in front of each unit, were used in anticoincidence to reject charged particles from background processes.

The solid angle of collection of the neutrons was about 50%, but as only $\sim \frac{1}{3}$ of the neutrons that passed into the scintillator interacted, the total efficiency of the ring was $\sim$ 15%.

The neutron time of flight was determined from the time difference between a pulse from the principal beam counter S_2 (Fig.2.1) and a pulse from the neutron counters. Accurate timing, based on the arrival time of a pulse from the anode of a neutron counter photomultiplier tube, N_c, was not possible for pulses of small amplitude. To ensure that only large N_c pulses were used, we also demanded that the signal from the last dynode, N_d, should be large. The complete coincidence that signalled a neutron (or photon), CO1, is represented as $N_c N_d \bar{A}_{1-6}$, where the accurate timing information depended on N_c. The r.m.s. timing error was estimated to be $\pm$ 0.83 ns.[26]

2.3 The Beam

For the ϕ search experiment, the need for a high intensity negative pion beam of well-defined momentum was met by the two stage beam designed by D.C. Mason to operate in the region of 1.3-1.8 GeV/c. This same beam was used without modification for the ϕ decay experiment. (Fig.2.2).

Negative pions produced at $\sim 0^o$ from an internal copper target (10 cm x 1 cm^2), in Octant 6 of the 7 GeV proton synchrotron Nimrod, were swept out of the machine by its own fringe field. The first beam line element, a Type I[27] Quadrupole, was made vertical focussing to compensate in part for the defocussing effect of the Nimrod fringe field. This magnet was positioned as close to the machine as possible in order to maximise its acceptance. A second similar magnet followed with horizontal focussing. This doublet magnetic lens formed a primary image of the internal target at C1 (Fig.2.2). Particles of the desired momenta were selected by the bending magnet BM1, and the collimator, C1, which limited the momentum bite to about 2%.

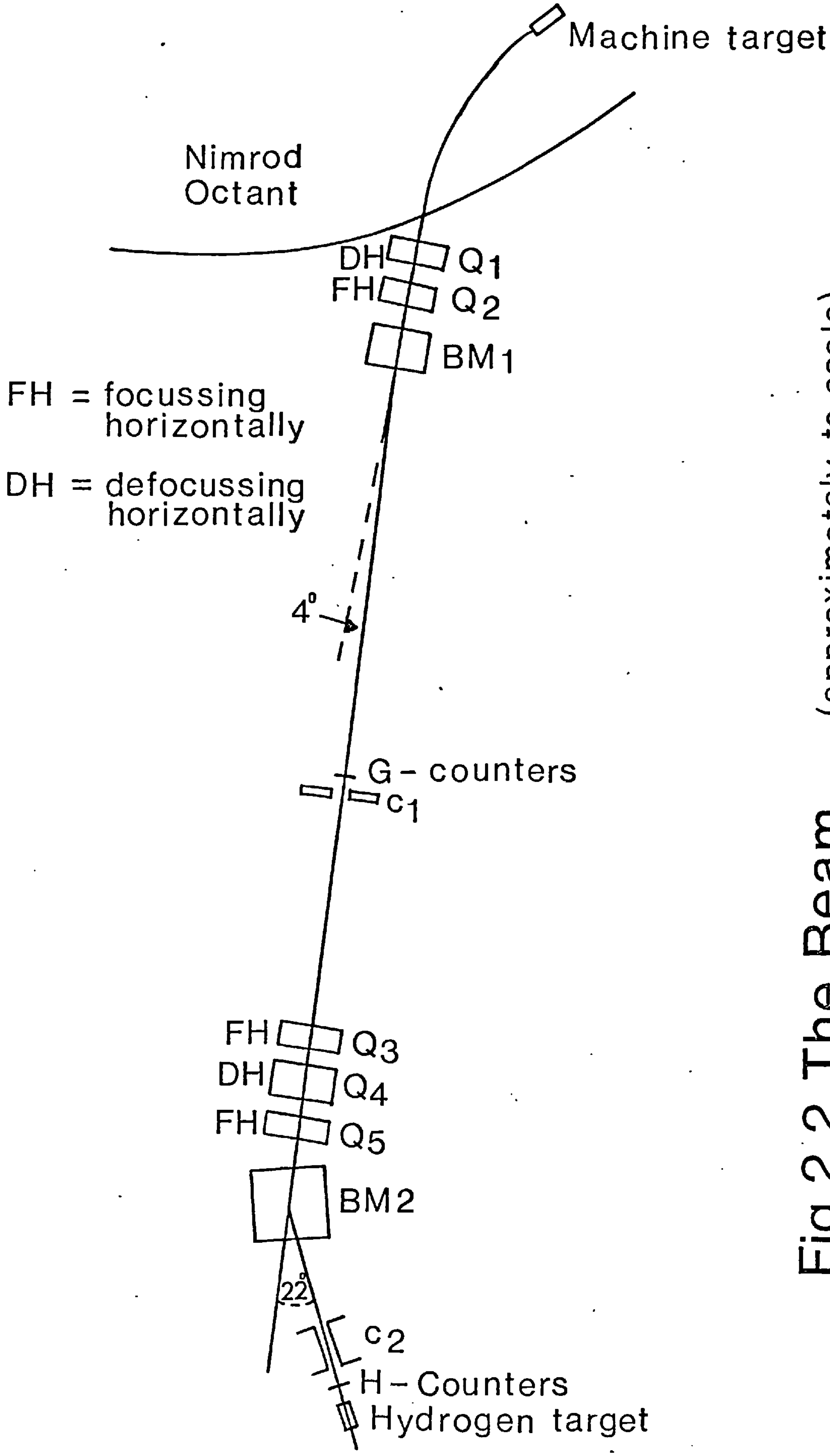

Fig.2.2 The Beam (approximately to scale)

The beam then passed on to the second stage which served two main functions. One was to cancel the dispersion introduced by the first stage, and the other to measure the beam momentum in conjunction with a counter hodoscope (see Section 2.4). The quadrupole triplet and bending magnet of this second stage focussed the beam onto the liquid hydrogen target with a magnification of almost unity. The collimator, C2, was included to protect the spark chambers around the target from stray beam particles, which would otherwise have caused casual tracks that might have interfered with the detection of the wanted events.

The bending magnet BM2 had been tested for uniformity and shimmed, to compensate for path length inequalities, by A. Duane. The currents corresponding to various momentum settings had also been determined prior to the ϕ search experiment by A. Duane and D.C. Mason, using the standard floating wire technique in which the trajectory of a particle of momentum p may be simulated by a wire, carrying a current i and under a tension T, according to the analogue relation $p = 2.941\ T/i$.

A threshold gas Cerenkov counter had been used to determine the beam composition, which was found to be (78 ± 4)% pions with 22% electrons and muons. The anti-proton and kaon content was estimated to be less than 1%.

2.4 The beam momentum measurement - the hodoscope

Two sets of vertical finger counters, G_{1-6} and H_{2-5}, mounted across the beam (Fig. 2.3) in the conjugate planes of the second stage of the beam (Fig. 2.2), were used to signal the lateral displacements of each beam particle from the beam axis. The widths of the fingers at G and H, 8.0 mm and 8.8 mm respectively, were matched to allow for the horizontal magnification of 1.1. Each set of counters was housed in a light-tight box, and aluminium foil cylinders surrounding each of the 3 mm thick fingers guided the scintillation light to the appropriate photo-multipliers.

From the horizontal displacement from the beam axis in both G and H planes, the momentum of each particle could be deduced. As G and H were at conjugate planes, for a particular momentum and a particular G counter, the H

Fig. 2.3 The Hodoscope

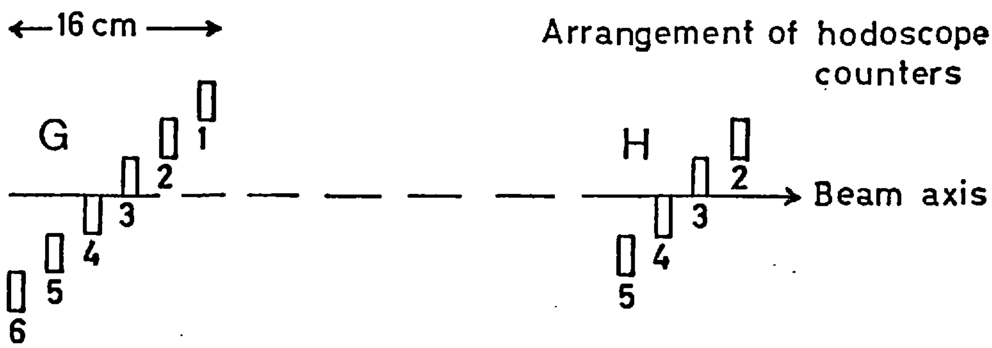

The GH combination of each momentum channel

Momentum channel	Counter Combination			
2	G 1 H 2			
3	G 2 H 2 +	G 1 H 3		
4	G 3 H 2 +	G 2 H 3 +	G 1 H 4	
5	G 4 H 2 +	G 3 H 3 +	G 2 H 4 +	G 1 H 5
6	G 5 H 2 +	G 4 H 3 +	G 3 H 4 +	G 2 H 5
7	G 6 H 2 +	G 5 H 3 +	G 4 H 4 +	G 3 H 5
8	G 6 H 3 +	G 5 H 4 +	G 4 H 5	
9	G 6 H 4 +	G 5 H 5		
10	G 6 H 5			

used

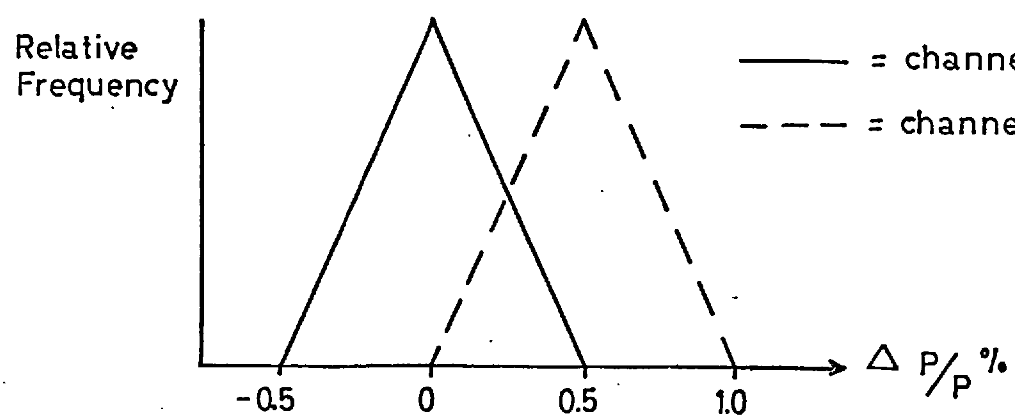

Momentum distribution in neighbouring hodoscope channels counter triggered was defined uniquely. Consequently multiple Coulomb scattering in the counters was unimportant. Many combinations, such as G_3H_4 and G_2H_5 corresponded, within the resolution, to particles of the same momentum. Such groups, therefore, were added electronically to form momentum 'channels', $p_{\pi i}$, i = 2,10 (Fig. 2.3). Due mainly to the finite finger widths, the momenta thus defined were not unique but fell within a triangular distribution of full width at half height of 0.5%. Only the four central channels were used as, in the outer channels, the flux was lower and also the detection efficiency for neutrons associated with ϕ production was less.

2.5 The Hydrogen target

Apart from the usual thermal insulation and safety precautions necessary with a liquid hydrogen target our main requirements were that the beam should encounter a minimum of material, apart from liquid hydrogen, and that the side walls of the vessel should be thin. The latter stipulation was necessary to reduce the probability of producing electrons by photon conversion in the walls of the target.

The liquid hydrogen was contained in a 'sausage' of 0.01" thick Mylar, 32.3 cm long and 6.5 cm in diameter (Fig. 2.4). To choose the target length a number of factors were considered; the low $\phi \longrightarrow e^+ + e^-$ rate necessitated a long target, whereas secondary products from a shorter source would be easier to collect. Also, although not of great concern in the ϕ decay, due to the increased ionisation loss in the long target, the beam momentum at the point of interaction would be more uncertain.

The outer vacuum vessel, the same as that used in the $\omega \longrightarrow e^+ + e^-$ experiment,[2] was made of a thin 0.025" aluminium cylinder fitted with 0.005" Mylar end windows. The flange at the downstream end of the target was essential for mechanical reasons and did not interfere with the lepton pair detection.

2.6 The ϕ search experiment

The apparatus used in the ϕ search is shown in Fig. 2.5. Due to the low production cross-section anticipated, a secondary selection system, sensitive to the most abundant decay mode $\phi \longrightarrow K^+ + K^-$, was incorporated in a bid to

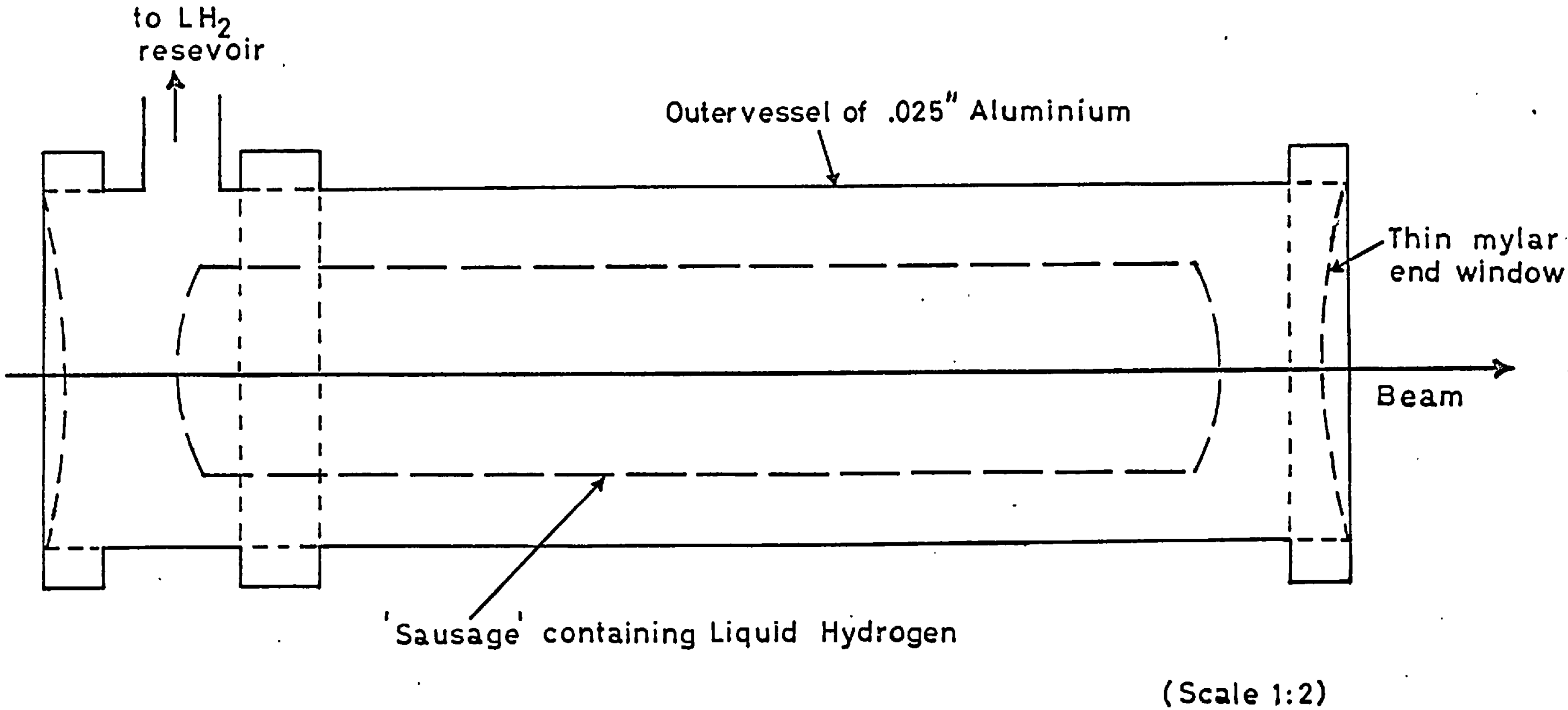

Fig. 2.4 The Hydrogen Target

Fig.2.5 Apparatus used to detect the reaction $\pi^- + p \longrightarrow n + K^+ + K^-$

(Not to scale)

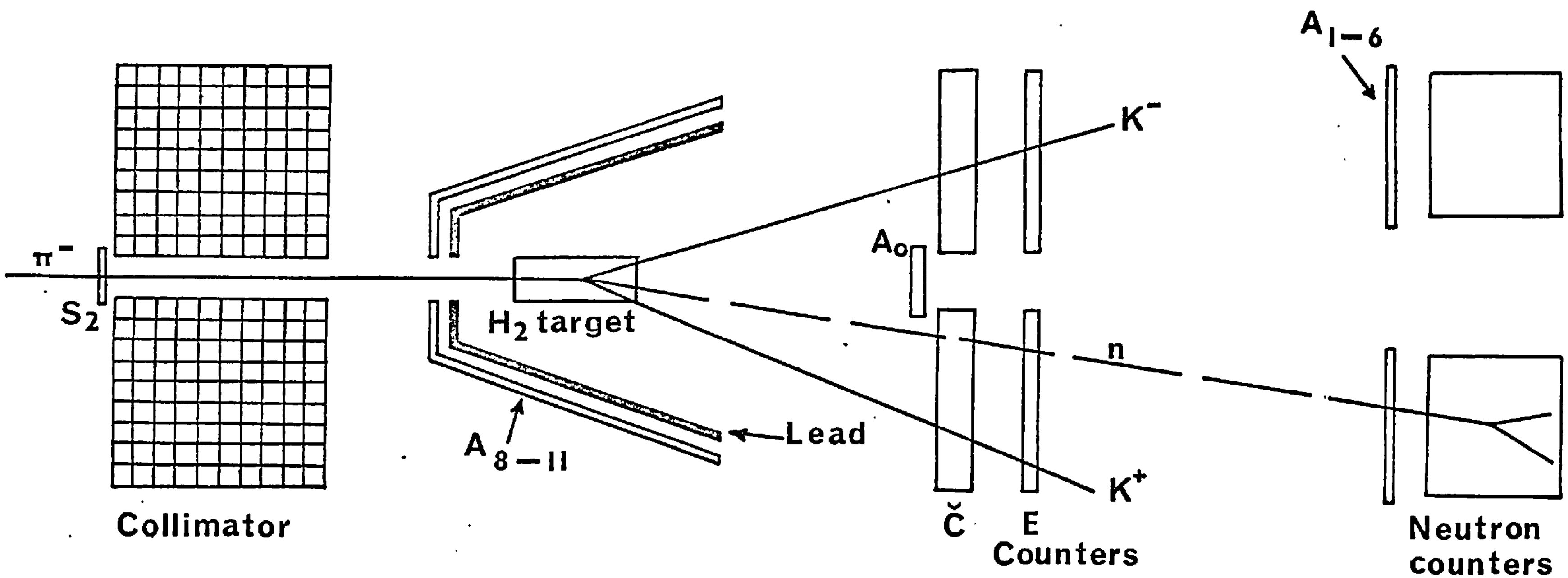

reduce the preponderance of pion backgrounds. A detailed account of this experiment may be found in reference 3 or 4. The secondary selection of the kaons was carried out using four large scintillation counters and a threshold Cerenkov counter. Due to the low Q value of this decay, ~ 32 MeV/c^2, the kaons were confined kinematically to a forward cone, and the four 'E'-counters registered $\sim 50\%$ of the decays. Generally, the velocity of the kaons was below the Cerenkov threshold, whereas the faster pions from background processes were detected. Thus this counter, in anticoincidence in front of the E-counters, afforded a considerable reduction in non K^+K^-n events. In this way signals from any two of the four E-counters, with no Cerenkov pulse, indicated a possible dikaon event. The lead-lined counters A_{8-11}, principally intended to veto wide angle photons from π^o decays, suppressed the background further.

The logic throughout the experiment employed the R.L. series units. Discriminators standardised the pulses from each photomultiplier tube, and these standard pulses were interrogated by the rest of the logic system. Only when all the desired conditions were fulfilled, was a master trigger pulse produced.

Subdivisions of the logic may be given as follows:

$S_2 P_\pi \overline{A}_7 \overline{A}_o$ ..... beam particle interacts

$N_c N_d \overline{A}_{1-6}$ ..... neutron (or γ) detected

$E\ \overline{C}\ \overline{A}_{8-11}$ ..... K^+K^- signature

and the master trigger may be expressed as the product of these three terms.

For each master trigger, a pulse, the amplitude of which was an analogue representation of the neutron time of flight, was 'kicksorted' by a Laben 512 channel pulse height analyser. In this way a 'time of flight' spectrum was obtained. A typical example is shown in Fig. 2.6a. The peak indicated at 13.3 nsec, termed the 'fast peak', is due to particles of $\beta = 1$. Times of flight are determined relative to this peak.

Twenty-four time of flight spectra were obtained at various beam momenta ranging from below the K^+K^-n threshold, 1492 MeV/c, to above the ϕ threshold at 1620 MeV/c. Each spectrum was normalised to 10^8 beam particles after allowing for high rate effects. The major rate effect was known as

Fig. 2.6

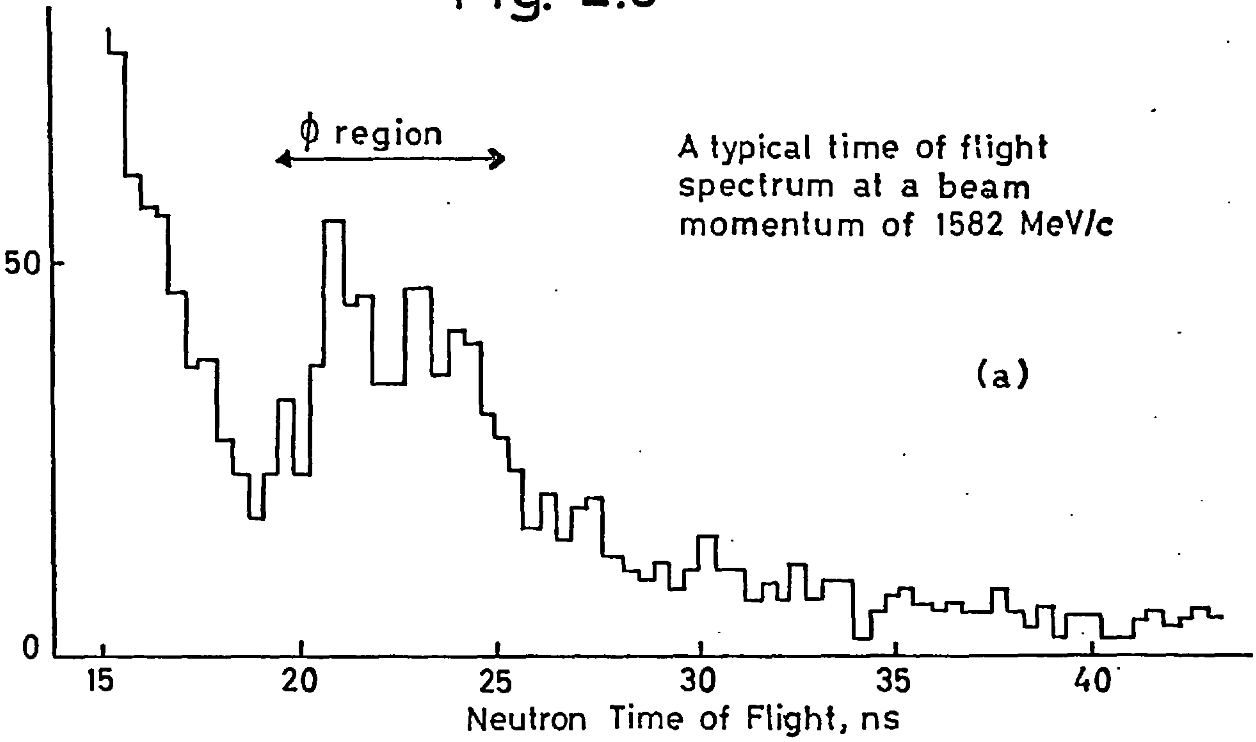
ϕ region
A typical time of flight spectrum at a beam momentum of 1582 MeV/c
(a)
50
0
15
20
25
30
35
40
Neutron Time of Flight, ns

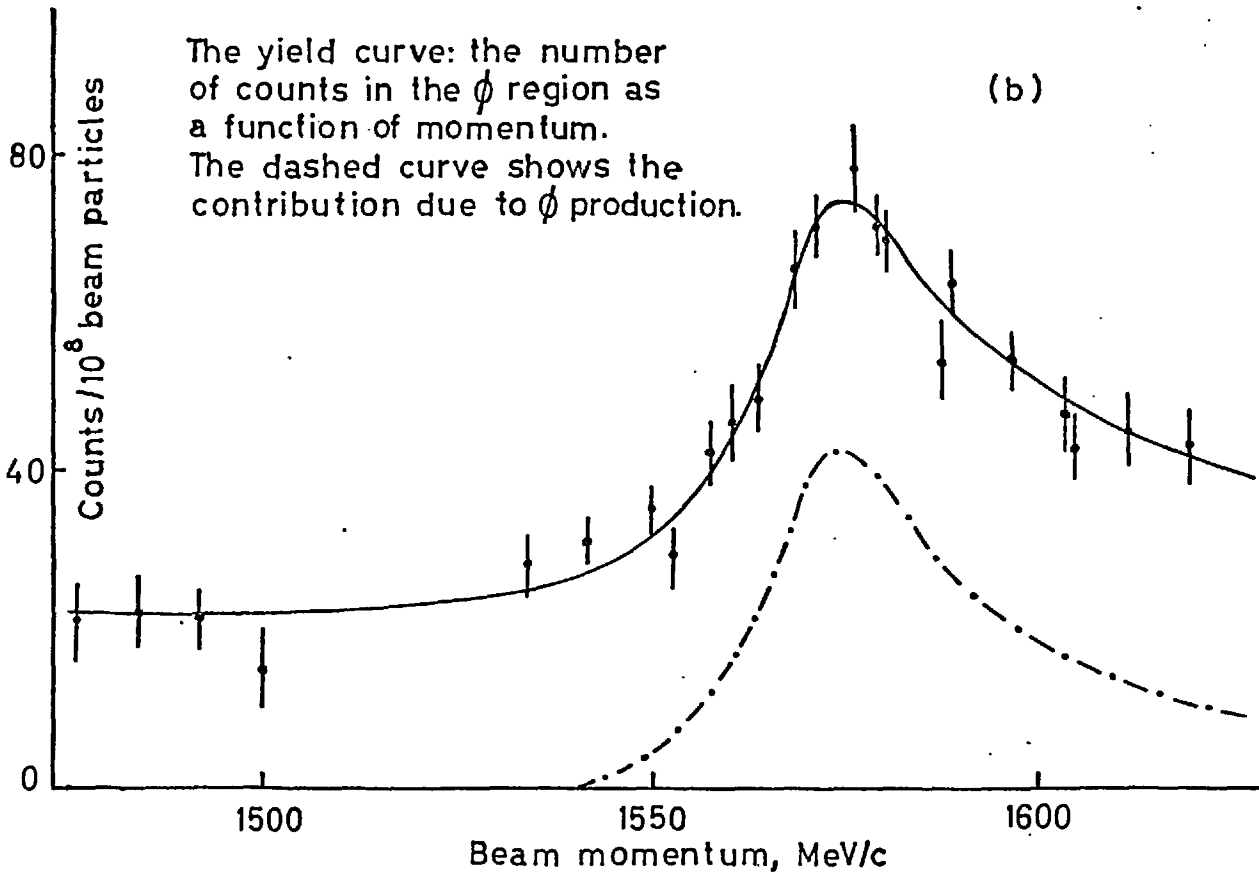
The yield curve: the number of counts in the ϕ region as a function of momentum.
The dashed curve shows the contribution due to ϕ production.
(b)
Counts/10^8 beam particles
80
40
0
1500
1550
1600
Beam momentum, MeV/c

'occupancy', the result of casuals in the veto counter A_o, situated just in front of the Cerenkov counter, Fig. 2.5. The loss of good events incurred was a function of beam rate but, on average, was $\sim$ 10%. For each spectrum, this loss was monitored continuously and allowed the necessary corrections to be made.

The equivalent counter in the $\emptyset$ decay was A_{10} and, as the rates in, and the pulse widths of, both counters were almost identical, the loss would be very similar in both experiments. Hence in the eventual normalisation, errors in the estimation of the occupancy would tend to cancel.

From Monte Carlo calculations at 1580 MeV/c, a time of flight gate was chosen to include all but a negligible number of $\emptyset$'s. The total number of counts in the appropriate kicksorter channels were found for each spectrum. These numbers, corrected for casual counts which, like occupancy, had been monitored continuously, were normalised to 10^8 beam particles and are shown as a function of beam momentum, p_π in Fig. 2.6b, the 'yield' curve. The rapid rise at $\sim$ 1560 MeV/c is evidence of $\emptyset$ production as opposed to other sources of K^+K^- pairs. The relative momenta were not sensitive to hysteresis in the bending magnet BM2, as each was set from an n.m.r. frequency. However, the absolute values were uncertain due to the $\sim 0.3\%$ error in the floating wire calibration. The ϕ mass, deduced from the yield curve using the nominal p_{π} values, was found to be 1016.5 ± 2.5 MeV/c^2. To produce the accepted value[25] of 1019.5 ± 0.6 MeV/c^2, the necessary change in the momentum scale was found to be 4.3 ± 1.5 MeV/c. This is consistent with the error in the floating wire result. The actual momenta used in the ϕ decay could now be deduced from the n.m.r. frequencies used.

The contribution to the yield curve from non K^+K^-n events was estimated as follows. At long times of flight where the $K\bar{K}n$ contribution was small, the total number of counts (normalised) was found to vary only slowly with momentum. The number of non $K\bar{K}n$ events in the ϕ region should also not vary appreciably with momentum and therefore the backgrounds above and below threshold in the ϕ decay would be very similar. The amount of this non K^+K^-n background present in the ϕ search was deduced from the data below the K^+K^-n threshold.

The non-resonant K^+K^-n contribution was found from the 1620 MeV/c data in which the ϕ would have a small effect.

In Fig. 2.6b the continuous line shows the best fit to the data for a ϕ production cross-section rising linearly with c.m.s. momentum, p*, with isotropic production and decay of the ϕ, superimposed on non-resonant kaon and constant pion backgrounds. The dashed curve shows the estimated contribution due to ϕ production.

For the ϕ decay normalisation we needed to know, as a function of p_π, the number of ϕ's that would be produced per 10^8 beam particles, in which the corresponding neutron was detected. From the ϕ search analysis at this stage, the yield of detected $\phi \longrightarrow K^+ + K^-$ was known and thus from a knowledge of the branching ratio for $\phi \longrightarrow K^+ + K^- = 0.48 \pm 0.03$, and the K^+K^- detection efficiency, we could deduce the quantities required.

The geometric efficiencies of the K^+K^- detection system were found from Monte Carlo calculations assuming isotropic ϕ production and decay. The program also allowed for loss of kaons which either were faster than the Cerenkov threshold, or decayed in flight. Apart from the geometric efficiency and the two losses mentioned above, all of which could be estimated accurately, the corrections in the K^+K^- detection efficiency were small. The kaon loss due to detection of δ-rays, produced in the Cerenkov counter, was found to be $3 \pm 3\%$ by both experiment and calculation, and the effect of kaon interactions in this counter was estimated to be $3 \pm 2\%$. The total detection efficiency for K^+K^- from ϕ decay was estimated to be 0.34 ± 0.01.

Other losses were common to both search and decay experiments and would cancel on normalisation. These main losses included such factors as: beam attentuation along the target, 0.96; beam constitution, 0.78 ± 0.02; neutron interaction products resulting in a veto pulse in A_{1-6}, 0.97 ± 0.02; neutron counter efficiency, 0.28 ± 0.03. These factors were necessary only to deduce the ϕ production cross-section.

Spark chamber photographs of the K^+K^- tracks had been taken concurrently and allowed an analysis of the K^+K^- angular distributions. A detailed account of this aspect of the ϕ search experiment may be found in reference 3.

The data were found to be consistent with a simple S-wave model and, using this model, the total cross-section was found to be $(0.28 \pm 0.07)p^* \mu b$, where p^* is measured in MeV/c. To date, the only experiment with which the results of the ϕ search can be directly compared is that of Hess et al.[28] The results of both experiments are shown in Fig. 2.7. The only point, in the data of Hess et al., in the p^* region relevant to the ϕ search is consistent with the ϕ search results.

Fig. 2.7

Comparison of ϕ production cross-sections from the ϕ search experiment and that of Hess et al.

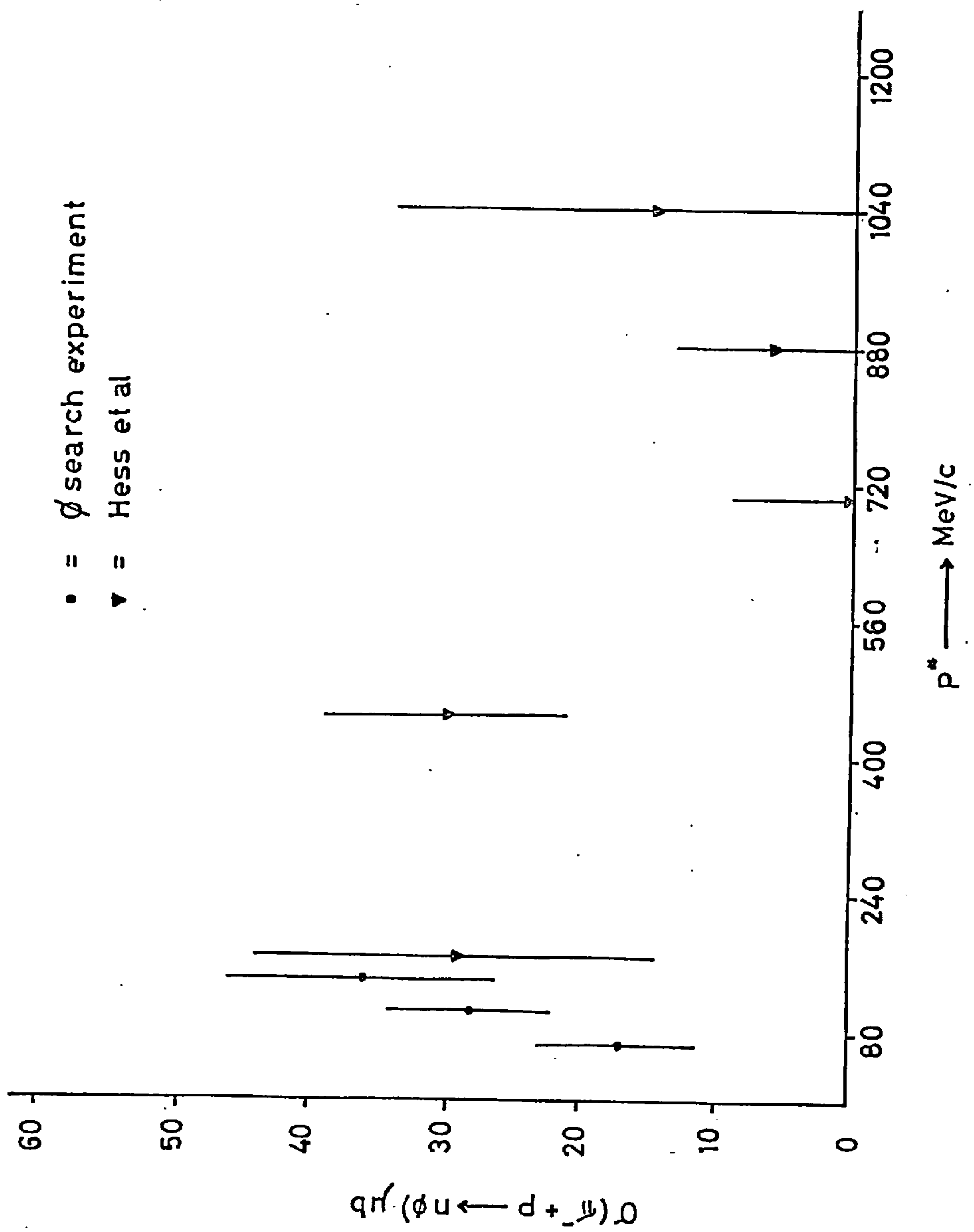

CHAPTER 3

THE ELECTRON PAIR SECONDARY SELECTION SYSTEM

3.1 Introduction

As the ϕ mesons were to be produced near threshold, electrons from $\phi \longrightarrow e^+ + e^-$ would be of relatively low momenta, 400-800 MeV/c, and would be emitted over a wide range of angles in the laboratory. To detect the electron pairs efficiently, spark chambers interleaved with lead plates, as had been used successfully in the $\omega \longrightarrow e^+ + e^-$ experiment,[2] were considered to be the most practicable.

In the ω experiment, the first of the series, six thin foil optical spark chambers, alternated with five lead plates, each of ~ 1 radiation length, were placed on each side of the target and the multiplication in the electron showers, recorded on film, could be examined after each radiation length of lead. An improved version of this system was used in the ϕ decay experiment to resolve the electrons in copious pion and photon backgrounds.

3.2 The spark chambers

Spark chambers display single tracks efficiently, but suffer from 'robbing' when required to support multiple tracks.

Observation of multiple tracks was of vital importance in the electron shower detection and, to reduce the effects of robbing, four gaps were used in each chamber module. Scattering within the chambers was made negligible by using thin, 0.001" aluminium foil plates, and consequently the chance of a photon conversion in the plates of the chambers nearest to the target was also negligible.

Were the efficiency of a module to be 100%, then each track would appear as four colinear sparks. In practice, the efficiency would fall short of this ideal, but as only two of the possible four sparks are necessary to define a track, the loss of tracks is relatively insensitive to the loss of sparks.

Experience had shown that a loss of sparks of about 10% could be expected in supporting single tracks, and that a loss of this order was insensitive to small changes in the operating conditions. For multiple tracks the loss would be greater, but provided the single track response did not deteriorate, then the number of shower particles resolved by the chambers would not depend significantly on the operating conditions. This independence of conditions was important as the showers in the decay experiment were to be compared later with those of beam electrons which had been photographed some years ago using a similar arrangement of chambers and lead plates.

3.3 Location of the chambers

As the decay rate of $\phi \longrightarrow e^+ + e^-$ was anticipated to be small, efficient collection of the lepton pairs was desirable, and a number of geometrical arrangements of the spark chambers was envisaged with this aim in view. A bank of chambers at an angle on each side of the target, Fig. 3.1 as in the ω experiment, was considered to be the only practicable solution, and efforts were made to maximise the acceptance of this configuration.

To attain the optimum response from counters, which were placed between the spark chambers, the electrons from ϕ decay should enter the chamber banks normally. The mean opening angle of the decay products indicated that chambers at $\sim 35^\circ$ to the beam would be most suitable. A smaller angle, however, would result in an improved collection efficiency and a compromise value of 25° was chosen.

Fig. 3.1 The arrangement of the spark chambers around the hydrogen target. Each chamber is off-set with respect to its neighbour as is indicated.

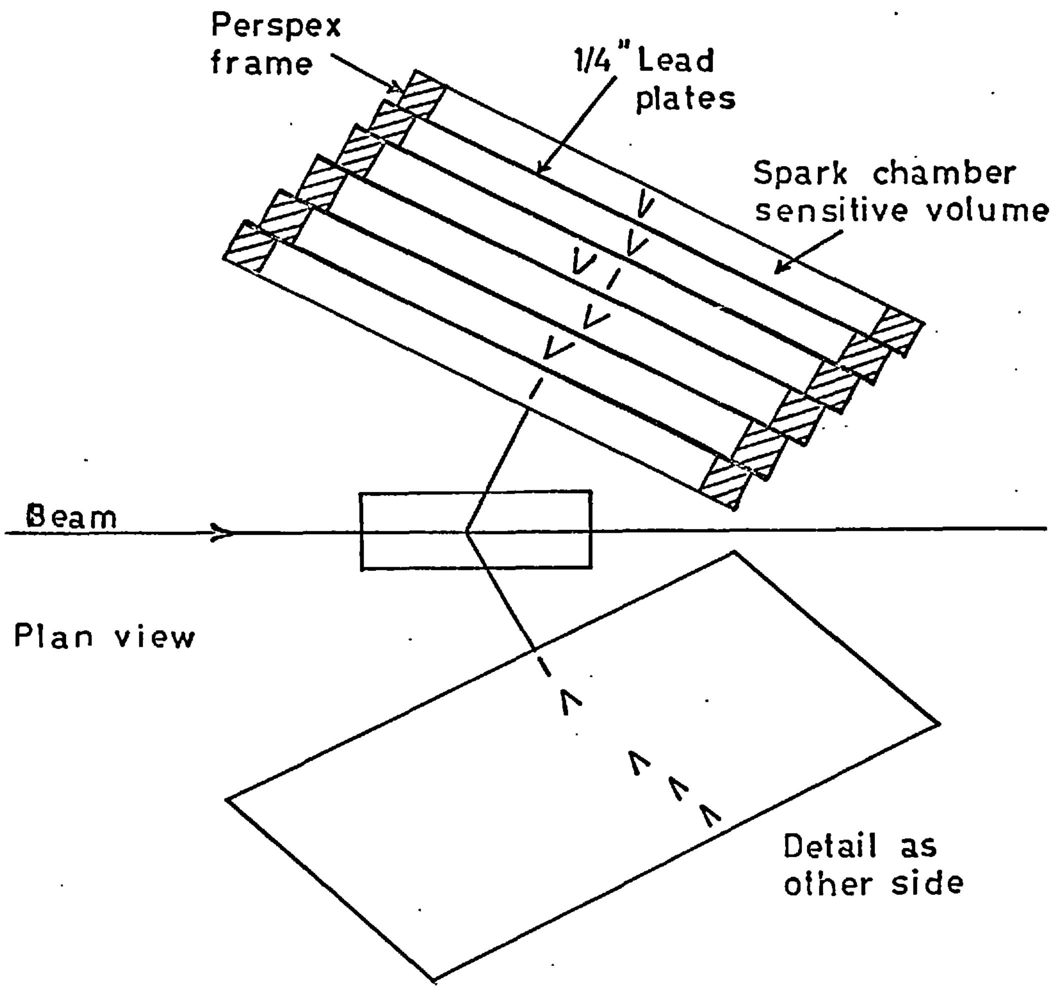

Chambers of a larger area than those actually used would of course have increased the acceptance of the system. Their size, however, was limited to 75×75 cm^2, both by the width of the aluminium foil available and the maximum dimensions of the mirrors (needed to view the chambers) that could be manufactured at the time. Furthermore, the additional electrons collected by larger chambers would be at smaller angles to the plates and their showers would differ structurally from normally incident electrons.

Thinner modules would also have led to improvement by reducing the overall thickness of the chamber banks. This, however, would have entailed decreasing the plate separation from $\frac{1}{4}$" and would automatically have magnified any undesirable effects due to non-uniformity in this separation. Furthermore, a substantial reduction in the depth of each chamber bank would modify the spread of any electron showers, and not permit a straightforward comparison with the calibration electron photographs (see Section 5.2).

By reducing the distance between the two banks of chambers the acceptance could have been increased. This could only be done at the expense of introducing an excess of troublesome interactions in the perspex frames due to particles in the fringes of the beam. A separation of 6 cm between the edges nearest to the beam was chosen. Beam interactions in the lead plates were of even more concern than those in the perspex frames. To reduce troubles from this source, the areas of lead near the beam were cut away from the two inner plates on both sides. This had the added advantage that, without cost to the electrons, the losses due to neutron interactions were almost the same as in the ϕ search experiment, the results of which could therefore be used for normalisation without an additional neutron loss correction. Metal supports were of course avoided in this region.

As in the ω experiment, each module was offset with respect to its neighbour as shown in Fig. 3.1. With this staggering, the shower from an electron directed along PR (Fig. 3.2a) could be sampled in each chamber, whereas without staggering (dashed outline) this same electron would leave the chamber fiducial volume at an early stage. The converse would apply to an electron along PQ, but as relatively few electrons from ϕ decay would have angles of more than 90° to the beam, their loss would be unimportant.

Fig. 3.2

a) Staggering of the chambers increases the acceptance.

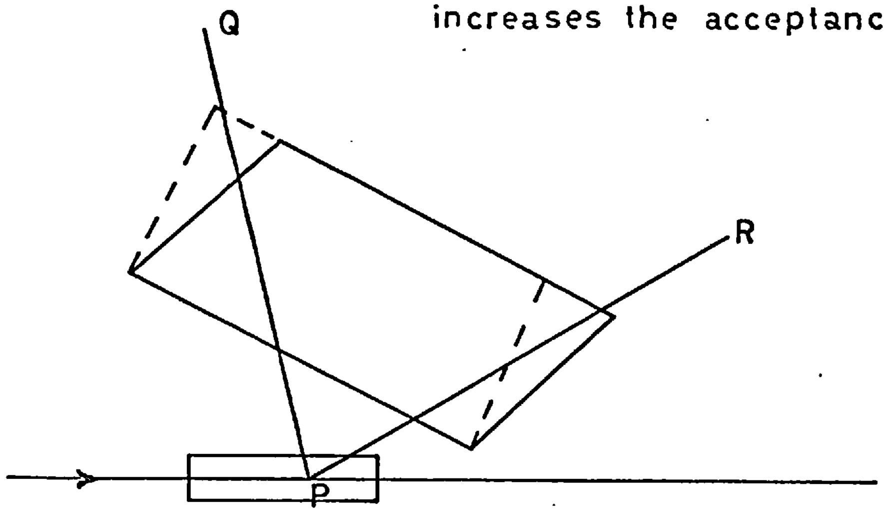

b) The degree of staggering is chosen such that, if a forward electron is just accepted at S, then its partner is just collected at T.

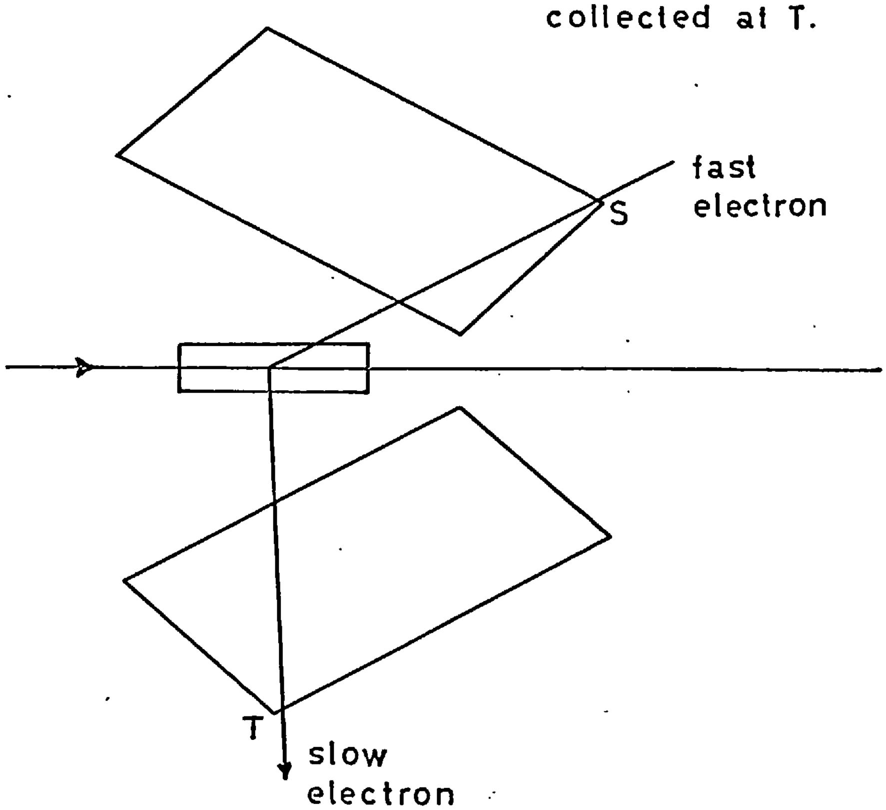

The nett effect of staggering was to increase the acceptance of $\phi \longrightarrow e^+ + e^-$ events.

A rough estimate was made of the optimum position of the centre of the hydrogen target with respect to the inner chambers. At the centre, decays of $\phi \longrightarrow e^+ + e^-$ in the horizontal plane were considered. The degree of staggering was chosen such that if the faster electron were to pass into the chambers close to 'S' (Fig. 3.2b) then its slower partner on the other side would just be accepted near 'T'.

Once the position of the outer chambers had been determined, the final location of the chamber system could be chosen with respect to the target. Monte Carlo $\phi \longrightarrow e^+ + e^-$ events were generated along a long hypothetical target. The distribution of events, in which both electrons passed into the outer chambers, and the relative position chosen for the actual 32.3 cm long target, are shown in Fig. 3.3.

In this way the acceptance of the chamber configuration used was maximised. Using a simple S-wave model, Monte Carlo calculation showed that of all $\phi \longrightarrow e^+ + e^-$ decays, in which the corresponding neutron was detected, the fraction

Fig. 3.3

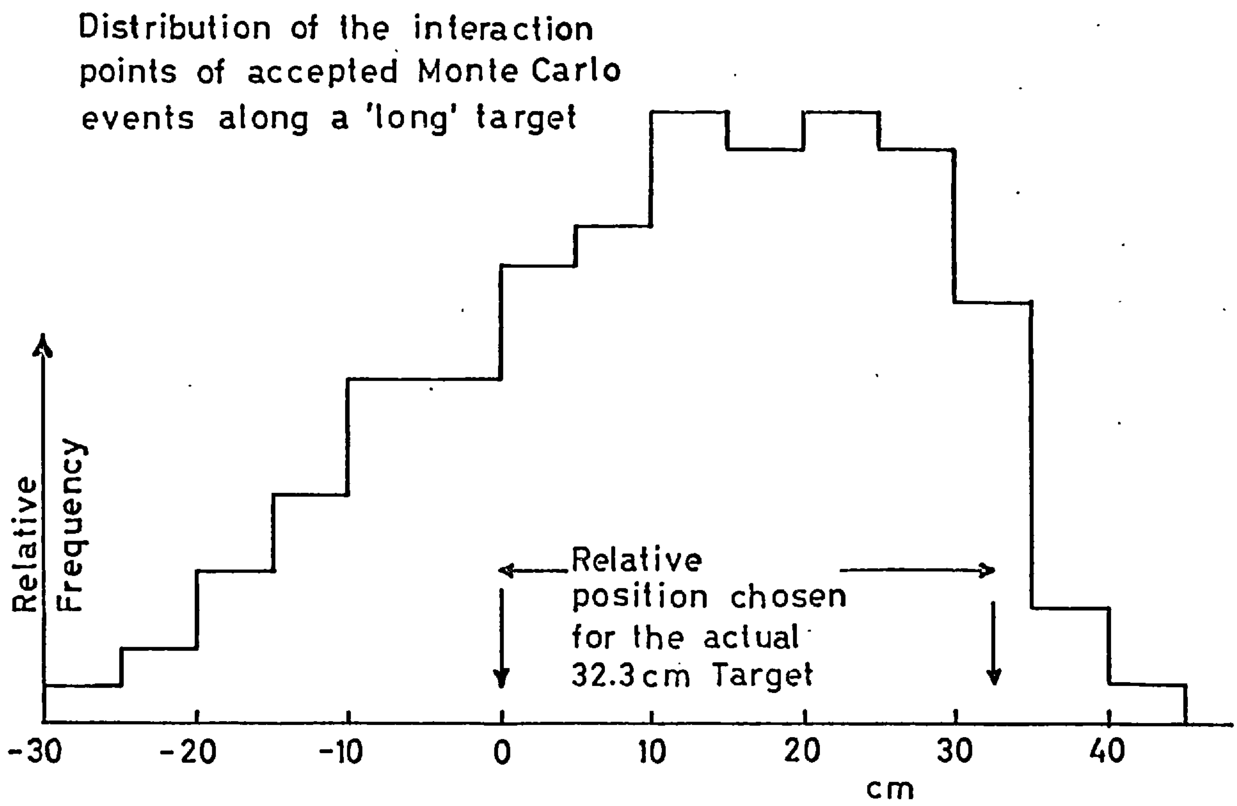
Distribution of the interaction points of accepted Monte Carlo events along a 'long' target
Relative Frequency
Relative position chosen for the actual 32.3 cm Target
-30
-20
-10
0
10
20
30
40
cm

in which both electrons would pass into the sensitive volume of the outer chambers was 22%.

3.4 Selection of charged secondaries

Due to the low ϕ cross-section, the production rate of $\phi \longrightarrow e^+ + e^-$ per unit beam was estimated to be an order of magnitude lower than the corresponding ω rate. It follows that, as in the ω experiment in which there was no secondary selection, proportionately more photographs would be necessary in the ϕ experiment. The 500,000 frames from the ω experiment had placed a considerable strain on our scanning resources and the prospect of several millions from the ϕ decay seemed formidable. Therefore, although an electronic secondary selection system would introduce bias problems, rejection of events, of a type unlikely to be electrons, was unavoidable.

One obvious technique was to incorporate counters to detect the entry of a charged particle into the chambers on each side of the target, and thereby to prevent wastage of film on events without tracks in both banks of chambers. These counters could not preceed the inner spark chambers for the same reason that required thin walls to be used for the target vessel. In addition, multiple Coulomb scattering in the counters would mar the incident particle direction information available from the inner chambers. Similarly, counters placed after the first lead plates would fail to record any electrons which happened to convert in the lead. To avoid a significant loss of $\phi \longrightarrow e^+ + e^-$ events, the counters would need to be efficient, and set between the inner chambers and the first lead plates. There was no point in making these counters larger than necessary, as any surplus scintillator in positive logic was a potential source of background. Monte Carlo techniques were used to simulate ϕ decays, and from the population of the electrons in the planes of the inner chambers, the minimum size and optimum positions of the counters were deduced. The counters, S_3 and S_4, were 34 cm x 41 cm x 1 cm thick. By demanding at least one charged particle on each side, we expected to reduce the trigger rate by a factor of about 4. This alone, however, would still result in an overwhelming number of photographs, and further selection was deemed necessary.

3.5 Sampling of electron showers

The majority of the triggers would be due to pion backgrounds. The interaction length in lead is ~ 25 radiation lengths and in general, pions, unlike electrons, would pass through the 5 lead sheets without interacting. It should be possible, therefore, to distinguish non-interacting pions from electrons by the absence or presence of showering.

Extensive work has been done on the development of electron showers in the energy range 100-1000 MeV, by Heusch and Prescott[29] whose results are in good agreement with the Monte Carlo calculations of Crawford and Messel.[30] Figure 3.4a shows the mean number, $\bar{N}$, of electrons in 400, 600 and 800 MeV showers as a function of depth of penetration measured in radiation lengths of lead. At 600 MeV the value of $\bar{N}$ is seen to rise quickly to a maximum of about 3 after 3 radiation lengths, and then to fall away slowly. A counter capable of distinguishing between 1 and more minimum ionising particles should therefore be able to segregate a non-interacting pion and the 'average 600 MeV electron'. The values of $\bar{N}$ given are averaged over many electrons, and

Fig. 3.4 a) The mean number of particles, $\bar{N}$, in electron showers as a function of penetration depth.

b) The maximum value of $\bar{N}$ as a function of energy.

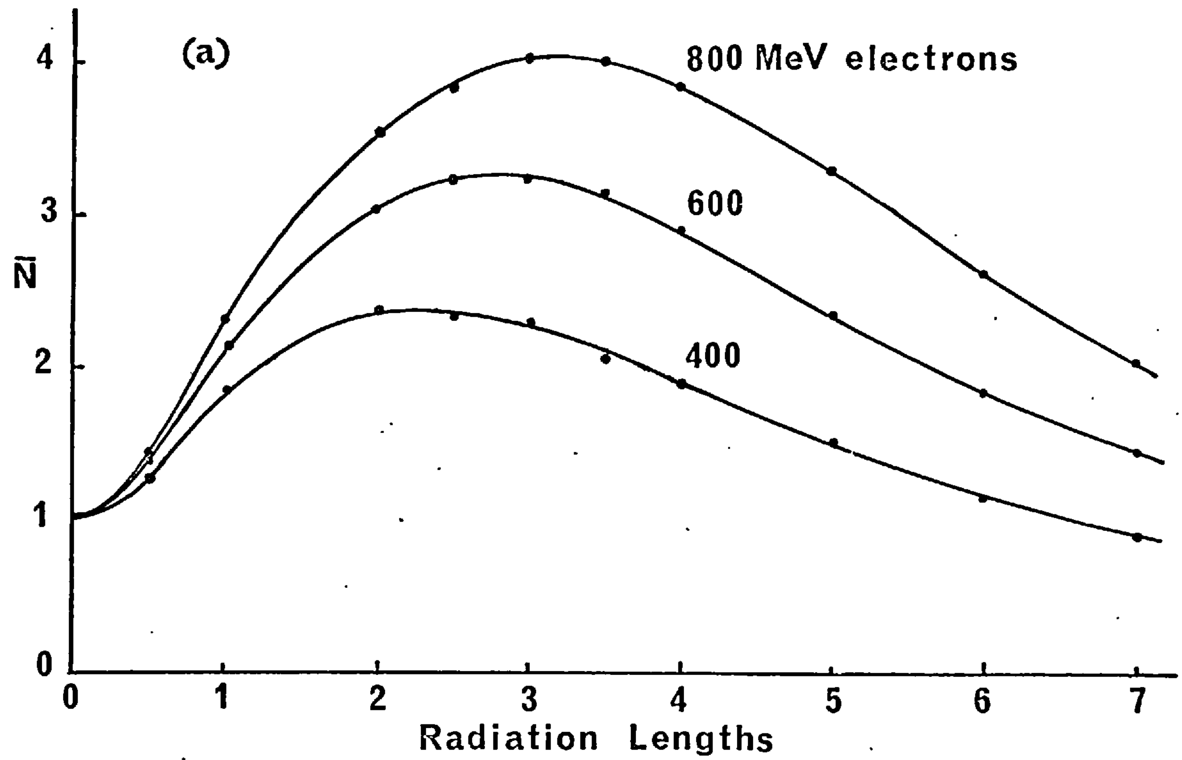

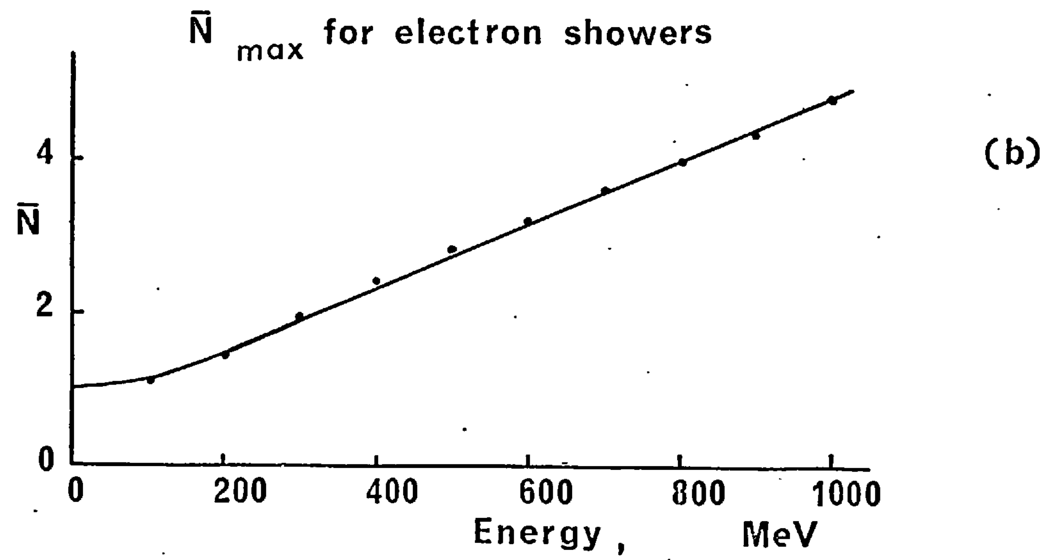

large fluctuations are found in individual cases. Values of one or even zero for N_e, the number of electrons at a given depth in an individual shower, are not infrequent, and a single counter biased to reject pions would incur an unacceptable loss of electrons.

By using counters to sample the showers at two points, instead of only at one, the effects of individual variations are reduced. The samples should be at points where $\overline{N}$ is close to the maximum, but should also be separated sufficiently to avoid strong correlations. After approximately 2 and 4 radiation lengths were the most suitable points.

If the gains of the counters were matched to give the same pulse height for normal minimum ionising (min I.) particles, then four such counters, two on each side of the target, Fig. 3.5, would have a mean total pulse height corresponding to $\sim$ 4 min I. for events with two pions, and to $\sim$ 12 min I., with a large spread, for events with two 600 MeV electrons.

Using the total, rather than the individual, pulse heights would have the advantage that the fluctuations in each counter would add statistically and have less

Fig.3.5 The apparatus used in the ϕ decay experiment

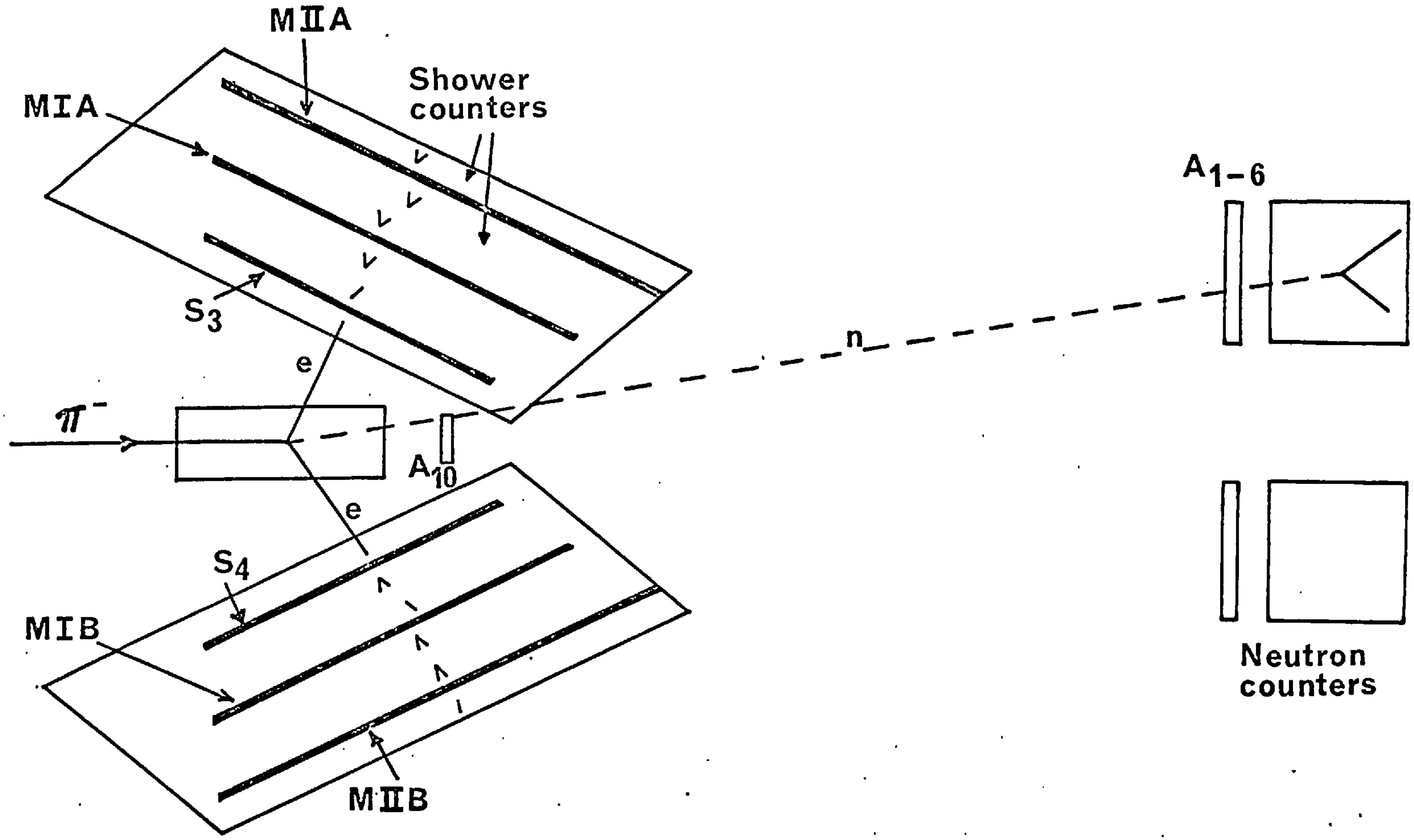

significance. Also, as the sum of the energies of the two electrons would be that of the ϕ and roughly constant, a low energy electron on one side would be partnered by a correspondingly high energy one on the other. Hence the total pulse height would not vary appreciably due to asymmetric events, as above 100 MeV the maximum value of $\bar{N}$ is a linear function of energy, Fig. 3.4b.[29] Discrimination against events with 4-5 min I. total pulse height could in principle be used to reject much of the pion background, provided the inevitable loss of electron events was not too great. This warranted further investigation.

The Monte Carlo program was adapted to estimate the total pulse height distribution to be expected from counters, used to sample the showers, after the second and fourth lead plates on both sides. The actual thickness of lead traversed by a particle depended on the angle of incidence, and due allowance was made for this in the estimation of $\bar{N}$ at each counter from interpolation of the results of Heusch and Prescott.[29] The standard deviations, σ , of the spreads in the values of N_e about the corresponding mean values $\bar{N}$, quoted in the same paper, were found to satisfy the following equations:

a) after $\sim 2\ X^{o}$: $\sigma = 1.025 x N_e - 1.04$ ... 3.1

b) after $\sim 4.5\ X^{o}$: $\sigma = 0.62 x N_e - 0.20$ ... 3.2

To fold in these fluctuations at each counter, random Gaussian errors, with the appropriate deviations, were added to the interpolated values of $\overline{N}$. For each event, the pulse height from each counter was assumed to depend linearly on the total ionisation deposited by, and therefore the total path length of, the N_e shower particles in the scintillator. The pulse heights, in min I. units, for each counter were added to give the distribution that could be expected from a set of 'perfect' counters.

To include the performance of actual counters, their intrinsic spreads had to be considered. Fig. 3.6a shows the pulse height spectrum of a typical scintillation counter subjected to normal minimum ionising particles. The spread, mainly due to photo-electron statistics, is defined as:

$$\text{Spread} = \frac{\text{Full width at half height}}{\text{Most probable pulse height}} \qquad \ldots 3.3$$

Fig. 3.6

Typical pulse height distribution from a counter subjected to normal minimum ionising particles

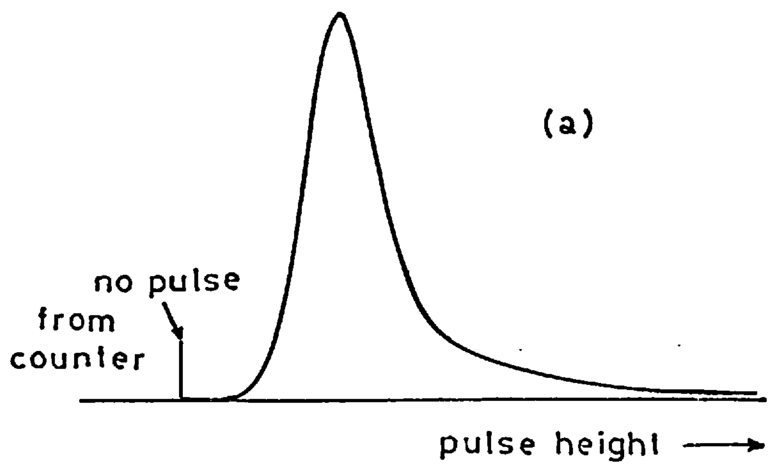

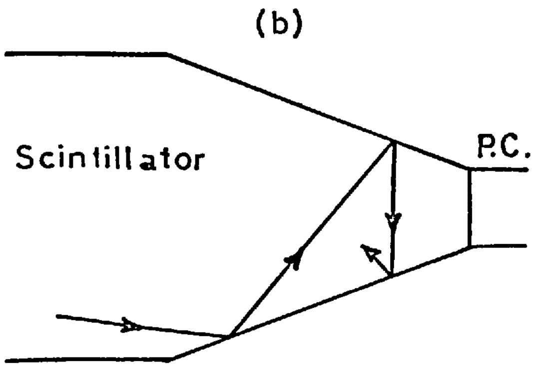

With a tapered guide, much of the light fails to reach the photocathode.

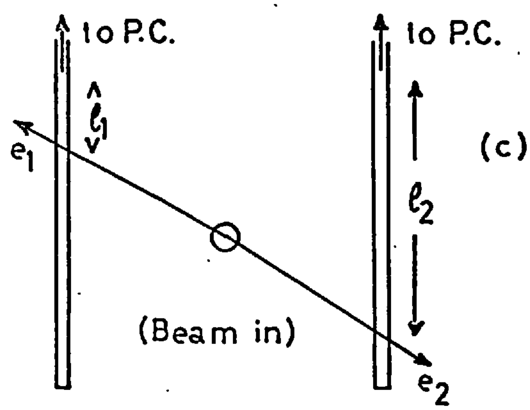

Since $e_1 e_2$ and the beam are nearly coplanar, the sum $\ell_1 + \ell_2$ is almost constant.

Experience indicated that a spread of 50% would be a reasonable estimate for calculation purposes. An accurate value was unnecessary due to the much larger effects of the electron shower fluctuations.

The distribution of total pulse heights expected for electrons from ϕ decays, including counter performance, is shown in Fig. 3.7. The corresponding distribution expected from the non-interacting pions in 2π n events is also shown. These results indicated that a discrimination level of about 7 min I. would considerably reduce the dipion background at little cost to the electrons. The production of some suitable high performance counters became essential.

3.6 The shower counters - design

The shower counters, sandwiched between the chambers, Fig. 3.8, played a vital role in the electron shower detection. To make full use of the 65 x 65 cm^2 sensitive area of the outer chambers, the shower counters, MIIA & MIIB, adjacent to these chambers needed to be of at least the same dimensions. In fact the scintillators used were 70 x 70 cm^2. This allowed for some lateral spread in the electron showers, and reduced biases against electrons

Fig. 3.7 The distributions of combined pulse heights expected from the four shower counters

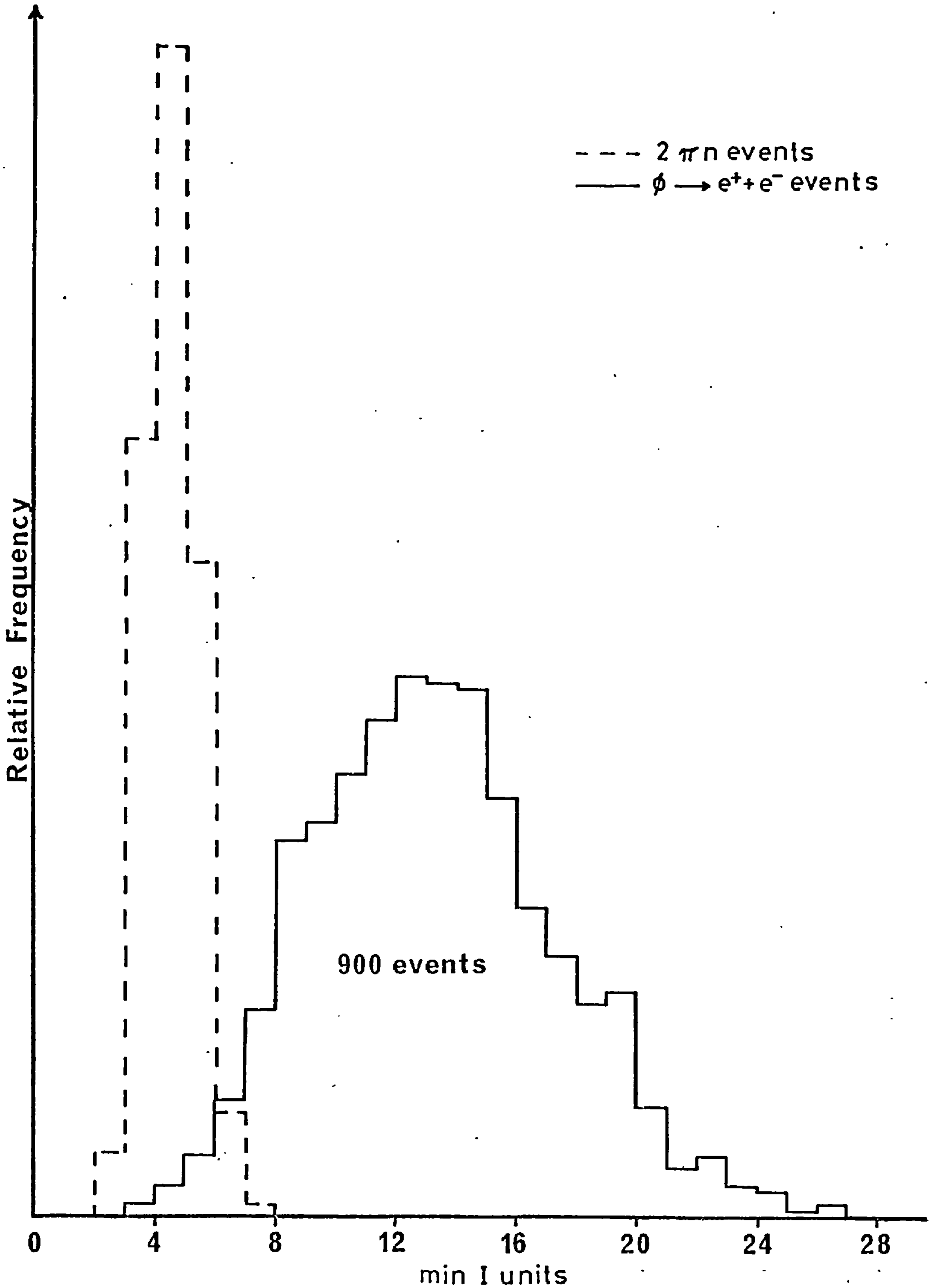

Fig. 3.8

Cross-section through one of the spark chamber banks.

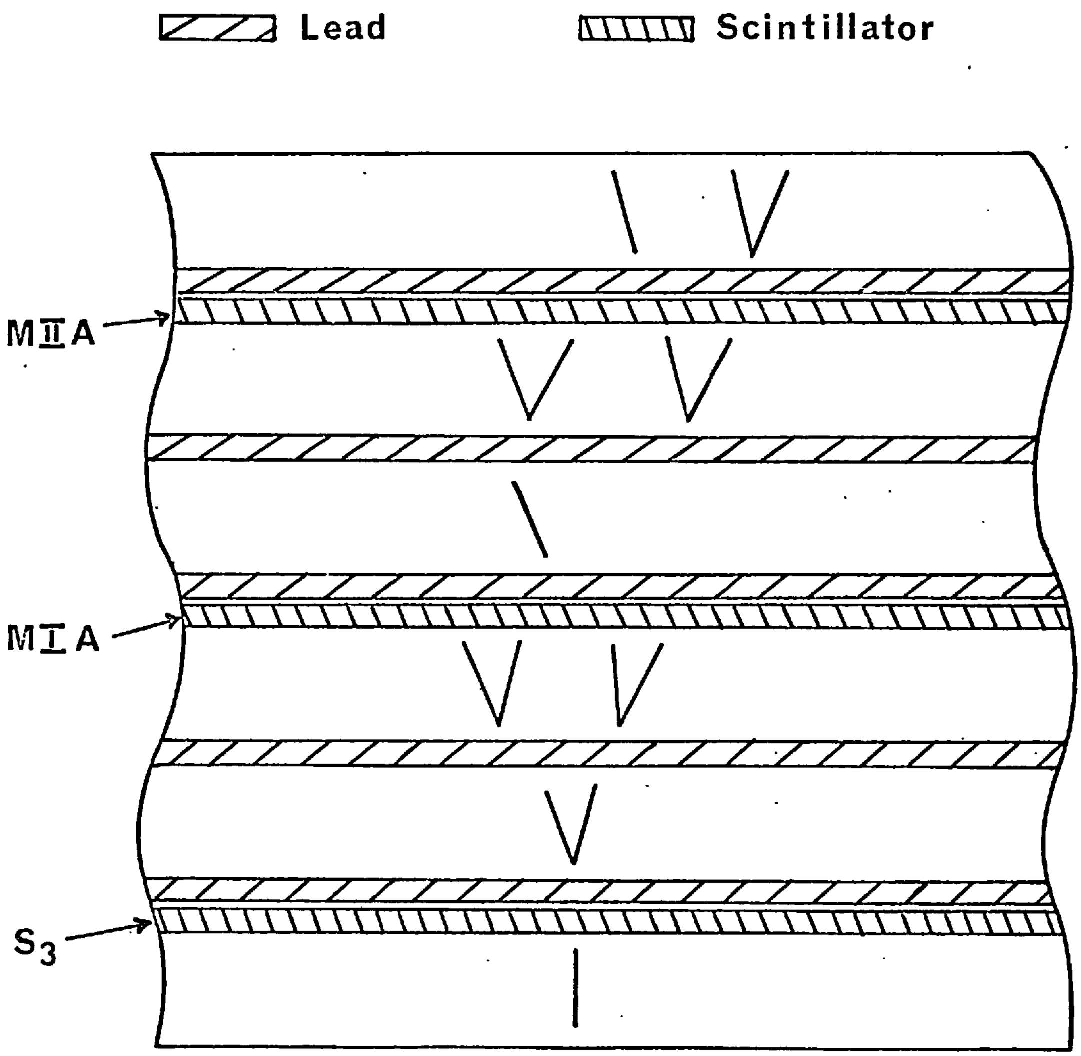

close to the edges of the chambers. The other shower counters, MIA & MIB, were only 60 x 60 cm^2 as, because they were nearer to the target, this size was ample to monitor any electrons that would also pass into MII. (The A and B notation is used only where the distinction is necessary).

Uniform pulse response is a result of an abundant supply of photo-electrons. The thickness of the scintillators, and therefore the supply of photons, could not be increased significantly beyond the 1 cm and ½" used for MI and MII respectively, without reducing the acceptance. Therefore, other means of improving the uniformity had to be sought.

The largest factor contributing to loss of light in scintillation counters is the light-guide itself. Liouville Theorem, applied to light-guides, states that the maximum flux of light at the photocathode is given by:

$$\text{(flux into P.C.)} \leq \frac{a}{A} \cdot \text{(flux into guide)} \qquad \ldots 3.4$$

where 'a' and 'A' are the respective areas of the photocathode and the light-guide near the scintillator. Absorption and reflection losses reduce the efficiency further.

The area at the edge of MII was 70 cm x 1.27 cm, i.e. $\sim$ 90 cm^2. To use the usual 2" 56 AVP photomultiplier tube, with an effective cathode area of 14 cm^2, would automatically have limited the light collection efficiency to $\sim$ 16%, and the advantages of a 5" 58 AVP with an effective area of 97 cm^2 from this point of view were obvious.

Even so the conventional fish-tail guide leads to gross loss of light as most of the photons do not reach the photocathode, but return to the scintillator after a few reflections, as indicated in Fig. 3.6b. If, however, the cross-section of the guide were constant throughout its length, losses due to such reflections would not occur.

Light-guides, using a number of twisted perspex strips to exploit this fact had been made and tested.[31] The uniformity of counters employing these fluted light-guides was stated to be considerably better than counters of the same dimensions using standard fish-tail guides. Our counters were larger; similar light-guides, using thicker perspex strips, would be essential to attain the required response. The thickness of the strips, $\frac{1}{2}$", was chosen to be equal to that of the larger scintillators. The width of the strips, however, depended on a number of factors. A square cross-section of the combined strips at the photo-tube end of the guide would result in the minimum light loss, and suggested 7 strips, each about 8.5 cm wide, for the smaller counters. Narrower strips, however, would not only be easier to bend but would also reduce the overall thickness of the light guide. Eight strips, 7.5 cm wide, were chosen for the 60 cm MI, and nine similar ones for the larger counters, MII.

The length of the strips was not critical. They had to be sufficiently long to assume their final position without excessive curvature, yet form a reasonably compact light-guide. The absorption length in perspex is $\geq$ 120 cm [31] and the loss of light in the 70 cm long strips chosen was unimportant.

3.7 The shower counters - manufacture

The technique of bending the ½" thick perspex strips was developed at Imperial College by R.F. Hobbs and D.J. Scholes.

As total internal reflection is the chief mechanism that confines the light in its guide, it was essential that the bending process should not degrade the polished surfaces of the perspex. To avoid 'blistering' of the perspex, careful temperature control was found to be necessary.

The strips were heated to 146°C in an oven. After an hour at this temperature, the pliable strips were twisted to the required shape and held in a jig, which was at the same temperature. Care had to be taken to avoid contact between the hot strips which readily coalesced. The strips were allowed to cool whilst secured in the jig and, when cold, were machined to ensure uniform surfaces at both the phototube and scintillator ends.

After removal from the jig, the separate strips were given their final polish. They were reassembled and bonded to a 5" diameter perspex disc at the phototube end and a length of ½" square perspex at the scintillator end. Figure 3.9 shows one of the four guides at this stage of the manufacture.

Fig. 3.9

Each strip was wrapped loosely in aluminium foil to assist the light transmission, and the guide as a whole was made light-tight. To avoid the problem of wrapping a cumbersome completed counter, the scintillator, like the light-guide, was prewrapped, and after glueing only the region near the join between the two parts needed further attention. Special housings, with mu metal shields, were designed to grip securely around the necks of the counters and ensured good optical contact between the 58 AVP phototubes and the light-guides. These housings were 7" in diameter, but the actual separation of the scintillators within the chamber banks was to be about 4". Furthermore, the steel structure supporting the hydrogen target reservoir happened to coincide with the optimum positions for the phototubes. Consequently, the light-guides of all six counters, the inner counters, S_3 and S_4 included, had to be offset by carefully predetermined amounts in order to fit them physically into the system. To accommodate these various offsets the jig was modified after the manufacture of each light-guide.

3.8 The shower counters - performance

The uniformity tests used the first shower counter to be made, MIA, which, unfortunately, was later found to have a defective junction in addition to badly crazed scintillator, and consequently it gave sub-optimal results. Even so, the response, determined from radio-active source measurements, was found to be uniform within $\pm$ 20%. A similar uniformity had been found, by another group,[31] for counters using $\frac{1}{4}$" strips and 2" photo-multipliers. With $\frac{1}{2}$" strips and 5" tubes, the response of the shower counters could only be better. The faulty scintillator in MIA was replaced, and all four counters were tested in the beam. With the use of a thin layer of Silicon grease to improve the optical contact at the light-guide phototube junction, the spread in pulse heights produced by beam particles, incident normally at the centre of each counter, was found to be $\sim$ 45%.

Absorption losses in the scintillator would not be important. As the neutrons collected would have relatively small transverse momenta, the e^+e^- pairs from ϕ decay and the beam axis would be almost coplanar. From Fig. 3.6c, the summed path lengths, $l_1 + l_2$, of direct scintillation light is independent of the decay plane. Non-uniformities would tend to cancel on the two sides and, as the absorption length of scintillation light in NE 102A is ~ 90 cm,[31] any residual effect would be small.

To use the Monte Carlo results shown in Fig. 3.7, it was essential that the tubes should respond linearly to multiple tracks. A particle, incident at 60^{o} is equivalent to two particles that are normal to the scintillator, as such a particle has twice the normal path length. Tests of the four counters in the beam showed no departure from linearity for twice minimum ionisation. It was intended that the mean pulse height, from single, normal, minimum ionising particles should be less than 1/5 of the tube saturation level, and then the counters could be assumed sufficiently linear up to ~ 5 min I. (Later evidence showed some non-linearity; see section 4.6).

Early tests showed long term drifts in the mean pulse height. These were attributed partly to changes in temperature. A monitor of the gains of the shower counters, using their response to single minimum ionising particles, would need to be incorporated into the data runs. Non-resonant $2\pi n$ events were thought to be suitable candidates for this calibration.

Although changes of a few per cent in the gain and therefore in the effective bias level, would alter the trigger rate appreciably, it may be seen from Fig. 3.7 that the estimated loss of electron pair events, using a cut-off of 7 min I., would not be affected significantly. Therefore, provided the gains of the individual counters could be held constant within about 5%, then the shower counters would serve their purpose adequately.

CHAPTER 4

THE SYSTEM, OPERATING CONDITIONS AND DATA TAKING

4.1 Introduction

In this chapter the integrated system is described first and then the conditions under which it was run. In addition an account of the procedures necessary to ensure the stability of these operating conditions in obtaining the data is given.

4.2 The experimental arrangement near the hydrogen target

The counters, spark chambers and lead plates were installed as indicated in Figs. 3.5 and 3.8. Mirrors were used to combine the stereo views of both sets of spark chambers, which were recorded on film using a single camera,[32] as is outlined in Fig. 4.1. The optical path length, 10 metres, was made the same in all four views so that each would suffer the same demagnification onto the film, and also each image would be in focus. The film used throughout was unperforated 35 mm 4-X. This film is more sensitive than 3-X and permitted a smaller lens aperture, f/11, which improved the depth of focus over that realised in the ω experiment.

The mirror system used in the ϕ decay

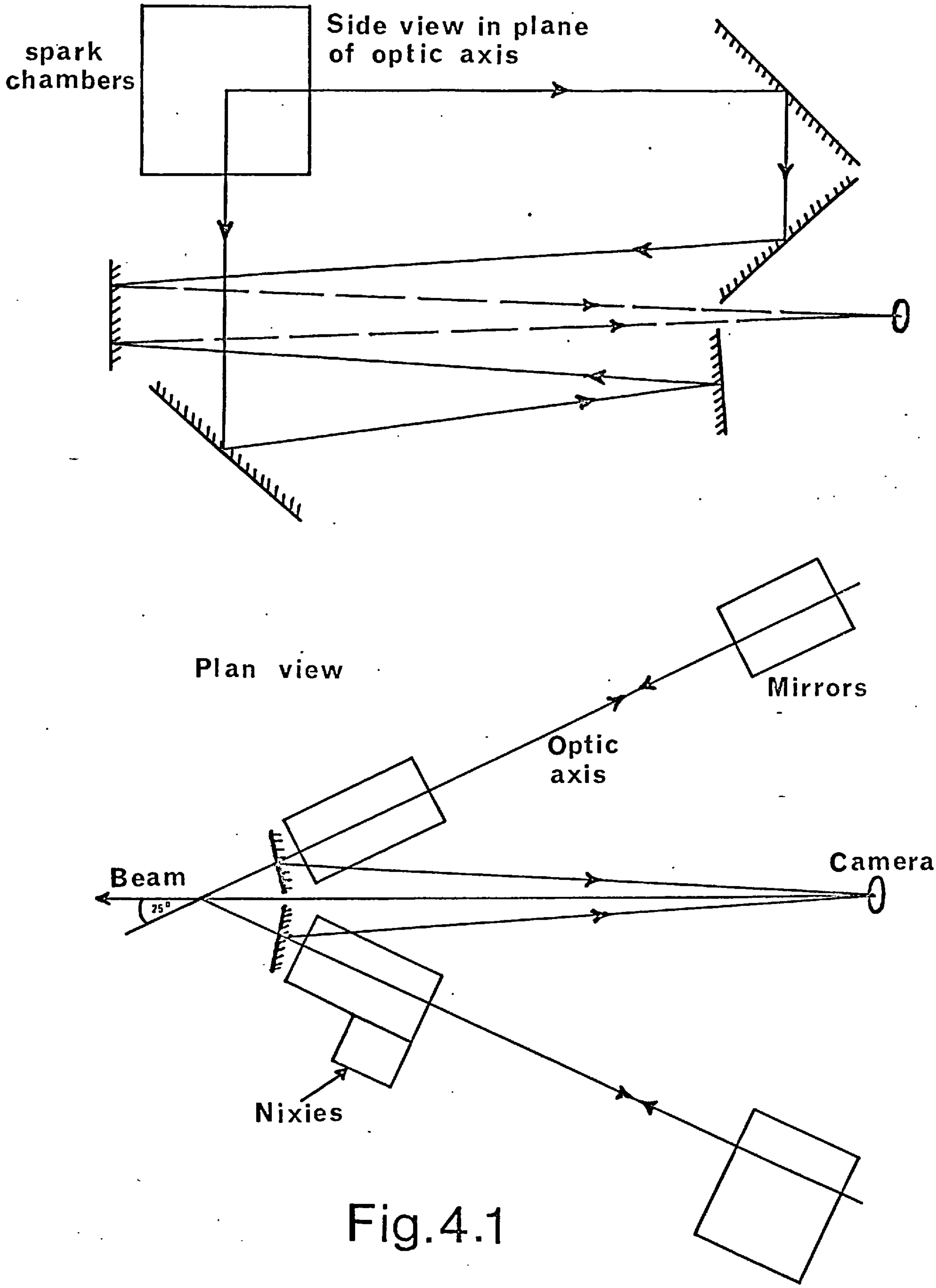

Fig.4.1

Each mirror, of front silvered plate glass, was lightly clamped to an aluminium support, and care was taken to avoid bowing of the glass which would have resulted in image distortion. The aluminium was mounted on a 3-point ball joint suspension to facilitate easy adjustments of a few degrees. The required positions and inclinations of the mirrors had been predetermined, and only small final changes proved necessary.

Nixie tubes mounted along side one of the chamber banks gave a digital display of information relevant to each trigger. This information was photographed along with the tracks in the spark chambers and comprised:

1) Event number.
2) τ_n - a number that bore a known linear relation to the neutron time of flight.
3) WP_π - the momentum channel number relevant to the trigger.
4) W.N.C. - a number from 1 to 6 indicating which neutron counter had fired.
5) M.P.H. - a number that had a known linear dependence on the combined pulse height of the four shower counters.

In each view a series of small cross marks, the spatial positions of which were known to within 1 mm, were illuminated by flash lamps and photographed together with the sparks at each trigger. The relative positions of the tracks could be measured with respect to these fiducial marks to allow later reconstruction of the events by computer.

4.3 The Logic

The master trigger was the final product of a large, complicated system of fast logic. Where possible, Rutherford Laboratory logic units were used, and standard techniques [4] were employed to ensure correct relative times of arrival, to within ~ 1 nanosecond, of the various pulses at all stages of the logic. Care was taken to minimise dead-time and casual veto losses by using short, typically ~ 10 nanoseconds, pulses, particularly where high rates were encountered. The resolving times of the coincident units that involved high rates were also minimised to reduce spurious casual triggers. Fan units and scalers at major stages in the logic facilitated access to information at each point without disturbing the running of the system. Many features, additional to the basic experiment, were built into the system including a complete monitor of ϕ meson production using the K^+K^- decay mode as in the ϕ search experiment.

The block diagram, Fig. 4.2, illustrates the basic features of the logic. Pulses from the hodoscope counters, G_{1-6}, H_{2-5}, determined the momentum of each beam particle (section 2.4). The hodoscope signal was combined with that from S_2, the principal beam counter, at the coincidence unit $CO_{\pi\ i}$. A beam particle destined to miss the useful volume of liquid hydrogen produced a signal in the veto counter A_7, which was then used in logical anticoincidence. Thus the logic, $S_2 P_{\pi\ i} \bar{A}_7$ defined a useful beam particle of known momentum.

An 'OR' unit combined the four (or three) $CO_{\pi\ i}$ signals to form $\Sigma\pi$, i.e. the useful beam in all the momentum channels used. At this point the signal from A_{10}, the veto counter just dowhstream of the target, was added in anti-coincidence. The logic thus formed, $\Sigma\pi \cdot \bar{A}_{10}$, was therefore a signature of a beam particle interaction.

The neutron (or gamma ray) signature, $N_c N_d \bar{A}_{1-6}$, or CO1

Basic Selection Logic Fig.4.2

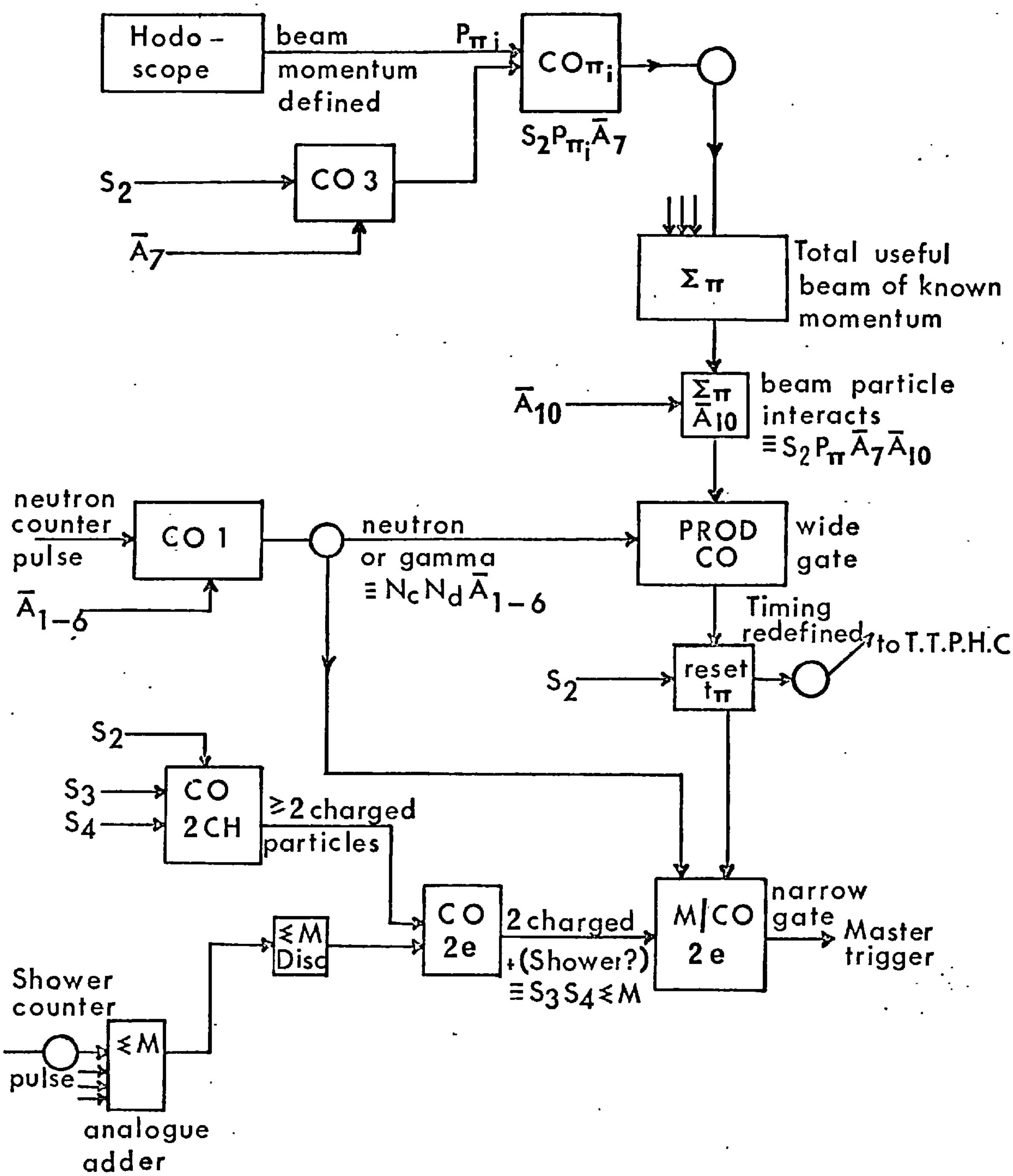

was combined with the beam signal at the 'prod CO' unit. The accurate timing signal from S_2 was reintroduced at the next unit, 'reset t_π ', to restore the timing of the system. The logic at this stage implied that a useful beam particle had interacted in the target and a neutron (or gamma) from this reaction had been detected. Up to this point, the main theme of the logic was common to both ϕ search and decay experiments, which, in principle differed only in the secondary selection of the K^+K^- and e^+e^- pairs.

The electron selection logic is sketched in more detail in Fig. 4.3. 'CO 2CH' detected coincident pulses from the inner counters, S_3 and S_4, (S_2 was included to define the timing). Each pulse from the shower counters was attenuated so that the respective fan units did not saturate for less than 8 minimum ionising particles. After further attenuation, four pulses were combined using an 'analogue adder' which in turn supplied its own fan unit 'Σ M'. One output of this fan was directed to the Fast Linear Gate (FLG), the purpose of which was to integrate the charge in the combined pulse over a period of 50 nanoseconds at each master trigger. The output of the FLG, which was suitable for digitisation,

Fig. 4.3 The Electron Selection Logic

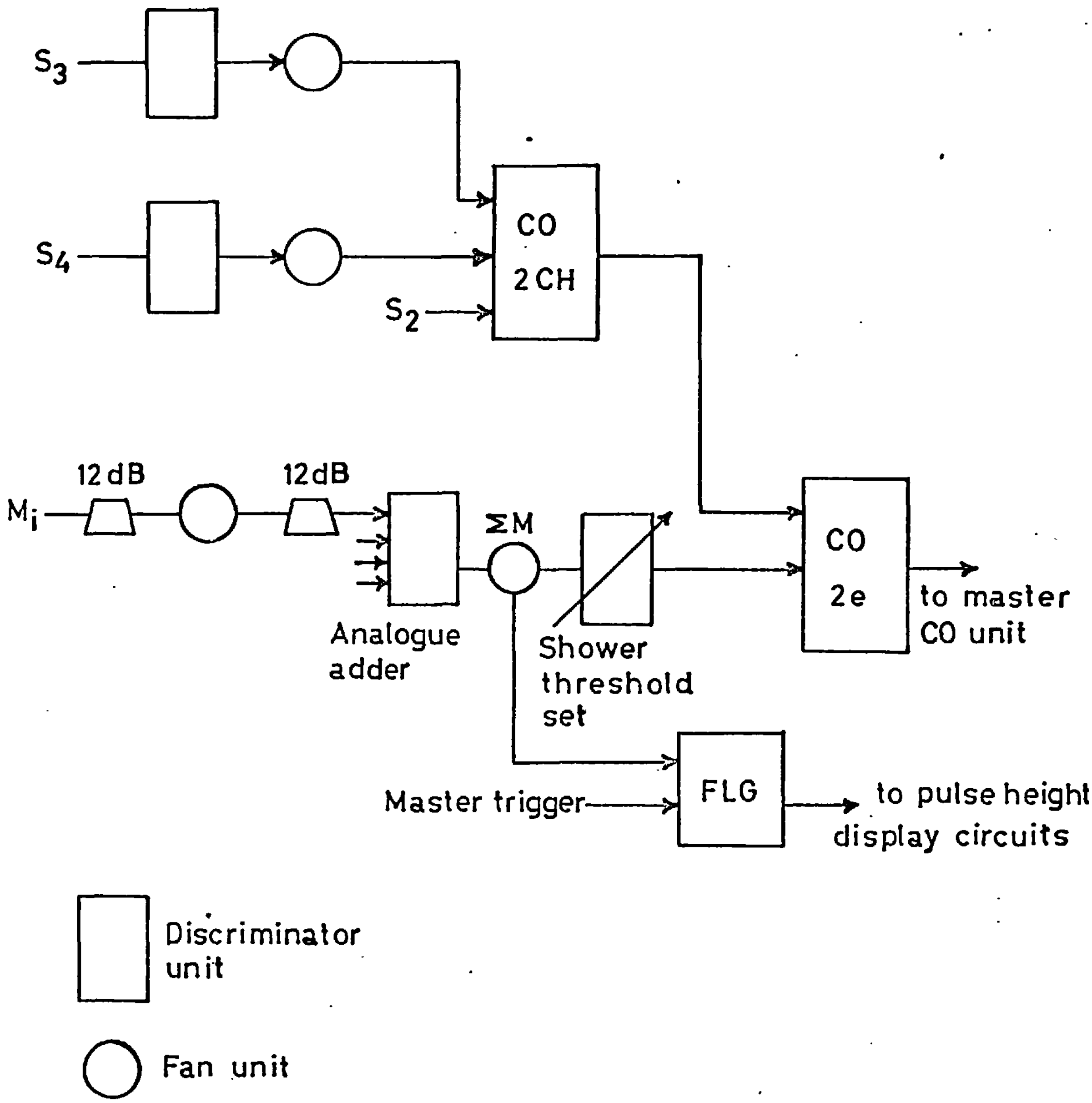

supplied the shower counter pulse height display circuits. A further output of the ΣM fan fed the all-important ΣM discriminator. The bias level of this unit, which was adjusted to reject a large fraction of background events, is discussed in section 3.5. 'CO2e', combined the outputs of 'CO 2CH' and the ΣM discriminator, and signalled that there had been charged particles in each set of spark chambers together with some evidence of a secondary interaction.

Finally, the outputs CO 2e, CO1 and 'reset t_π' were interrogated at the coincidence unit M/CO2e, at which the time of flight gate was formed. This gate restricted the accepted neutron velocities to a region which, in the signal runs, corresponded to a missing mass range centred on the ϕ mass with a full width at half height of ~ 15 MeV/c^2. The gate settings are discussed in section 4.5.

Hence only when all conditions were satisfied, (i.e. useful beam particle interaction, neutron within the required velocity range, one or more charged particles on each side with some evidence of a secondary multiple process) was a master trigger produced. To avoid an unreliable dead time correction at each master trigger the fast electronics was inhibited for 40 msec, the dead time of the camera, while the slow logic took control. During this time the spark chambers were fired, the tracks were photographed and the camera was prepared for the next frame.

To sweep away icnisation caused by the passage of earlier particles, a clearing field of 40 V was maintained between adjacent plates of the spark chambers. The chambers were sensitive for only ~ 1 μsec. and it was important to activate the chambers very shortly after the passage of the trigger particles. The delay through the logic was minimised by careful design and also the master and slave spark gaps, which drove the chambers, were adjusted to breakdown rapidly. The total delay time from the passage of the trigger particles to the firing of the chambers was about 700 nsec. Tests had shown that this delay, combined with a clearing field of 40 V, did not impair the chamber efficiency significantly.

4.4 Choice of beam momentum

Ideally, the branching ratio, $\phi \longrightarrow e^+ + e^- / \phi \longrightarrow$ total, would be determined from a comparison of yield curves for the e^+e^- and K^+K^- decay modes. However, because of the low value anticipated for this ratio it was only practicable to measure the yield at two points, one below threshold and the other where the $\phi \longrightarrow e^+ + e^-$ yield would be optimum. The difference between the yields of electron pair events at these two momenta, suitably normalized to the same number of effective pions would indicate the presence or otherwise of the decay $\phi \longrightarrow e^+ + e^-$ and purely from this point of view the exact operating momenta would not be critical. However, in order to quote a branching ratio the yield of ϕ mesons must be known and as this was a more sensitive function of momentum and also, as it was intended that further $\phi \longrightarrow K^+K^-$ data would be taken concurrently, the individual momentum channels were used.

Of all beam-line elements, BM2 was the most critical as the field of this magnet was used in determining the beam momentum. Due to hysteresis, its field was set, not from measurement of the current but by reference to a nuclear magnetic resonance frequency. The correspondence between frequency and momentum was known from the ϕ search and floating wire measurements. As hysteresis effects in the other beam-line elements were small, the currents were set to the values used in the ϕ search runs at the relevant momenta.

In deciding the actual operating conditions there were a number of general considerations. In the final selection of events, resulting from the application of all the shower and kinematic criteria, there would remain some events, arising from background processes, which would be indistinguishable from any genuine examples of $\phi \longrightarrow e^+ + e^-$. The number of these ultimate background events, which would be roughly proportional to the total of the photographs taken, could not be estimated with any certainty and it was not known whether any examples of $\phi \longrightarrow e^+ + e^-$ would eventually appear significant in the presence of these background events. The expected yield of $\phi \longrightarrow e^+ + e^-$ events per photograph needed to be optimised. This condition is reached for each parameter when the detection efficiency for $\phi \longrightarrow e^+ + e^-$ is maximum. However, to use a very small range around the maximum has two serious consequences. Not only would there be a substantial loss of potential $\phi \longrightarrow e^+ + e^-$ candidates, but also in many cases the loss would be difficult to estimate. In general, therefore, the various limits applied were such that losses were of only a few per cent and as only ~ 20 final events were anticipated, accurate estimation of these losses was unnecessary.

The detection efficiency for neutrons associated with ϕ mesons, determined from Monte Carlo computations, is shown as a function of momentum in Fig. 4.4. The fraction of e^+e^- decays, from these ϕ's, accepted by the chambers was independent of momentum in the range 1520 to 1600 MeV/c. For the signal runs, bearing in mind the need for data rich in $\phi \longrightarrow e^+ + e^-$, only 3 momentum channels were used at 1574, 1582 and 1590 MeV/c, ($P_{\pi 5}$, $P_{\pi 6}$ and $P_{\pi 7}$, respectively).

To enable direct comparison of the events in the runs above and below threshold, the classes of background processes which initiate the triggers in both cases should be the same. The central momentum channels for the two therefore were not separated more than necessary. Just below the ϕ threshold was the most suitable operating point. A fourth momentum channel, $P_{\pi 4}$, was included to increase the rate of data accumulation. The momenta used were 1526, 1534, 1542 and 1550 MeV/c. Only negligible numbers of ϕ's could be produced by pions near the upper limit of this range.

Fig. 4.4 The collection efficiency of the neutron counters as a function of momentum determined from Monte Carlo computations

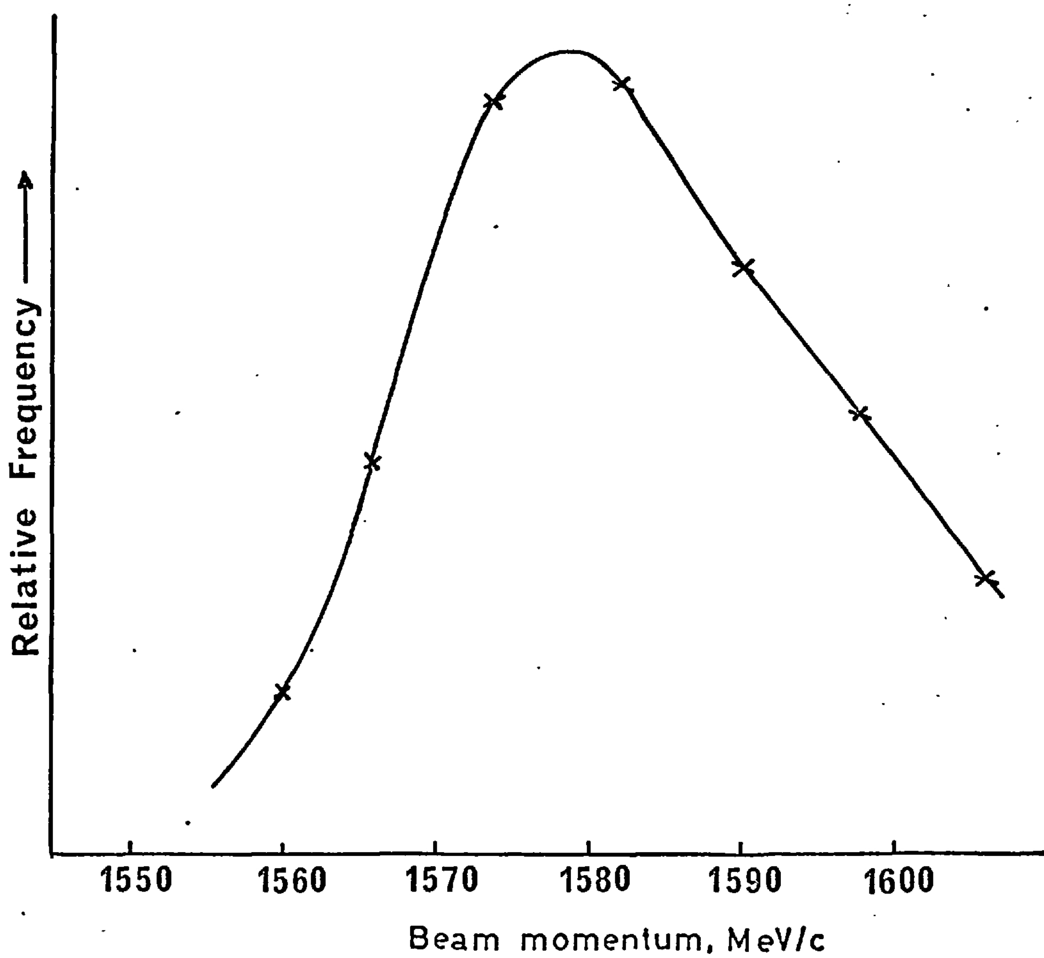

4.5 The neutron counters and time of flight gates

The neutron counters and associated logic were operated under identical conditions, both electrical and geometrical, to the ϕ search. Relative to other errors, differences introduced by small changes in (say) the N_d discriminator bias level or photomultiplier gain were negligible; consequently the efficiency for detection of ϕ associated neutrons was the same in both search and decay experiments.

The neutron time of flight was determined from the delay between pulses from S_2 and CO1 relative to the delay produced by $\beta = 1$ particles. These small time differences between the pulses were typically ~ 10 ns, and initially were converted to a pulse height using a Time to Pulse Height Converter (TTPHC). The analogue pulses produced were kicksorted using a Laben 512 channel pulse height analyser. In this way a nanosecond was represented as 2.57 kicksorter channels. The kicksorter played no essential role in the ϕ decay proper, but was an invaluable tool in checking the functioning of many aspects of the system. The linearity and reliability of both kicksorter and TTPHC had been demonstrated in earlier experiments [4,33] and only occasional detailed calibrations were necessary. Simple checks which would quickly indicate a serious malfunction were more frequent.

The timing response of the neutron counters, the beam counter S_2, and the associated logic was checked at the end of every five films ($\sim$20 hours) using the 'fast peak'. Essentially, the fast peak was the time of flight distribution of beam particles scattered into the neutron counters. Counters A_{1-6} were used in coincidence to select charged particles. As this peak was almost entirely due to particles of $\beta = 1$, its width at half height of $\sim$ 2 nsec gave a measure of the timing resolution. Any significant change in either the width or position of this peak indicated a fault.

The uniformity of the TTPHC and associated logic over all times of flight considered was tested, also after every five films, using a 'white spectrum' - the distribution of time differences between random S_2 pulses and pulses from a 20 Mc/s oscillator. Within statistics this distribution should be flat in the region considered.

Similarly, using the white spectrum technique, the widths and positions of the ϕ and K 'gates' were checked. These gates determined the range of neutron velocities accepted at the master coincidence unit. Fig. 4.5 shows the neutron time of flight distribution of accepted Monte Carlo-generated $\phi \longrightarrow e^+ + e^-$ events. Few events are found outside the range 19.8-25.0 ns and therefore, for the signal runs, the gate was intended to eliminate potential triggers outside this region. The actual gate edges used corresponded to 19.2 and 25.0 ns and only times of flight between these limits were considered.

No similar stipulations were necessary in the background runs. Although using an identical gate would simplify the normalisation between the ϕ and K runs, to increase the rate of data accumulation, the background gate was widened to include times of flight from 17.3 to 26.3 ns.

4.6 Setting of the shower counter bias

The gains of the four shower counters were matched in situ using interaction products from the target selected by the full logic requirement with the exception of the shower counter demands. These products were assumed to consist predominantly of fast pions from $2\pi n$ events.

Fig.4.5
Monte Carlo time of flight distribution

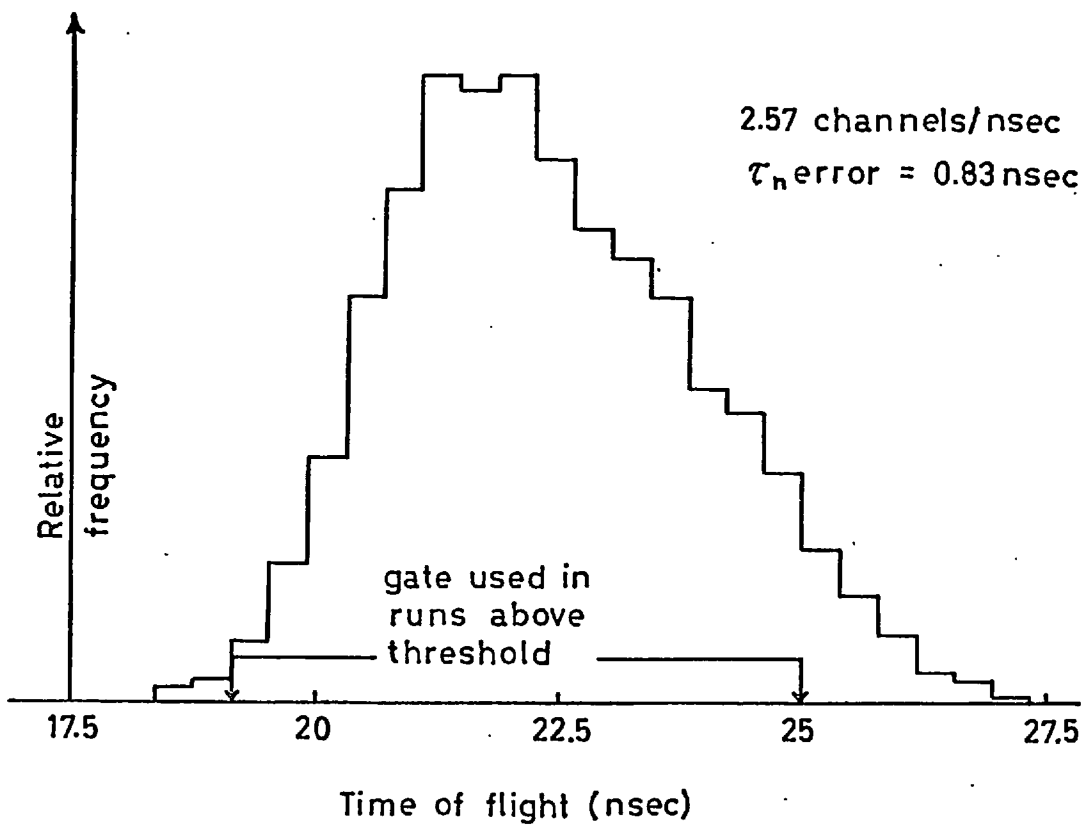

After every five films, the performance of each counter was checked by kicksorting its output via the fast linear gate, as described in section 4.3. This test would have shown any significant change in either gain or spread. In practice no deterioration in spread was recorded and the gains remained constant within 5%. Changes of this order had $\sim$ 15% effect on the trigger rate but the alteration in loss of $\phi \longrightarrow e^+ + e^-$ events was estimated to be negligible.

The threshold of the Σ M discriminator was set by reference to the Σ M pulse height spectrum, indicated in Fig. 4.6. The pedestal, at O, corresponds to no pulse from the shower counters, and the peak, P, attributed mainly to single minimum ionising particles crossing each counter, was assumed erroneously to be equivalent to 4 min I. units. (The subsiduary peak, R, is due to events in which the particles miss some of the four counters). A similar spectrum (dotted line) is taken with a threshold requirement on the total pulse height from the four counters. Since both the electronics and shower counters are linear in the range used for this calibration, the number of channels from O to Q, where Q is the half-height as shown, gives a measure

Fig.4.6 Setting the shower counter threshold

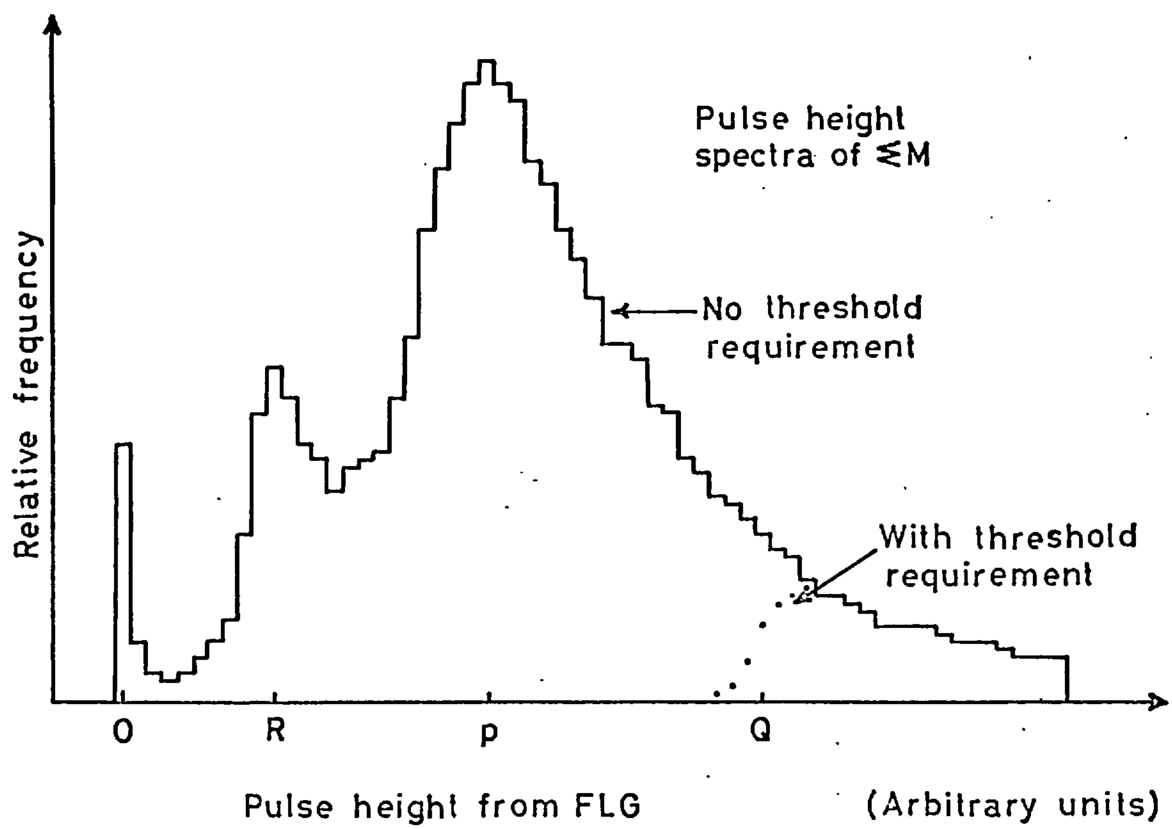

of the pulse height threshold relative to OP. Thus to set a threshold of (say) 7 min I., the ΣM discriminator is adjusted until the ratio OQ/OP = 1.75.

For the first 50 films the bias had been estimated to correspond to 6.8 min I. units, but was increased in later films to 7.7 to reduce the number of frames per unit beam. The loss of electrons assuming the counters to be linear was estimated to be less than 7% at either bias.

The Monte Carlo generated pulse height spectrum for $2\pi n$ events (Fig. 3.7) indicated that a mean value of 4.5 min I. should have been used above instead of only 4 min I., but it was found later (section 6.4) that few $2\pi n$ events were present. The particles which produced the ΣM spectra were estimated to be from multi-pion events and, due to the more varied angles of incidence to the counters, OP was equivalent to greater than 4.5 min I. A better approximation to the true value for OP in min I. units was found using the mean pulse height expected from the two charged pions of $3\pi n$ events. OP was estimated to be equivalent to 4.6 ± 0.15 min I. units which inferred that the two thresholds used were 7.8 and 8.8 min I. The error of about 5% in the estimation of these biases arises from both the uncertainty in the value of OP and the drifts in the gains of the counters.

Due to non-linearity of the phototubes the loss of electrons was greater than estimated previously. Departures from linearity were shown to be negligible below 3 min I. and $\sim 10\%$ at 4 min I. To revise the estimated loss incurred by the ΣM threshold, we considered the curves in Fig. 4.7 which were generated by the Monte Carlo program and show the percentage loss of $\phi \longrightarrow e^+ + e^-$ events as a function of bias. For the dashed curve, the maximum pulse height from each shower counter was limited to 4 min I. The continuous curve, which had no limit imposed on the individual counter outputs, was obtained by integration of the Monte Carlo pulse height distribution (Fig. 3.7) for $\phi \longrightarrow e^+ + e^-$ events. The true losses were estimated to be between the two curves in Fig. 4.7, and were found to be $(9 \pm 3.5)\%$ at 7.8 min I. and $(15.5 \pm 5.5)\%$ at 8.8 min I. The errors include the uncertainty in the bias settings.

4.7 Spark chambers and photography

One of the more significant factors contributing to the efficiency of the spark chambers was known from experience

Fig.4.7 The loss of $\phi \rightarrow e^+ + e^-$ events in the electronic selection as a function of ΣM bias.

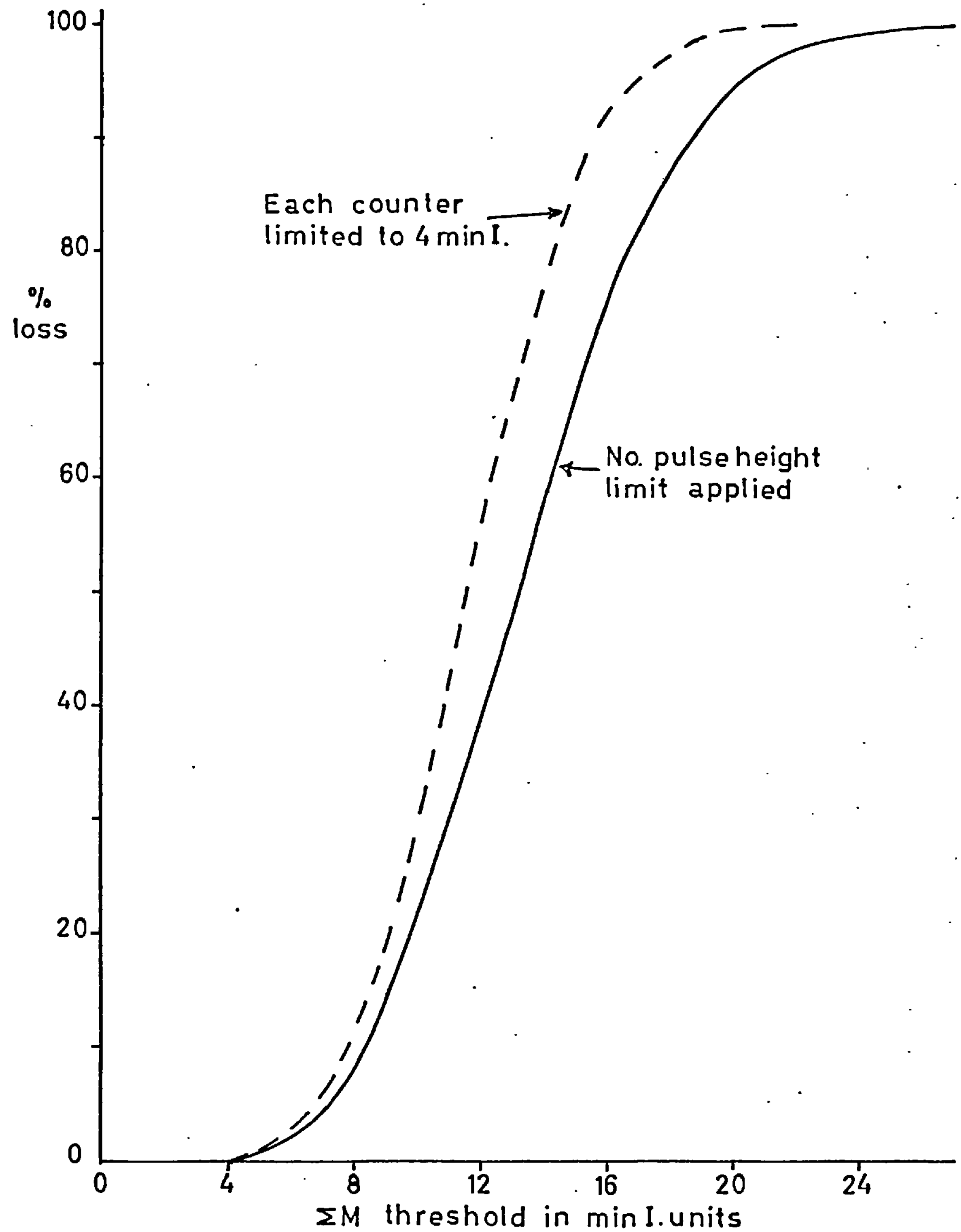

to be the purity of the gas mixture. To remove residual air, the flow of the Helium-Neon mixture through the chambers was started ~ 48 hours before filming. Entry of further impurities into the chamber volume was prevented by maintaining small excess pressure, ~ 1 cm of oil, in the chambers throughout the run. A rough indication of the degree of purity, was available from the colour of the sparks which, in pure HeNe, appear orange-pink but become more blue with increasing contamination. Other factors contributing to the efficiency, such as the clearing field and master gap speed, were checked periodically.

At the end of each film, the last three feet or so were developed locally and examined. From these samples of the films, the test strips, the proper functioning of many parts of the apparatus were checked. Such items included: the camera, the various Nixie data displays, the flash lamps, the spark chambers, the master gap and, to some extent, the logic. Faults in both the pneumatic camera and the H.T. circuits could often be detected readily by an audible change in the operation of the camera or in the breakdown of the master gap or spark chambers.

4.8 General running - data taking

Assuming a Branching Ratio of ~ 1 in 10^3 and using estimates of the beam intensity, the full logic trigger rate, the detection efficiency for e^+e^- and the ϕ yield, about 20 examples of $\phi \longrightarrow e^+ + e^-$ would be recorded in $\sim$100,000 photographs. A similar number of frames would be necessary below threshold and the total filming time was estimated to take about 80% of the 16 days available. Only 20% of the time would be left to accommodate inefficiencies and it was necessary, therefore, to streamline the data taking.

To minimise loss of time, of the numerous performance checks necessary, only those that could not be carried out sensibly while actually taking data were done between films. While the camera was being unloaded and reloaded with new film, the readings of all the scalars, which recorded the total counts in key parts of the logic, were noted. The apparatus was then run for 10^7 beam particles and the scaler readings were compared with standard values. This quick check would show a serious fault in the logic or in the newly loaded camera which was run under observation during this time. If no fault was immediately obvious, the scalers were reset and the film proper was started. This procedure took about 5 minutes, which, compared to the 3-4 hours needed to complete a film, was small.

After the start of the film, many other items were checked: the Nixies displaying sensible numbers - both flash lamps, used to illuminate the fiducial marks, working - tracks in the spark chambers - etc. The developed test strip and the counting rates from the previous film were examined. These rates had good statistics and presented a valid check on the stability of the system.

In addition to the above, at the end of every 5 films ($\sim$18,000 photographs) the shower counter performance, and the time of flight response and gate positions were checked. These more complete checks usually took 2-3 hours.

The 200,000 photographs were expected to fill approximately 70 reels of film, 35 above and 35 below threshold. Runs above and below threshold, or 'signal' and 'background' were ascribed the code letters 'ϕ' and 'K' respectively. In principle, all 35 ϕ films could have been taken followed by the 35 K films, but ideally, ϕ and K films should have been alternated to balance the effects of any long term drifts in the eventual comparison of the two. Furthermore, had there been a major breakdown of either Nimrod or our experiment after (say) 20 films, then with equal quantities of ϕ and K in hand, it might have been possible to extract a lower limit for the Branching Ratio, whereas with 20 ϕ films only, the problem of background subtraction would have become extremely difficult. However, as the change from ϕ to K, or vice versa was very time consuming - the beam momentum had to be altered in addition to resetting and checking the time of flight gate - alternation of ϕ and K films was impracticable. To compromise, ϕ and K films were alternated in batches of ten or fifteen.

At intervals of about 20,000 frames, 2000 events, in which there was no shower requirement in the trigger, were photographed. It was intended that these events which, at the time, were assumed to arise largely from non-resonant $2\pi n$, would be used to test the reconstruction and fitting programs.

In all about 235,000 frames were taken and subjected to further analysis.

CHAPTER 5

THE CRITERIA AND THEIR APPLICATION

5.1 Introduction

The anticipated branching ratio, $\phi \longrightarrow e^+ + e^- / \phi \longrightarrow$ total, was $\sim 10^{-3}$ and a rough calculation showed that, unless this estimate was very low, there would be only about 20 examples of $\phi \longrightarrow e^+ + e^-$ in the 220,000 photographs taken during the data run. The problem, therefore, was to reject the non-electron pair events, in the most efficient way, until the numbers were at a level where the $\phi \longrightarrow e^+ + e^-$ events, if they existed, would appear significant.

It was intended to reduce the data in several stages. First of all there would be a scan of all the events using very weak criteria that would eliminate obvious non-candidates. The resulting few thousand frames would then be subjected to more rigid criteria and the accepted events would be measured and kinematically fitted. The nature and number of the candidates that would survive the applications of both the kinematic and shower requirements were uncertain, and further steps would be developed if they proved necessary.

It was important that the criteria should be objective and effective in their role of background reduction without incurring a significant loss of electron pairs. The cost to genuine events was deduced by applying the same criteria to photographs of electron showers.

5.2 The calibration electron experiment and comparison with the ϕ decay

An experiment was performed, in June 1965 prior to the ϕ search, to examine showers produced by 300, 450, 500, and 650 MeV/c electrons. The momentum distribution of electrons from ϕ decay ranged from 400 to 900 MeV/c. The apparatus used is sketched in Fig. 5.1a. A threshold gas Cerenkov counter, in coincidence with the scintillation counters, S_1, S_2, was used to select electrons in a beam comprising 78% π, 10% μ and 12% e. The beam was incident on a spark chamber-lead sandwich which, with the exception of the inner and shower counters, was identical to either bank of chambers in the main experiment. Photographs of the electron showers were taken using the mirror system, outlined in Fig. 5.1b, which was similar in principle to that used in the main experiment.

Fig. 5.1 The Calibration Electron Experiment

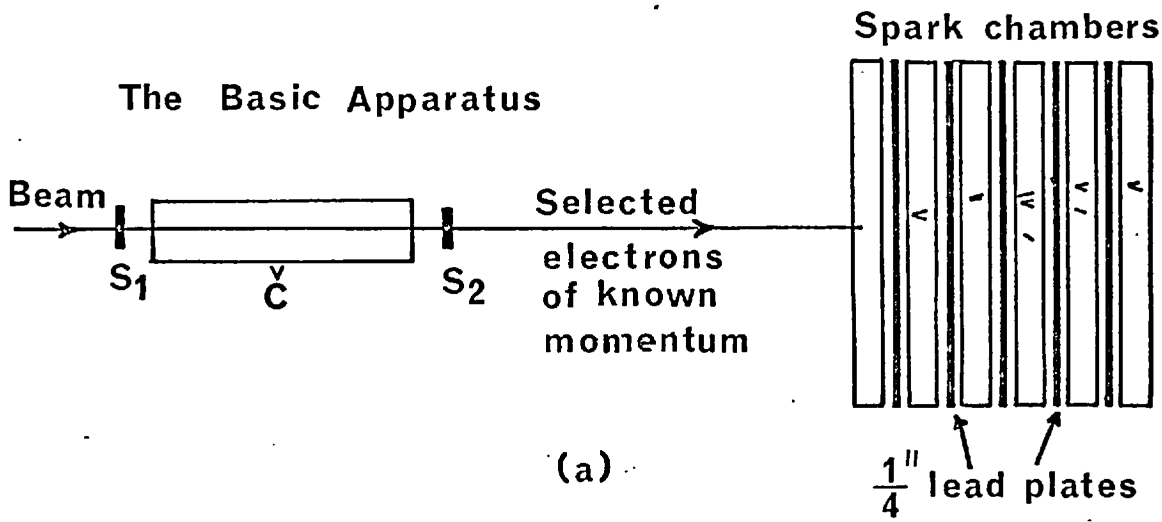

(a)

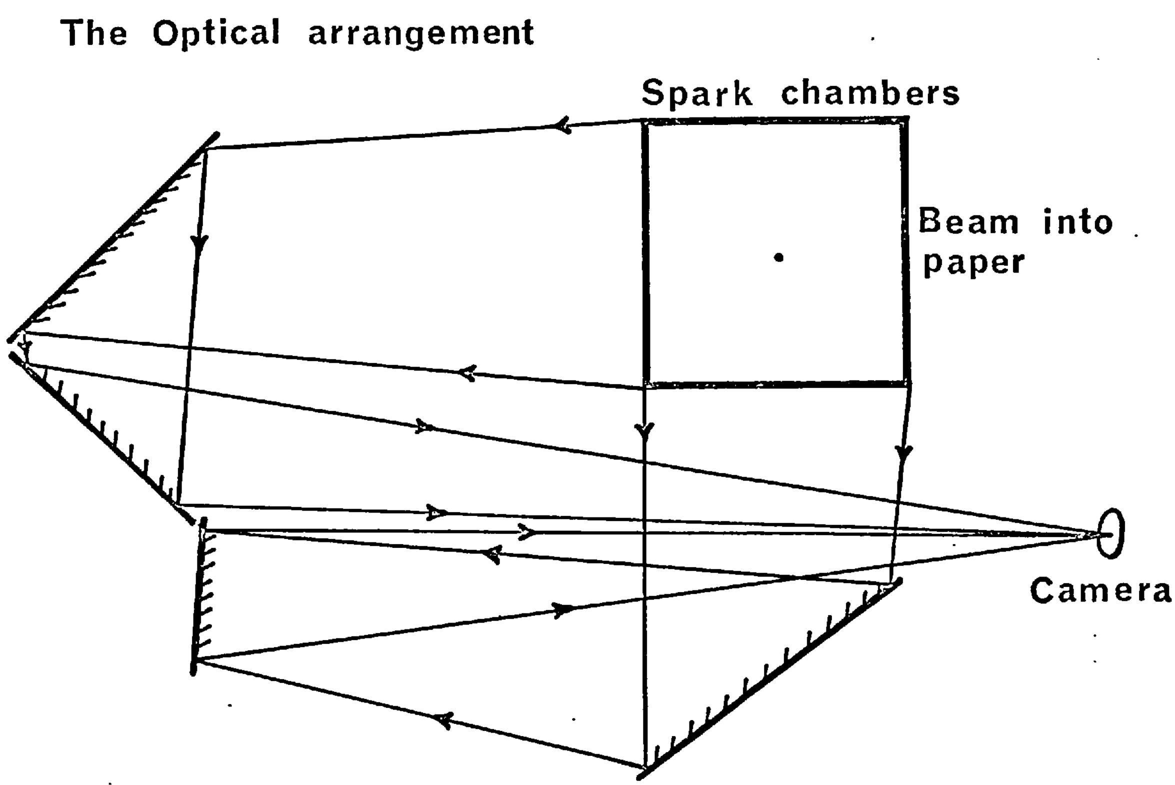

(b)

The Cerenkov counter was shown to have a high muon and pion rejection efficiency. This was born out by the infrequency of non-interacting tracks, typical of muons, and to a lesser extent of pions, on the film.

In both calibration and ϕ decay experiments the spark chamber efficiency needed to be high to allow true representation of the electron showers. The single track response of the chambers was used to test the relative efficiencies of the individual modules. Of the ϕ decay chambers, apart from one which had a persistently poor gap but was otherwise good, the individual efficiencies were almost equal and showed a mean loss of sparks of 3%. The chambers used in the calibration electron experiment were similarly uniform and had an average spark loss of 3.75%.

In electron showers, the importance lies in the representation of multiple tracks. For the different numbers of tracks supported, the relative numbers of tracks with 4, 3 and 2 sparks are shown in Fig. 5.2 for both the ϕ decay and the calibration electron chambers. The individual plots have been normalised to have the same number of tracks with four sparks from both samples. In both sets of results,

Fig.5.2 The relative efficiencies of the ϕ decay and Calibration electron chambers as a function of the number of tracks supported.

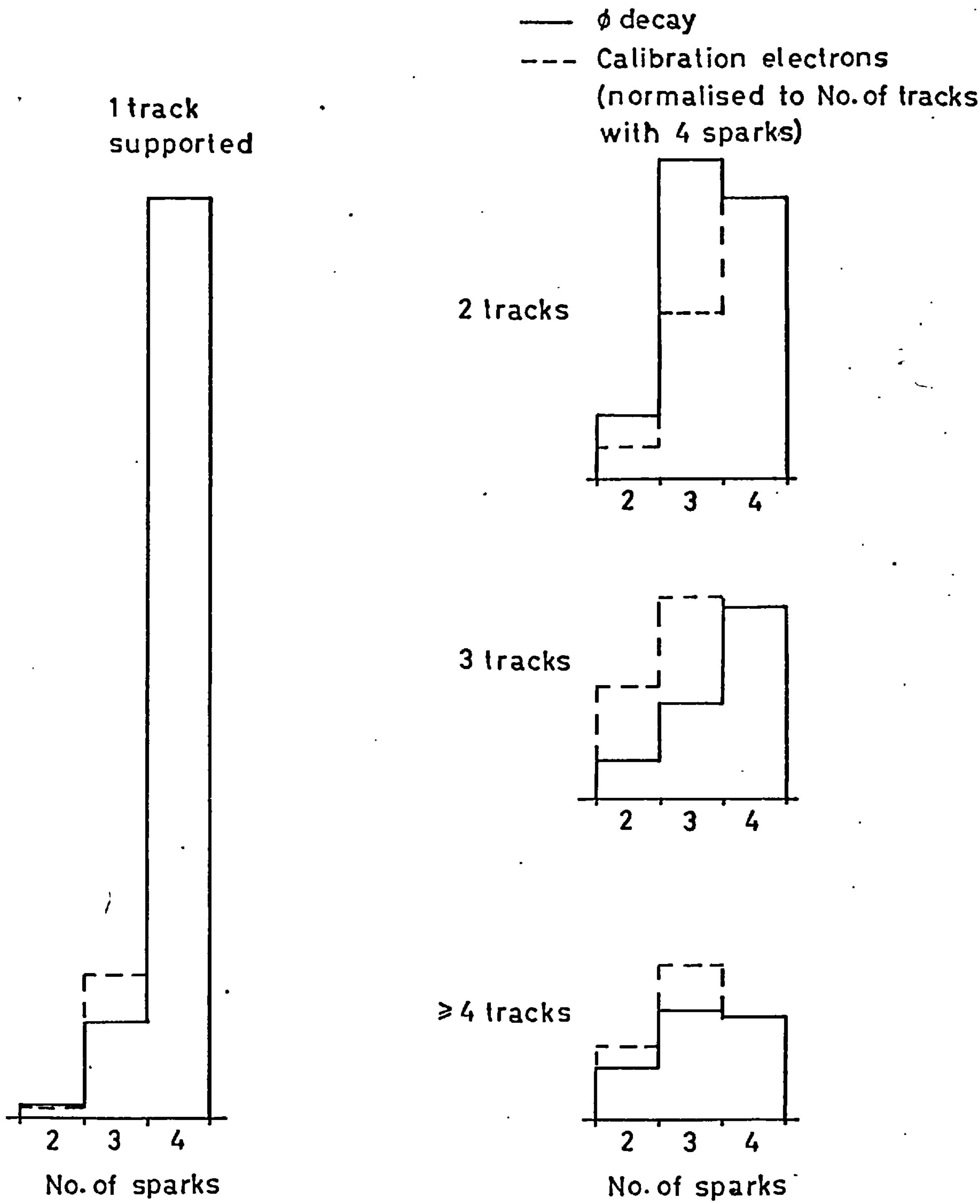

the histograms for 4, 5 and 6 supported tracks have been summed to improve statistics. In each case care had been taken to ensure that the tracks considered were correctly timed relative to the trigger pulse since chamber efficiency is a function of this time. As 2 sparks are necessary to define a track, the histograms were valid only for 2, 3 and 4 sparks, none of which constituted an actual loss of tracks. The comparative track efficiencies were estimated therefore from the proportion with 2 sparks. The percentages of tracks with only 2 sparks are summarised in Table 5.1 for the ϕ decay and the calibration electron chambers.

Table 5.1

Percentage of tracks with 2 sparks

No. of tracks supported	ϕ decay	Calibration experiment
1	1.2 ± 0.4	1 ± 1
2	10.5 ± 2.6	7 ± 2
3	13.5 ± 5	22 ± 3.5
≥ 4	21.5 ± 7	22 ± 3

The overall efficiency is seen to be better in the ϕ decay, and consequently, this response compensated qualitatively for the additional casual tracks that were present in the ø decay film. Furthermore the relatively high loss in supporting 4 or more tracks in any one chamber was not important as the loss of a whole track in the presence of several others would not alter the shower appearance significantly.

Again the appearance of the showers would differ if the mean separation of the lead plates was not equal in the two experiments. In practice, the mean distances between the plates were 5.7 cm and 5.5 cm in the ø decay and calibration electron experiments, respectively. The difference was negligible. The effective radiation length of the lead-spark chamber complex was about 5 cm. The increased effective plate separation in the ø decay due to non-normal angles of incidence was relatively unimportant as few electrons from ø decay, entering the chamber fiducial volume, would be very oblique. Therefore, apart from a 10% difference in the optical magnification, the showers on the film from the main experiment could be compared directly with the calibration electrons.

The mean number of tracks in the calibration electron showers in each chamber, determined from the 450 and 650 MeV/c data, are shown in Fig. 5.3 as a function of penetration depth in radiation lengths. The results of Heusch and Prescott[29] are shown for comparison.

The agreement is fairly good and shows that almost all particles in the showers were resolved by the spark chambers. Furthermore, the agreement justifies the use of the Heusch and Prescott data in the Monte Carlo calculations of the total pulse height distributions expected from the shower counters.

5.3 The preliminary criteria and the initial scan

The initial criteria were very loose and easy to apply. They were based largely along the lines of the criteria used in the ω experiment and were orientated towards rejecting background events quickly rather than selecting electrons.

In the ω experiment, each event was examined for 'showers' in which the total number of tracks exceeded a minimum. Due allowance was made for 'non-ionising links' in assessing the showers. Non-ionising links, the result of a photon being formed in one lead plate and converting in a subsequent plate, had been shown to be

Fig.5.3 The average number of electrons in a shower as a function of penetration depth

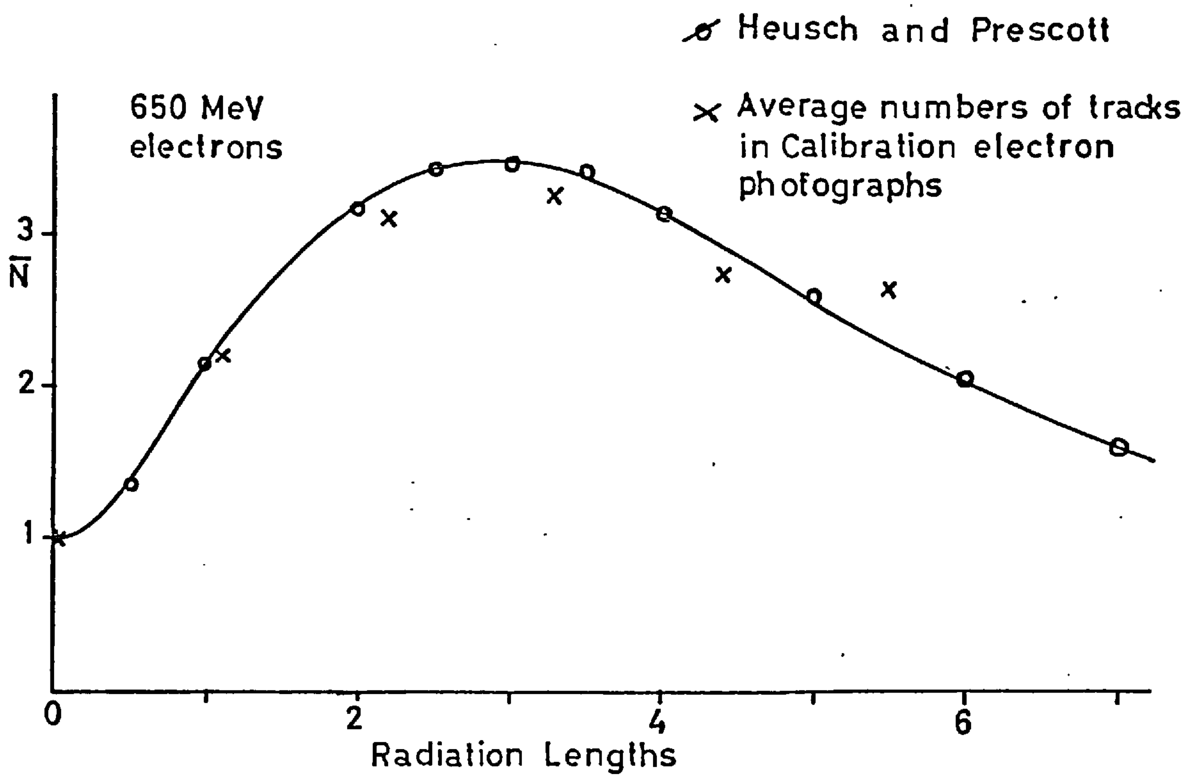

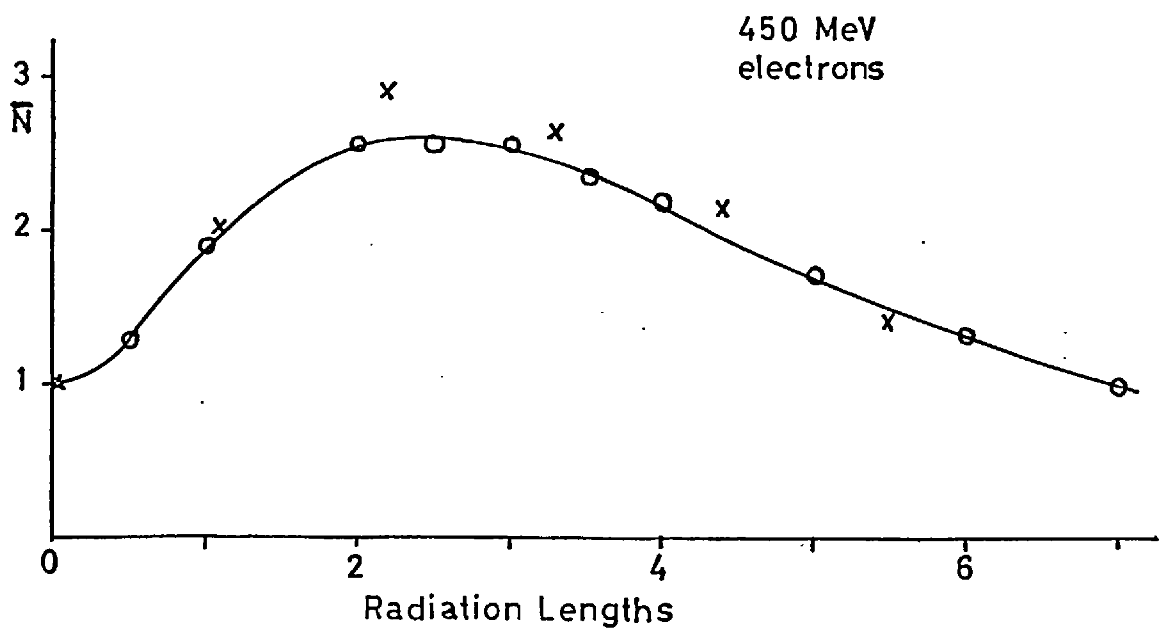

equivalent to two tracks.[1] All tracks that were considered to be part of a shower, were required to fall within a cone of half angle of 30°, where the axis of this cone was aligned along the incident track and its apex was in the first lead plate.

Due to the high beam rates used in the ϕ decay, there were many more casual tracks in the spark chambers than had been encountered in the ω experiment. To reduce the problem of casuals, a fiducial volume smaller than the ω cone, in which to define the showers, was necessary.

From the calibration electron photographs, plots were made of the lateral displacements, of the secondaries, from the incident track. In each view, the majority of each shower was found to fall within 5.4 cm (real space) of the incident track. As this restriction, compared with the ω cone, did not increase the secondary track loss significantly and also would reduce the number of events accepted due to casual tracks by an order of magnitude, the volume thus defined formed the basic fiducial volume for all the subsequent criteria.

In the ϕ decay, to assess the 'showers' a points system was devised. This system allotted one point for each interaction in which a secondary product was formed. Thus a pion with a single δ-ray scored 1 point; a non-ionising link received 2 points, since this was regarded as two interactions, one to form, and the other to convert the photon. In addition, although not of great significance in practice, scatters of $> 20^{\circ}$ scored a half point. Usually the number of points scored by a shower could readily be deduced from the various interactions; secondary tracks (e.g. δ-rays), non-ionising links and scatters. However in certain cases, the number of points was not defined uniquely as ambiguities could arise in the interpretation of the event. To resolve this uncertainty, the interpretation chosen was that which gave the minimum total of points. These ambiguities usually occurred only in complex showers and, as in such showers a knowledge of the exact numbers of points was unnecessary, misinterpretation was unimportant.

Few electrons from ϕ decay would be of less than 450 MeV. An examination of the calibration electrons of this energy showed that the proportion with less than two points was negligible. Similarly at 650 MeV, the mean electron energy that was expected from ϕ decay, the fraction with less than three points was small. Since the total energy of the two leptons would be roughly constant, a cut-off of six points for the pair would reject very few $\phi \longrightarrow e^{+} + e^{-}$ events. Thus for the events in the main experiment, to qualify as a candidate, a minimum of six points was required with not less than two from any one side. Less than 5% of the 220,000 photographs were expected to survive the application of the preliminary criteria.

The 220,000 events were scanned and subjected to the first criteria, by a number of people at Imperial College and at the Rutherford Laboratory. The loss of genuine events due to human factors is estimated later. For each event that passed the criteria, the event number and other digital data were recorded. Many events, due to the high beam rate, showed a preponderance of casual tracks and unless such events could be rejected clearly, they were recorded as candidates. Several minutes could be wasted on a complex event in attempting to correlate the mess of tracks in the stereo views, whereas the tougher criteria that were to follow in the second scan might reject the event in a matter of seconds. The number of frames wasted due to technical failures were noted to allow normalisation of the number of beam particles to the number of useful frames. This loss, of about 10%, was largely due to frames at the ends of the films that could not be projected. In all, about 4700 events survived the application of these first criteria. The first scan took about four months and during this time the reconstruction and fitting programs and second criteria were developed.

5.4 The reconstruction and fitting programs

Events are reconstructed[34] by reference to fiducial marks which, in our experiment, were crosses painted on aluminium frames in the planes ABCD and CDEF (Fig. 5.4). (For simplicity, one side only, the left, is considered below).

An optic axis was defined. This was a horizontal line that intersected the beam at 25° at a predetermined point 70 cm downstream of the target. This point, the origin, was such that the axis was the intended, effective line of sight from the camera to the centre of the chambers in the side view. The fiducials were measured with respect to a

Fig.5.4 The relative positions of the spark chamber banks in real space and projected film (table) space.

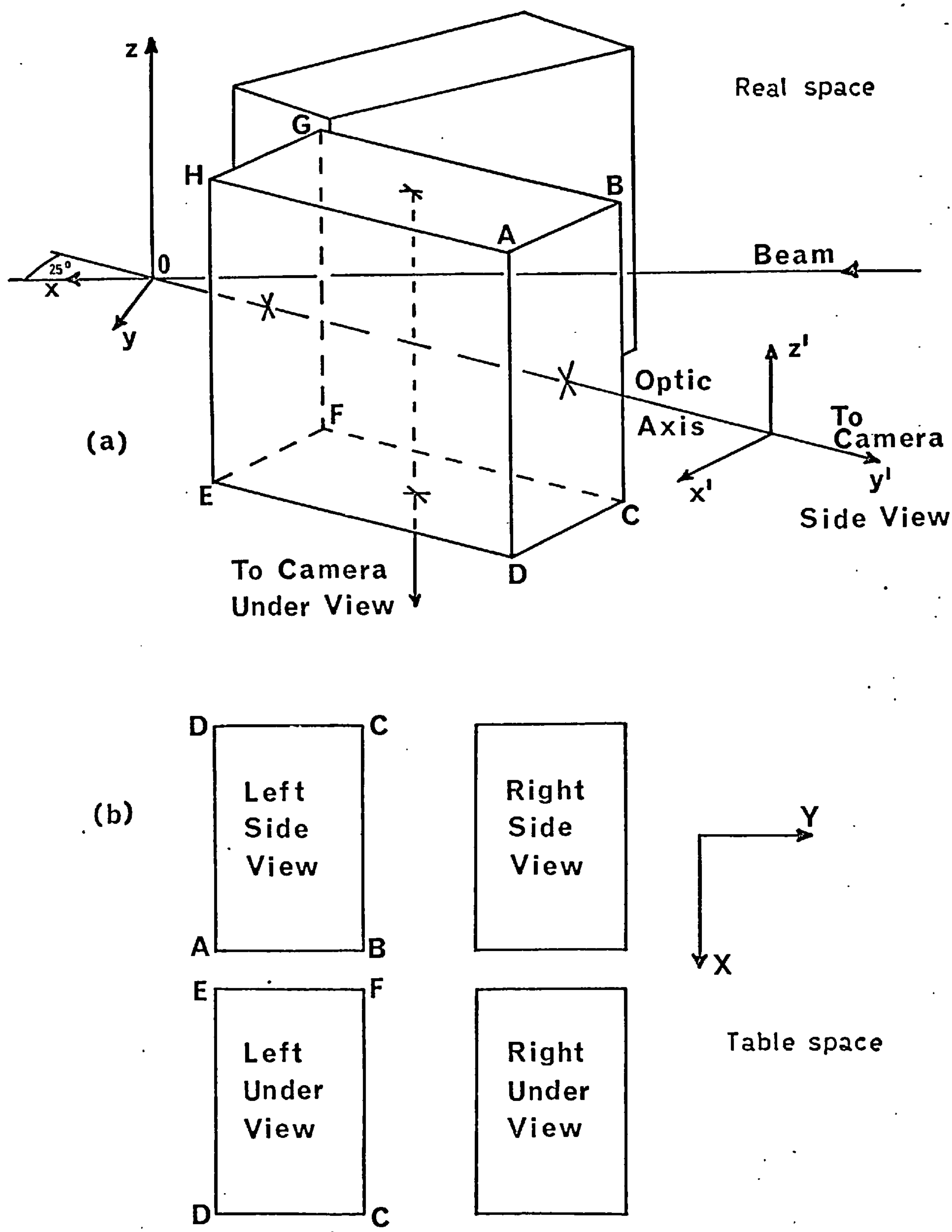

coordinate system with Oy' along the optic axis, Ox' horizontal and Oz' vertical as shown in Fig. 5.4a. The use of this system, rather than the main coordinate system based on the beam direction, Ox, implied that distances normal to the fiducial planes were less critical and only those in the fiducial planes required measurement to within 1 mm.

Images on the 35 mm film, when projected onto a DMAC Measuring Table, were about 0.4 x real size. The relative positions of the views of the chambers are shown in Fig. 5.4, in real space and projected film or table space. The coordinates corresponding to each point in the fiducial planes are related in real and table spaces by linear equations of the form:

$$\left.\begin{aligned} x'_s &= A_s X + B_s Y + C_s \\ z'_s &= F_s X + G_s Y + H_s \\ y'_s &= D_s \end{aligned}\right\} \quad \text{for the side view} \quad \ldots\ 5.1$$

and

$$\left.\begin{aligned} x'_u &\doteq A_u X + B_u Y + C_u \\ y'_u &= F_u X + G_u Y + H_u \\ z'_u &= D_u \end{aligned}\right\} \quad \text{for the under view} \quad \ldots\ 5.2$$

where X and Y are the coordinates in table space and x', y' and z' are the coordinates in real space as defined earlier. The reconstruction constants, $A_s - H_s$, $A_u - H_u$ were calculated using a modified version of a least squares fitting program, written by W.G. Jones. Four fiducial marks, one in each view and well separated from each other, were chosen to locate the 'standard frame' into which each measured event would be transformed. Using this same program and the known positions of depth fiducials in the planes EFGH and ABGH (Fig. 5.4), the effective camera coordinates for each view were estimated, and were found to be within a few centimetres of their design positions. Their exact locations were not critical as they involved second order effects only.

For each event measured, the relevant table coordinates (X,Y) were punched directly onto three 80-column binary cards. The first card held the necessary digital data, film number, event number, τ_n, etc., as well as the coordinates of the four standard fiducials. Four coordinates were punched onto the second card. Of these, t_u and t_s

(Fig. 5.5a), were at images of the same physical spark, usually the first spark of the incident track, in the two stereo views, LU and LS. t_u' and t_s' were further, although not necessarily corresponding, points along the line of the incident track. Similar information relevant to the track in the right-hand views, RU, RS was recorded on the third card.

Once measured, the events were ready for reconstruction using a modified version of a program written by W.G. Jones. First of all, the measured coordinates were transformed to the standard frame and, using the reconstruction equations, 5.1 and 5.2, the tracks were related to their real space images in the fiducial planes ABCD and CDEF. As the inner chambers were viewed in directions not quite parallel to their plates, the spark images recorded were partly reflections in the aluminium foil; their true positions, therefore, were distorted slightly and due allowance for these reflections was made in the computations.

Although the reconstructed values of t_s and t_u were purported to be images of the same physical point, due to measurement errors, lines constructed through $C_s t_s$ and $C_u t_u$

Fig.5.5 The coordinates measured for each event

(a)

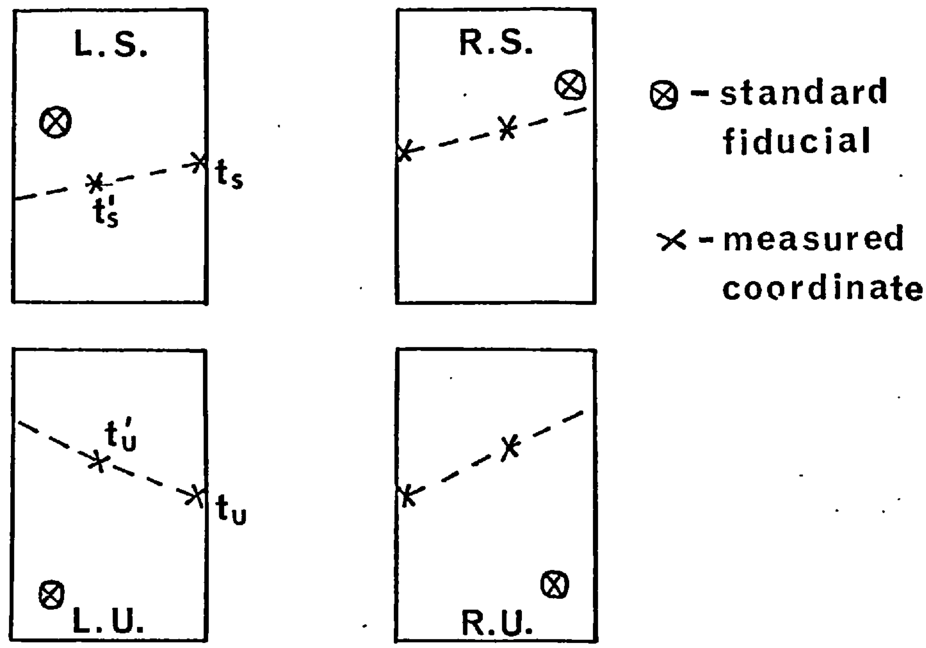

Reconstruction of the 'fixed' point, p

(b)

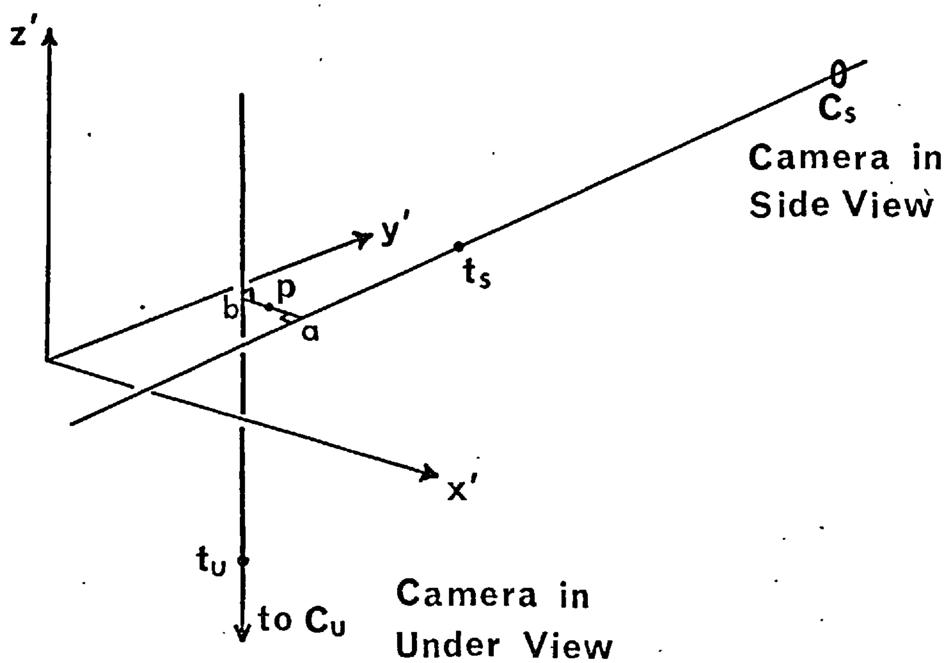

(Fig. 5.5b) in general did not meet. The 'fixed' point, p, on each track was taken as the mid point of the common perpendicular, ab. Planes were constructed, one through the reconstructed values of t_s and t'_s and the camera C_s, and the other through the reconstructed values of t_u and t'_u and C_u. From the line of intersection of these planes, the direction cosines of the track were estimated. The direction cosines of the other track were found similarly and the vertex in the target was calculated, again as the mid-point of the line of closest approach. Finally, the direction cosines were recalculated for each track from the coordinates of the vertex and the point, p. Throughout, the data were checked for consistency and measurement errors.

The reconstructed events were tested for consistency with the hypothesis $\pi^- + p \longrightarrow e^+ + e^- + n$ using a fitting program[34] written by D.C. Mason.

Any event purporting to be $\pi^- p \longrightarrow e^+ e^- n$ should be able to satisfy the condition that both energy and momentum must be conserved in the process. A particle i can be specified by its mass M_i, momentum p_i, and direction, given by the angles θ_i and ϕ_i defined in Fig.5.6. Conservation

Fig. 5.6 Definition of angles

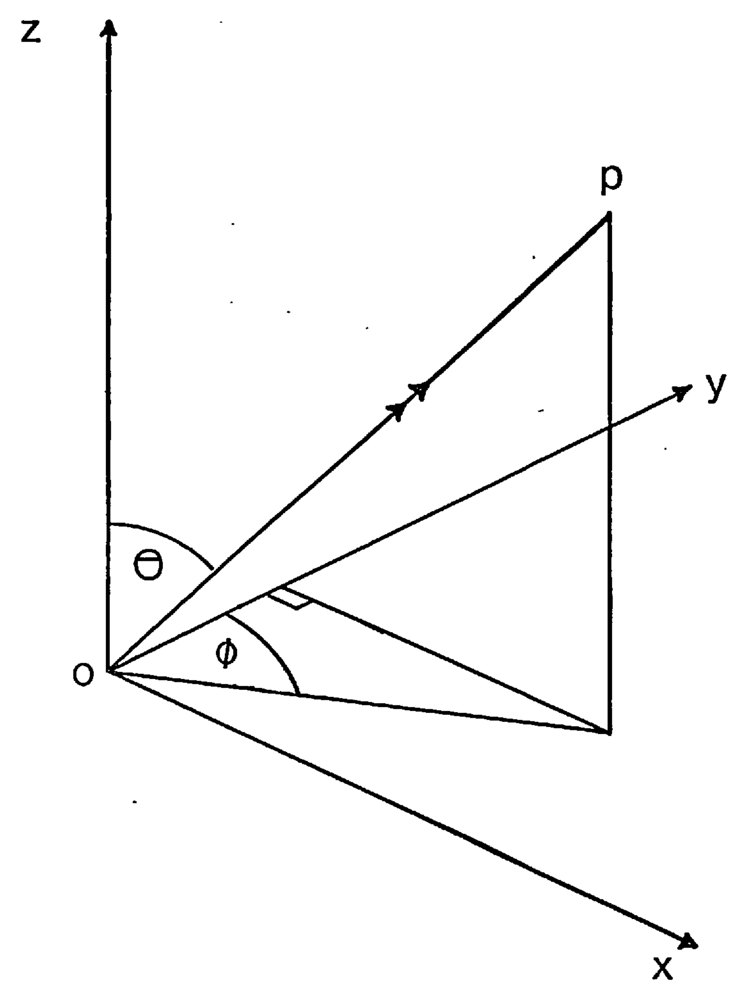

(Beam direction)

op = direction of particle

of energy and momentum can be translated into four equations, three for momentum conservation along each axis, and one for energy conservation. If we work in the laboratory frame:

$$\sum_{i=1}^{4} f_i \, p_i \, \sin\theta_i \cos\phi_i = 0$$

$$\sum_{i=1}^{4} f_i \, p_i \, \sin\theta_i \sin\phi_i = 0$$

$$\sum_{i=1}^{4} f_i \, p_i \, \cos\theta_i = 0 \qquad \ldots \; 5.3$$

$$\sum_{i=1}^{4} f_i \sqrt{(p_i^2 + M_i^2)} - M_p = 0$$

Index i runs from 1 to 4, since in this process there are four particles (π, n , e^+, e^-) with non-zero momentum in the laboratory frame. f_i is a factor which is -1 for initial state particles, +1 for final state particles; M_p is the proton mass.

In the case of an event where all the parameters are known, these equations will in general not be satisfied. This is because each parameter is subject to errors and uncertainties introduced by the apparatus or measurer. However, statistical methods exist, according to which, if small adjustments are made in a certain way to measured values of the parameters, the adjusted values of the parameters can be made to satisfy the conservation equations. Furthermore, it can be proved that, using these methods, the values of the adjusted parameters so calculated, represent the most likely estimates of the true values of these parameters. Such a statistical method (called a fitting process) can be employed whenever there is overdeterminancy i.e. whenever there are more equations linking a set of parameters, than there are unknowns among the parameters.

The kinematic information available for each event was the momentum vectors of both the pion and the neutron, and the direction cosines of both electrons (all measured in the laboratory frame). The only unknown quantities were then the momenta of the two electrons, so that the fit in our case was two-constraint - (number of constraints = number of equations - number of unknowns).

The method of least squares was the statistical method employed as the basis of the kinematic fitting. The basic operation performed was the minimization of the variable:

$$\chi^2 = \sum_{i=1}^{10} \frac{(m_i - m_i^o)^2}{\sigma_i^2} \qquad \ldots 5.4$$

under energy and momentum constraints (i.e. equations 5.3). Index i runs over all the measured parameters. m_i^o is the initial measured value of variable i, while m_i is the adjusted value obtained when χ^2 is minimised and the constraint equations satisfied. σ_i^2 is the estimated variance of the variable i. Since the constraint equations are non-linear, the minimisation process was iterative.

The least squares method demands that the variables used in the fit should be normally distributed. The θ and ϕ angles (see Fig. 5.6) were taken as the normal variables which described the direction of each particle (in the frame specified). The magnitude of the momentum of each particle was also considered as normally distributed, with the exception of the neutron, where the time of flight was taken as normally distributed instead. The main approximations involved in this formalism were that, in practice, θ and ϕ for the neutron were not really distributed normally, since the distributions of these parameters were limited by the finite dimensions of the neutron counters. Also, the input pion momentum was distributed triangularly rather than gaussianly.

The program was tested using Monte Carlo generated events, with normally distributed errors in the ten 'measured' parameters. Certain theoretical conditions were well satisfied by the fitted Monte Carlo events. Moreover, the same program had proved satisfactory in the ϕ search experiment. The use of the basic program in the ϕ decay was valid therefore and any errors in the fitting of the experimental events would be, in the reconstruction, in the values of the variances used, or in systematic errors in the parameters.

The normal variances, used in fitting both Monte Carlo and experimental events are given in Table 5.2. The estimate of the neutron time of flight variance was taken from reference 26. The variance in the pion angles was given by the divergence of the beam. The variances in the non-normally distributed parameters were as used in the ϕ search, in which the effect of assuming these parameters to be normally distributed had been shown to be small.

Table 5.2

Parameter Name	Standard Deviation
Neutron time of flight	0.83 nsec
Electron θ and ϕ angles	80 mrad ≠
Pion θ and ϕ angles	8 mrad
Pion momentum *	4.5 MeV/c
Neutron θ and ϕ angles *	25 mrad

* - normal distribution only approximates to true distribution.
≠ - see section 6.3 for the derivation of this number.

5.5 Development of the second criteria

While the preliminary scan was in progress, further criteria were developed. About 5000 first scan, S1, candidates were anticipated and it was intended that the second set of criteria should reduce the numbers to about 500-1000, at which stage it would be practicable to measure and fit the events kinematically. In eliminating the bulk of the remaining non-electron events, the criteria should be objective and insensitive to spark chamber performance. A 10% loss of genuine events was considered acceptable.

A sample of S1 candidates was examined on the DMAC measuring table. Many of the so-called showers which had satisfied the previous criteria were obviously due to pions with δ-rays or casual tracks. These secondaries, unlike those in electron showers, had no tendency to appear at an early stage, and therefore the points requirement of the first scan was tightened slightly to demand a minimum of one point in the first three chambers and two points in the first four. These two criteria, encoded '< 1 in 3' and '< 2 in 4', caused only a small additional loss of electrons and rejected a significant fraction of the background events.

Some events had been included in which a whole chamber had failed to fire along the line of an apparent pion track. Such cases, due to 'old' casual pions in which most of the ionisation had been swept away by the clearing field, constituted a technical 'non-ionising link'. To reduce the numbers of these events, we demanded that two points in the first four chambers should not be solely due to a non-ionising link - failure code ' <2 in 4 NI'.

Pions, the major element of non-electron 'showers', usually appeared as a series of colinear tracks. To test whether they could be recognised by their straightness, a template consisting of 6 pairs of parallel lines of separation 1 mm, 2 mm, ... 6 mm (table space) was made. Non-interacting pions, selected from a film in which there was no shower requirement, were tested to determine the minimum separation of lines within which the track could be contained. The 3 mm pair were found to accommodate $\sim 90\%$ of the tracks. A calculation based on multiple Coulomb scattering of a 600 MeV/c pion led to a similar separation. The 3 mm wide template could be used to reject pions effectively. To determine the corresponding loss of electrons, a sample of the 650 MeV/c electron photographs, the most likely to display straight tracks, was examined for 4, 5 and 6 colinear (as defined by the 3 mm template) tracks. In the first four chambers such tracks were found in about 60% of the cases. The '3 mm width' needed to be compounded with a points requirement. The following criterion was envisaged:

"If the total number of points in a shower is ≤ 6; then, if in the first n chambers (n = 4, 5 or 6), n tracks can be defined as 'straight' (as defined by the 3 mm template), there should not be less than (n - 1) points in these n chambers."

The failure code for this straightness criterion was '4 Str', '5 Str' or '6 Str' depending on the value of n.

A rough check indicated no appreciable loss of 650 MeV electrons. At lower energies, although the likelihood of scoring sufficient points would fall, not only would scattering out of the 3 mm width be more probable, but also there would be fewer tracks that could be straight. Higher energy showers should have ample points to be safe.

In electron showers, a certain degree of symmetry is found in the lateral spread of the secondaries. To test whether this feature could be exploited as a criterion, calibration electrons, at three momenta, were examined and the penetration depth at which the showers became 'symmetric' were noted. Here we define 'symmetric' as: "evidence of secondary track(s) on both sides of the incident track in each stereo view". Thus, in Fig. 5.7 which illustrates one view of a shower (A), the event becomes symmetric in the fourth chamber. The other example (B) is asymmetric. The distributions of chamber numbers at which each stereo view became symmetric are shown in Fig. 5.7 for three momenta. The overflow bins indicate asymmetric examples. To be effective in rejecting background events, symmetry was

Fig.5.7

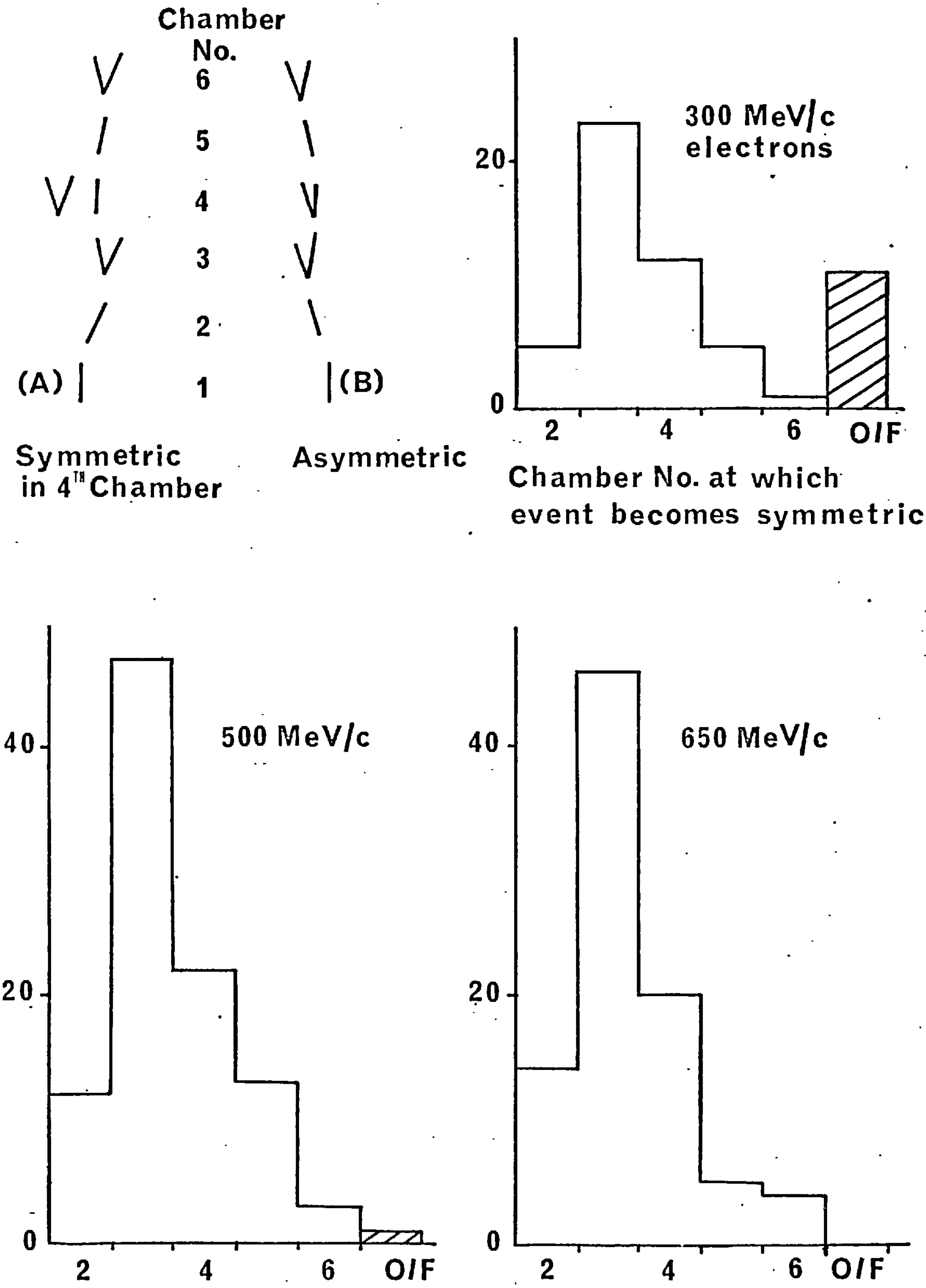
Chamber No.
6
5
4
3
2
1
(A)
(B)
Symmetric in 4TH Chamber
Asymmetric
300 MeV/c electrons
20
0
2
4
6
O/F
Chamber No. at which event becomes symmetric
500 MeV/c
40
20
0
2
4
6
O/F
650 MeV/c
40
20
0
2
4
6
O/F

required of both views for each 'shower'. The losses, therefore, would be double those indicated in Fig. 5.7 and to keep them at a low level all six chambers were used. Furthermore, to allow for misalignment along the incident track, the axis about which symmetry was required was modified by 2°. The template used is shown in Fig. 5.8. A shower which lay entirely to the right of AP or to the left of BQ, in either stereo view was defined as asymmetric (code 'A/S'). Again only tracks within the outer tramlines, KL, MN, at 5.4 cm (real space) from the input track centre were considered.

Some criteria, additional to the above, were introduced to dispose of certain classes of non-electron like events. These subsiduary criteria included:

a) Points must arise from >1 lead plate: failure code 'Sing. Int.'.

b) Points must arise from >1 chamber: failure code 'Sing. Ch.'.

c) Ignore:
   i) Back scatters from the first lead plate.
   ii) Non-ionising links of ≥ 3 chambers.
   iii) Non-ionising links that do not convert in a forward direction.
   iv) Obviously unassociated tracks.

Fig.5.8 The A/S Template

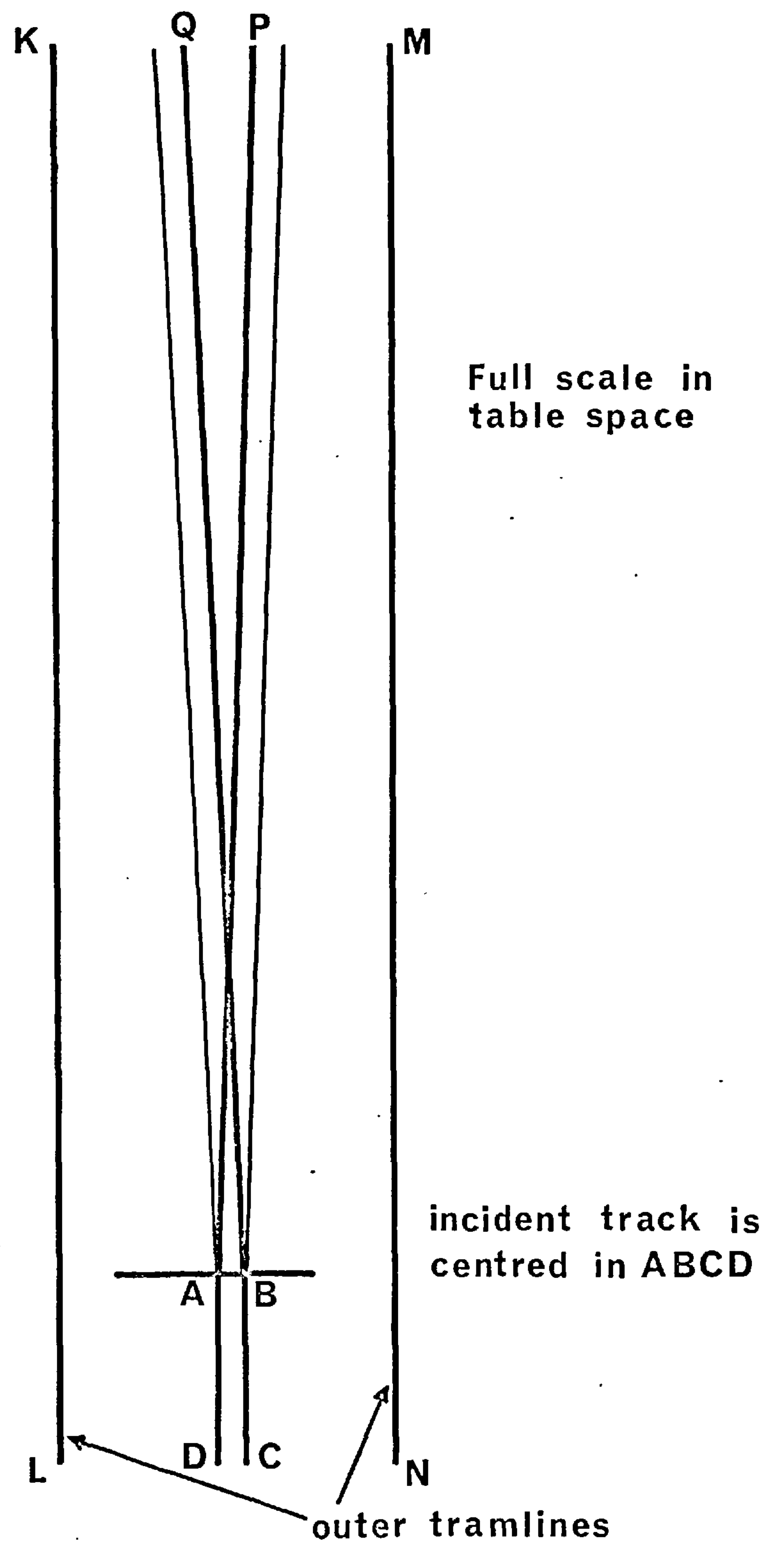

5.6 Effect of the criteria on electrons

The criteria were applied to about 3000 of the calibration electron photographs at the four momenta. For convenience, the failure codes of the criteria which include the preliminary scan requirements (code NC) are listed: NC; < 1 in 3; < 2 in 4; < 2 in 4 NI; A/S; 4 Str; 5 Str; 6 Str; Sing.Int. and Sing.Ch..

Calibration electrons remote from the beam axis tended to display weak showers and, as these examples were probably not of the nominal momentum, they could not be used to test the criteria fairly. About 75% of the electrons in the beam fell within a 5 cm square (table space), centred on the beam axis, and only electrons incident in this region were used to test the criteria directly. However, there would still be a small contamination of low energy electrons in this area and their effect was estimated as follows. The plane of the first chamber was divided into three zones (Fig. 5.9). Zone 1, the 5 cm square central region was surrounded by Zone 2 which was 8 x larger in area. Zone 3 comprised the remainder of the chamber. The criteria were applied to those Zone 1 and Zone 2 candidates with a single input track.

Figure 5.9

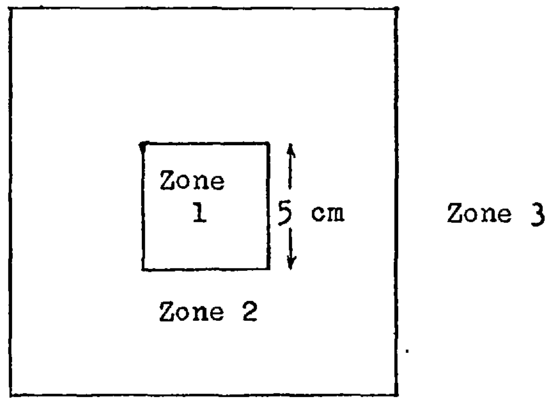

Fig. 5.9 Candidates in Zone 1, which is centred on the beam axis, are used to test the criteria. Candidates in Zone 2 are used to estimate the effect of low energy electrons in Zone 1.

Electrons of below the nominal momentum were postulated to have a uniform flux in both central zones, and to correct for these, of the Zone 2 criteria failures, 1/8 were subtracted from the Zone 1 failures. The losses at each momentum were estimated to be:

$$\text{loss} = \frac{\text{Zone 1 failures} - 1/8 \text{ Zone 2 failures}}{\text{Zone 1 candidates} - 1/8 \text{ Zone 2 failures}} \quad \ldots\; 5.5$$

Fig. 5.10 shows the combined losses of the first and second criteria as a function of energy. The upper (continuous) line indicates the loss with all borderline

Fig. 5 10 The combined loss of electrons due to the first and second criteria as a function of energy

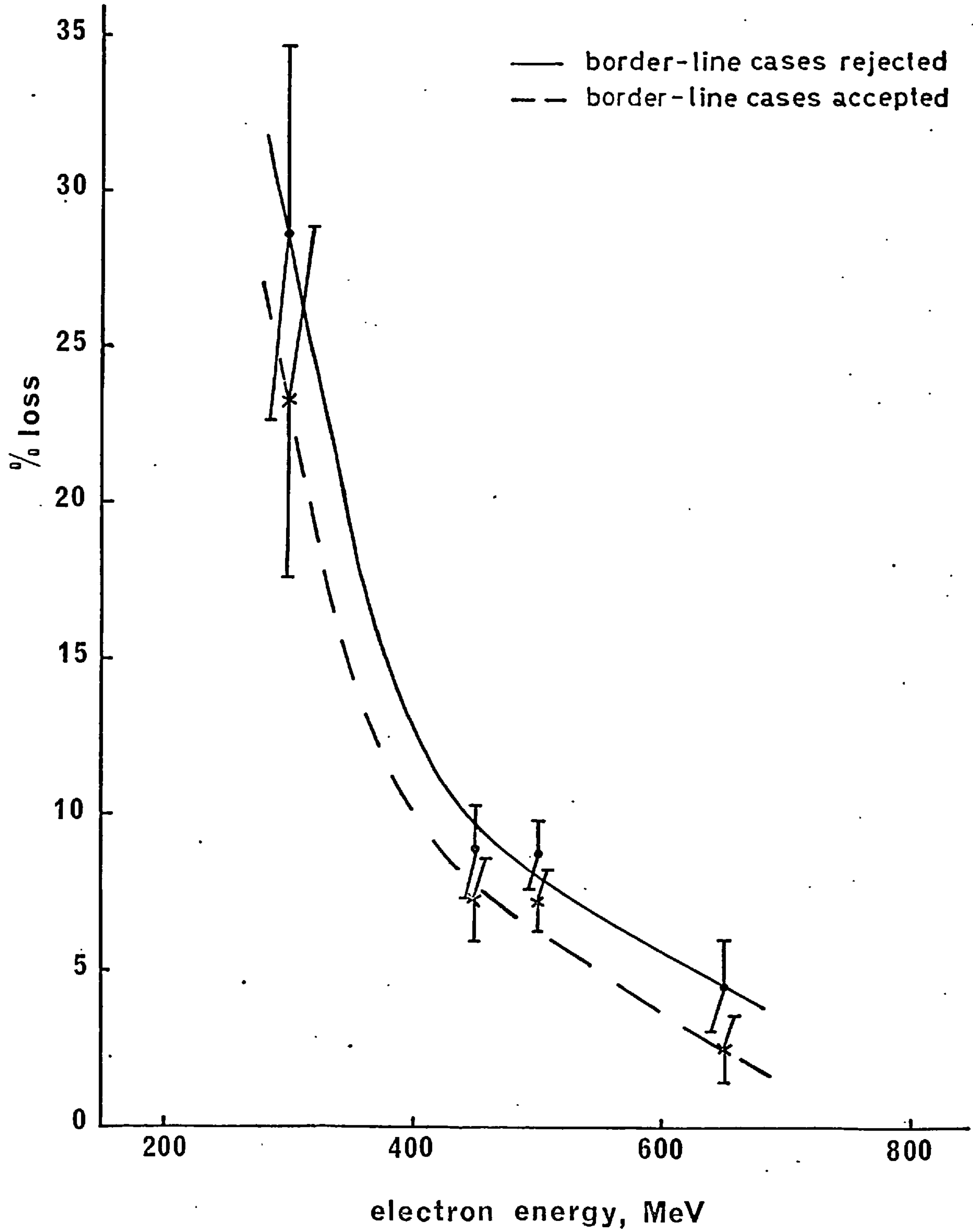

cases rejected and the lower (dashed) line indicates the loss with these same events accepted. The relatively small difference in efficiency due to these ambiguous events indicates the objectiveness of the criteria. The results at 300 MeV, based on a small sample of events using a slightly modified lead plate configuration, were used only as an indication of the trend at low energies. This uncertainty in the efficiency at low energies was unimportant as few ϕ decay electrons encountered would be below 400 MeV.

As film of showers at momenta greater than 650 MeV/c was not available, the losses at higher momenta were estimated. Since the probability of rejection would decrease with increasing $\overline{N}_{\gamma}$ and therefore with increasing momentum, a linear extrapolation to the free hand fit to the experimental points was used. The error in this estimate is comparable with the errors in the experimental values.

Since the total energy of the two leptons was roughly constant, it was possible to estimate the criteria loss of $\phi \longrightarrow e^+ + e^-$ events by reflecting the loss curves of Fig. 5.10 about the mean ϕ decay electron energy, 650 MeV, and adding. Fig. 5.11 shows the total losses due to the first and second criteria with border-line cases rejected (upper curve) and with border-line cases accepted (lower curve). In both cases the losses were found to be constant, within the experimental errors, from 430 to 880 MeV and since almost all the ϕ decay electrons encountered would lie within this energy range, the mean loss incurred by the criteria was estimated to be $(7.5 \pm 3.5)\%$.

5.7 Application of the second criteria

Working in pairs, to assist in attaining an unbiased application of the criteria, physicists subjected the 4700 first scan candidates to the second criteria. Each accepted event was measured and kinematically analysed.

As expected, many events that had caused difficulties in the first scan, fell readily to the new criteria. However, in events where there was a preponderance of tracks, not only were the tracks tedious to correlate in both views, but also, due to robbing, the efficiency with which genuine showers would be recognised was uncertain. It was necessary to eliminate the majority of such events in a way which was unbiased towards ϕ or K and could be assessed for later normalisation.

Fig. 5.11 The loss of $\phi \rightarrow e^+ e^-$ events incurred by the first and second criteria

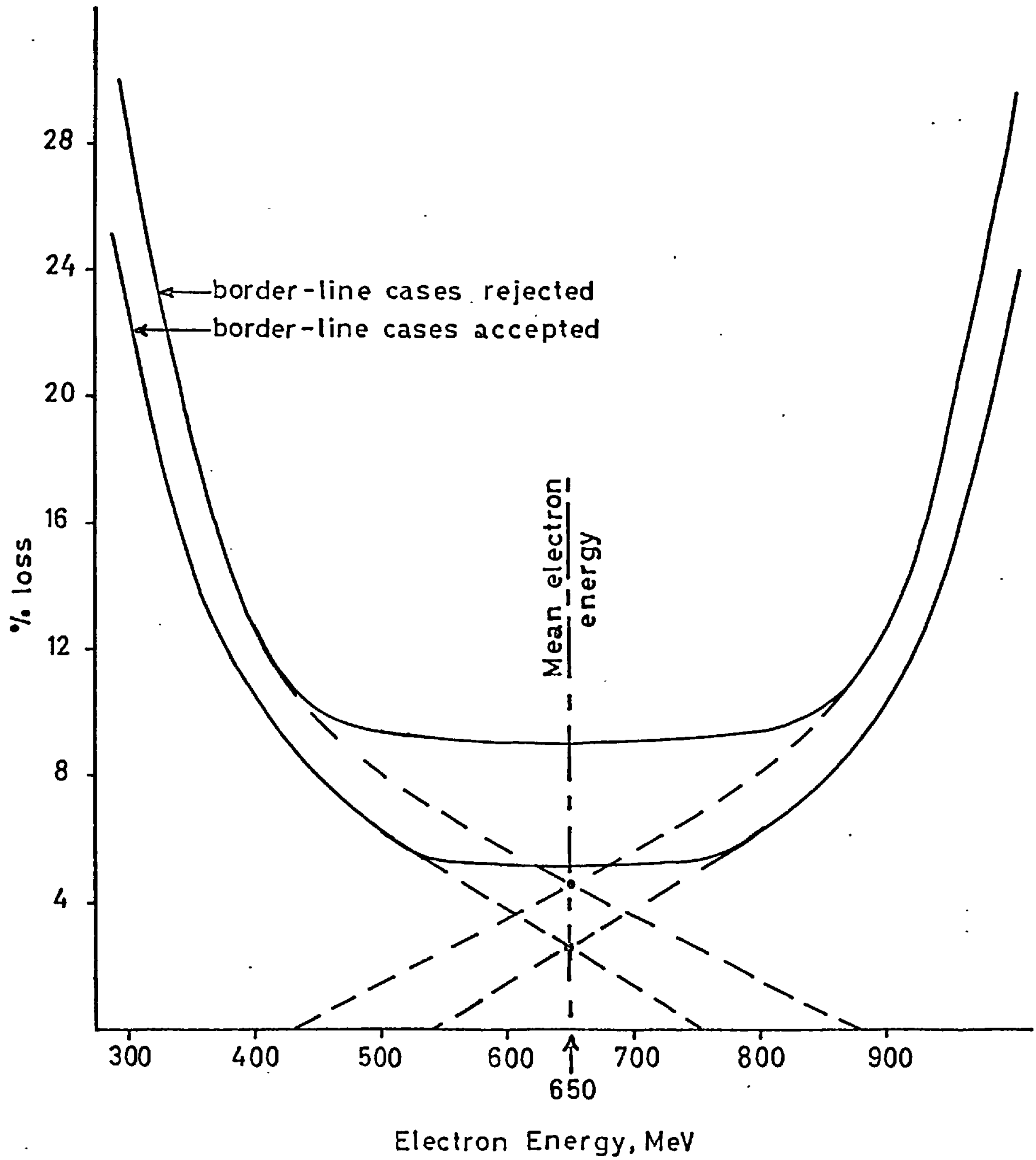

The distribution of the total number of tracks in the inner chambers is shown in Fig. 5.12 for samples from ten films. The shaded area indicates events where 3 or more input tracks were present on both sides. Events with 8 or more input tracks total and with 3 or more on both sides were rejected (code: $\geq$8T) as these would include the majority of the confused events. The average loss was estimated to be 5$\pm$1%.

No event of the 4700 could be rejected without a valid reason which was recorded against each event, e.g. a criterion failure code. Table 5.3 shows the relative effectiveness of each criterion for both ∅ and K events.

Table 5.3

Criterion applied	∅ events	K events
NC	520	459
A/S	444	471
< 2 in 4	326	397
< 1 in 3	276	297
4 Str	48	53
5 Str	66	58
6 Str	35	33
Sing. Int.	44	37
$\geq$ 8T	28	19
Non Hydrogen	115	134
$\geq$ 2 of above reasons	132	149
Accepted events	248	287
Totals	2282	2394

Fig. 5.12 The distribution of the number of tracks in the inner chambers. The shaded area represents events with ⩾3 input tracks on both sides.

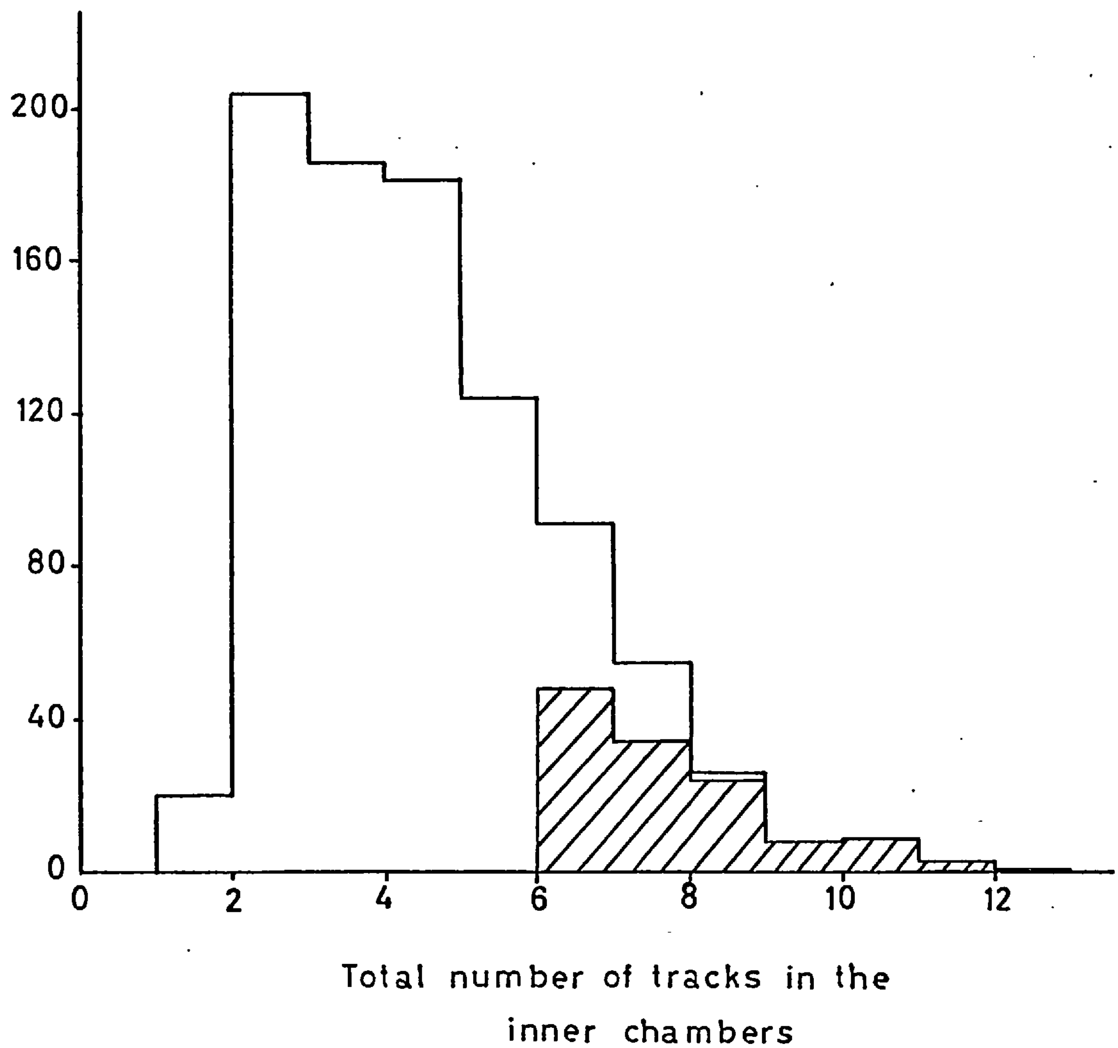

The number of non-candidates (NC) surviving to the second stage indicates the caution applied in the preliminary scan. Also the equality of the total number of ϕ and K first scan candidates shows impartiality, and the quantities against the individual criteria indicate a uniform application throughout. Moreover, the equality of the successful candidates, 248 from ϕ and 287 from K, was further evidence of unbiased scanning, and also demonstrated that $\phi \longrightarrow e^+ + e^-$ events were not present in numbers appreciably greater than was anticipated.

Many accepted candidates showed two closely spaced, almost parallel, input tracks. These events, arising from internal or external conversion of γ rays from π^0 decays, were termed 'Dalitz pairs'.[35] As unresolved pairs might contribute to the ultimate background, the 'Dalitz pairs' were not rejected at this stage.

Due to measurement errors, e.g. an incorrect fiducial, about 5% of the measured events were rejected by the reconstruction program. These events required remeasuring. As a greater part of time needed to right these errors would be occupied in loading films and locating frames, a complete remeasure of all 500 second scan, S2, candidates was performed. This remeasure was carried out by physicists working singly. It demanded a relatively small number of man-hours and had several advantages: each event had a further examination independent of the first measure, M1; the results of the first and second measures could be compared for consistency; and a further opportunity was presented for additions to the criteria. The only major addition to the criteria was concerned with the rejection of Dalitz pairs which constituted $\sim$ 25% of the remaining candidates. The photograph in Fig. 5.13 shows an event with three pairs of closely spaced, almost parallel input tracks, which are characteristic of Dalitz pairs. Although two input tracks are not obvious in the lower right view, their presence can be deduced by correlating the relative spark intensities with the upper view. A Dalitz pair was defined objectively as: "two almost parallel input tracks that originate from a vertex within the target and which are not separated by more than 15 mm (table space) in either view." This limit was chosen to include, with a margin of safety, all obvious Dalitz pairs in a small sample.

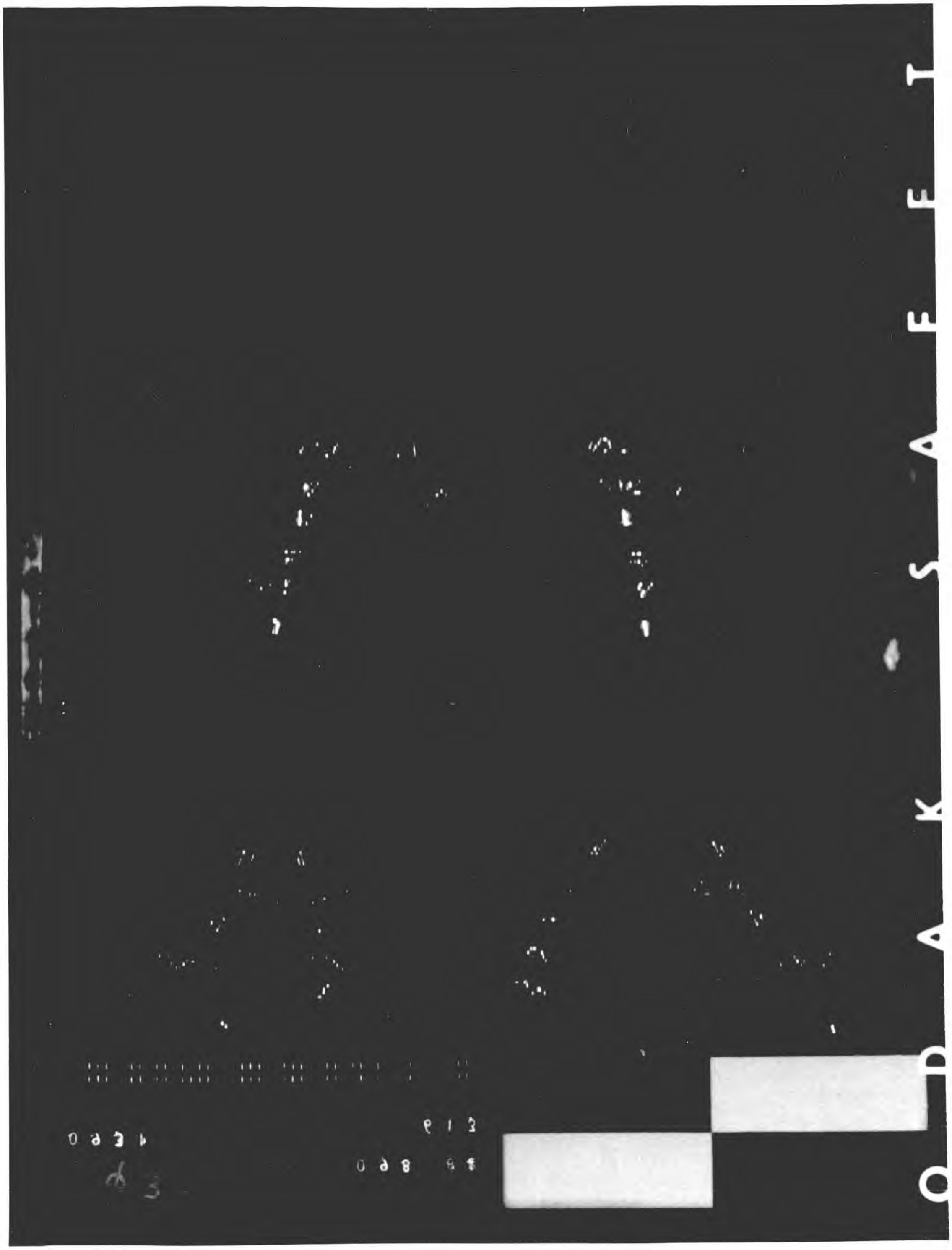

Fig. 5.13

The loss of genuine events, due to the proximity of an almost parallel, casual track was estimated as follows. For samples of consecutive frames on several films, the input track nearest to beam height in one view was assumed for this purpose to be the main track of a candidate. Any further tracks incident in the region corresponding to the shaded area in Fig. 5.14 were tested for a hydrogen vertex with the main track.

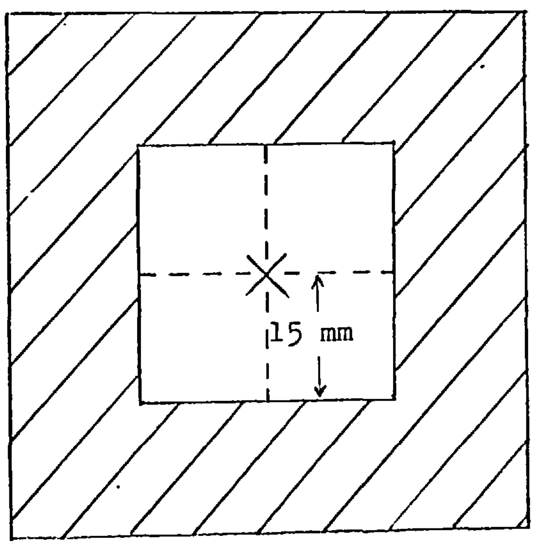

In plane of spark chamber with an input track at centre.

Fig. 5.14 A Dalitz pair requires a second input track, approximately parallel to the first which is centred at X, falling in the unshaded central region. The proportion of 'casual Dalitz pairs' is found by considering tracks which fall in the shaded area.

The fraction of each sample with such a vertex was noted. Additional tracks in the central (unshaded) area were ignored to eliminate genuine Dalitz pairs. A uniform flux of casuals was assumed in the central and shaded regions, and therefore, allowing for both sides in the ϕ decay experiment, the measured casual rate was 1.5 x the rate in the central area. The loss of $\phi \longrightarrow e^+ + e^-$ events introduced by rejecting candidates which fulfilled the Dalitz pair definition was dependent on beam rate and was found to vary from $(0.5 \pm 0.5)\%$ to $(1.3 \pm 0.7)\%$. Although this second measure presented an opportunity to digitise certain shower information, e.g. the number of tracks in each chamber, this would have been time consuming.

The results of the first measure had shown that one additional item of information was necessary - an indication of accuracy of measurement. The direction measured from 3 or 4 colinear sparks would be more accurate than, say, the direction measured from 2 adjacent sparks. It follows, for example, that an event with a vertex computed to be just outside the limits of the target could be rejected in the former case, but would require further investigation in the latter. A complex set of rules, based on thickness, colinearity and number of sparks, was superseded by a 'satisfaction of measurement' criteria, which, although somewhat subjective, indicated adequately which events required additional tolerances. A digit on the second and third cards for each event indicated four classes of measurement, viz:

2 good	measurement - e.g.	3 or 4 clean sparks
3 fair	"	2 non adjacent sparks
4 poor	"	2 adjacent sparks
5 bad	"	2 thick adjacent sparks

To ensure no events were eliminated falsely, events other than obvious Dalitz pairs could not be rejected without a second opinion. During the second measure, about 180 events were rejected on criteria, non hydrogen and Dalitz pair grounds.

The results of both first and second measures were checked for consistency in all respects. Multiple measuring of a few events had shown that the coordinates of the hydrogen vertex could be reproduced within about 1 cm. The computed vertices in both measures were compared and discrepancies were noted. For each event, to ensure the same pair of tracks had been measured on both occasions, the coordinates of the point, p, (see section 5.4) were required to agree. Similarly, unreasonable discrepancies in the value of χ^2 were noted for further investigation. All but a few films had some events that needed to be rescrutinised and an almost complete re-examination was carried out in conjunction with A. Duane. The only frames not rescanned were those events with good 'satisfaction of measurement' codes in which both M1 and M2 gave consistent results in all respects. Particular attention was paid to events which had been accepted as good fits in the first measure, yet had not been measured a second time. One event, falsely rejected as a Dalitz pair, was retrieved. When necessary, events were measured a third time. In cases where only poor direction information was available from an inner chamber the vertex of secondaries in the first lead plate was used to give a better estimate of the true incident direction. Events for which the value of χ^2 was less than 16 were considered to be consistent with the hypothesis $\pi^- + p \longrightarrow e^+ + e^- + n$ (see section 6.4). During the third measure these events were examined in passing and six were shown to fail the criteria, but, to avoid bias, two further independent opinions were sought in these six cases.

All events of the 535 accepted in the second scan had either been rejected for a valid reason or had had two measures, the results of which were consistent. In all, the various shower criteria had reduced the 220,000 events to 349, 166 from ϕ and 183 from K. Again the equality of the numbers of signal and background events indicated both lack of bias towards either class and that $\phi \longrightarrow e^+ + e^-$ events were not significantly more plentiful than was anticipated. In the next stage of the data reduction the 349 events were tested with geometric and kinematic criteria. The limits and tolerances used are discussed in the next chapter.

CHAPTER 6

KINEMATIC AND ADDITIONAL CRITERIA AND NORMALISATION

6.1 Introduction

This chapter is concerned with the final stage of the data reduction. The validity and results of the kinematic analysis are discussed in addition to the design and application of further criteria. An account of the normalisation of the final events is also presented.

6.2 The validity of the reconstruction program

The main test of the reconstruction program came from the geometric analysis of the measured events. If the reconstruction is correct, the position of the target indicated from the distribution of the computed vertex coordinates (x_v, y_v, z_v) should be consistent with the expected position. The edges of the distributions for all the measured events were not sufficiently well defined to indicate more than qualitative agreement. Due to the high beam rate, many of the photographs showed the products of more than one interaction and, in cases where the shower criteria demanded that tracks from two independent interactions be measured, the computed 'vertex' would be meaningless. Information from vertices corresponding to genuine interactions is lost due to these casual vertices. For example, consider a 'vertex' computed to be at (-70.1, 0, 12). (The downstream end of the target is at (-70, 0, 0)). As the z_v coordinate is remote from the beam, this is unlikely to be derived from products of a single interaction and can be rejected. The x_v coordinate of this same event is close to the expected edge of the target and therefore the inclusion of this event in the distribution of x_v mars the observation of a sharp edge corresponding to the end of the target.

To attain distributions richer in genuine interactions, limits on the target were defined: $-108 < x_v < -66$ cms; $-5 < \genfrac{}{}{0pt}{}{y_v}{z_v} < 5$ cms. The limits on the actual target were: $-102 < x_v < -70$ cms; $-3.25 < \genfrac{}{}{0pt}{}{y_v}{z_v} < 3.25$ cms. The vertex distributions, excluding events outside the former limits, are shown in Fig. 6.1, together with the anticipated target position along the beam axis. Normal to the beam, the distributions of y_z and z_v are centred on the beam within ~ 2 mm and also the small number of events close to the $\pm$ 5 cms limits shows that these limits were justified.

Fig. 6.1 Distributions of the reconstructed vertices relative to the beam axis. a) horizontally b) vertically c) longitudinally

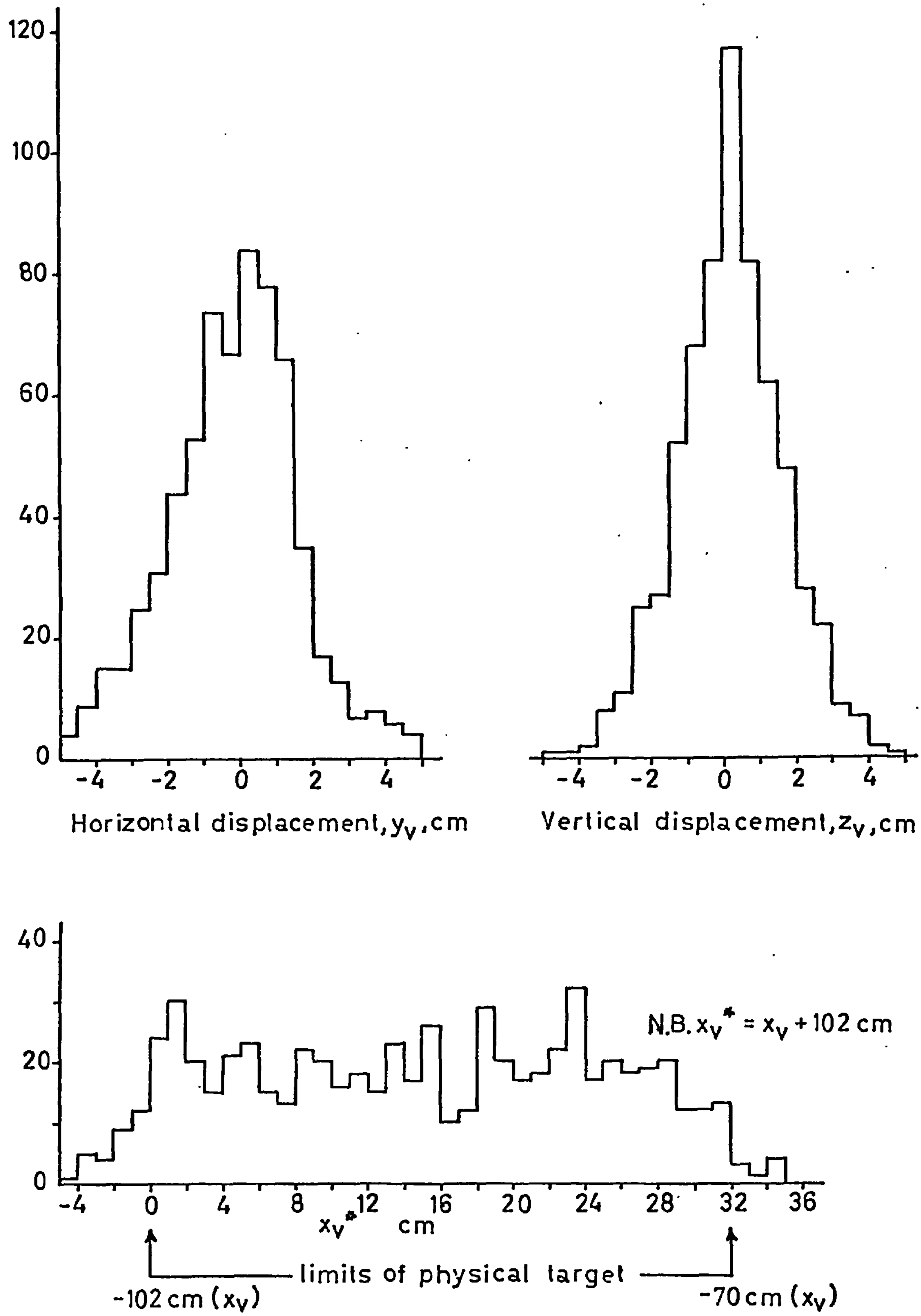

The sharp edge at -70 cm in the x_v plot shows clearly the edge of the target. The other end 32.3 cm away is not so well defined as, by being further from the chambers, vertices in this region are more susceptible to errors in measuring the tracks.

As described in section 5.4 the vertices are formed as the midpoint of the common perpendicular to both tracks. The track directions are adjusted to meet exactly; Fig. 6.2b shows the distribution of the angle, $\delta\theta_t$, through which each track was rotated, for events with accepted vertices. Events in which $\delta\theta_t$ exceeded 100 mrad. had also been removed from the distributions in Fig. 6.1. From the agreement between the computed and expected results the reconstruction was concluded to be satisfactory. Also photographs had been taken of wires stretched across the optical faces of the chamber banks. The reconstruction of these wires proved satisfactory.

6.3 Determination of the variance in the measured electron angles

A rough value of $\Delta\theta$, the variance in the measured angles, was found by assuming that a spark could be located

Fig. 6.2 Determination of the angular measurement error

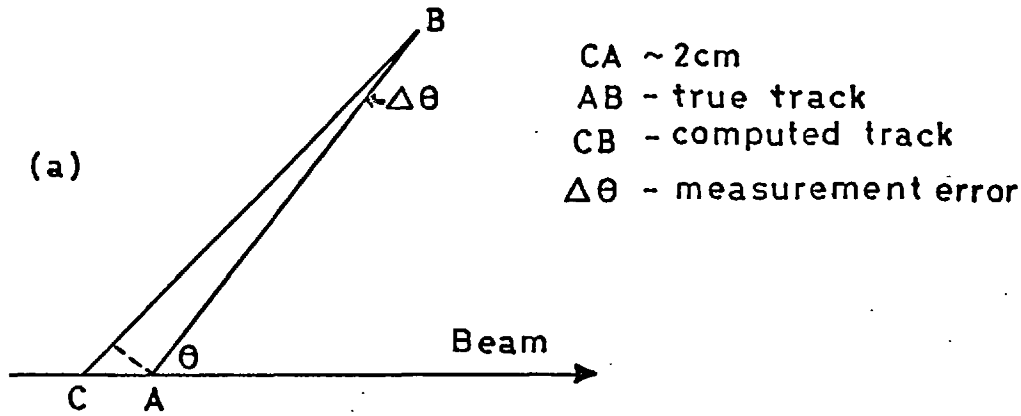

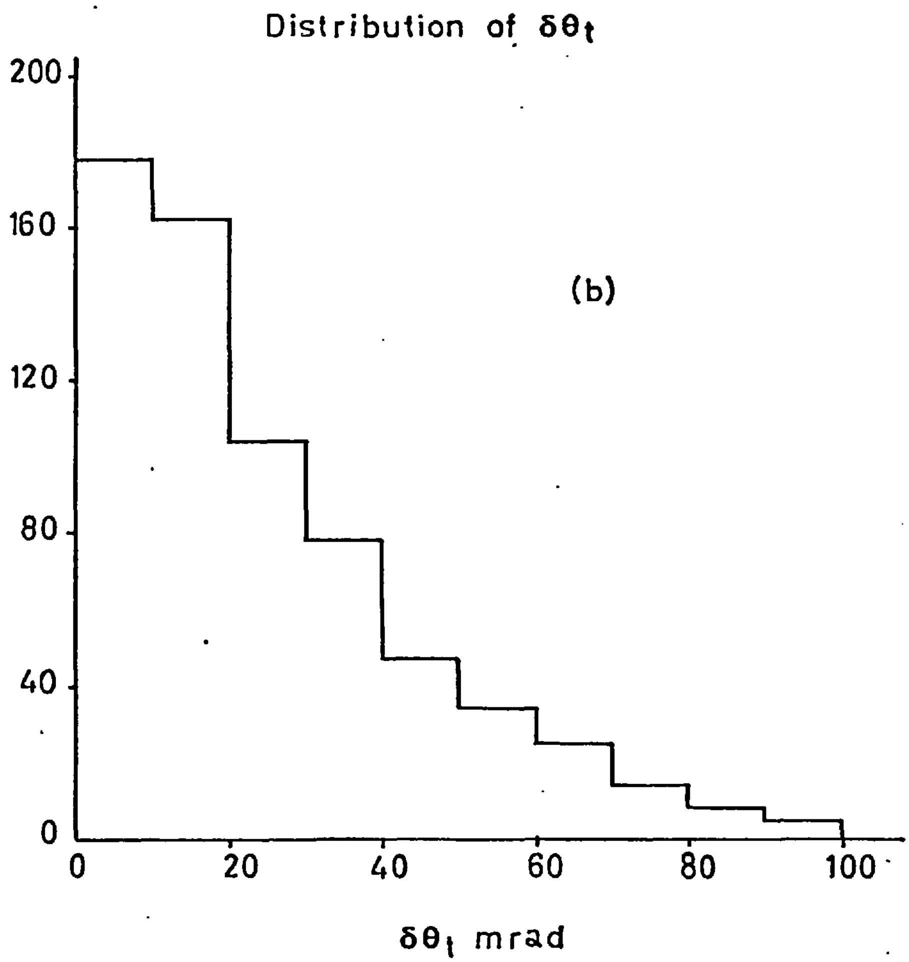

to within $\pm$ 1 mm and using the first chamber, an error of this order results in an angular error of ~ 56 mrad. A better estimate was obtained from the distributions of $\delta\theta_t$ and x_v.

From the histogram of $\delta\theta_t$(Fig. 6.2b) the standard deviation from zero was found to be $\simeq 30$ mrad. This error, $\delta\theta_t'$, is approximately the mean of the errors in the measurement of the two tracks, thus $\Delta\theta \simeq \sqrt{2}\delta\theta_t'$ and therefore $\Delta\theta = 42$ mrad. A second estimate used the x_v distribution. The computed vertex distribution along the beam direction extends ~ 2 cm beyond the geometric edge of the target as a result of measurement errors. In Fig. 6.2a the true track position, AB, at an angle θ to the beam is measured and reconstructed to be at CB where CA corresponds to the 2 cm discrepancy. Typical values of AB and θ are ~ 40 cm and $\sim 60^\circ$ respectively and therefore $\Delta\theta \sim 2.\sin 60^\circ/40 \simeq 43.5$ mrad. Thus the r.m.s. error in the measurement of the direction of the electrons was approximately $\pm$ 45 mrad. The value of the angular error, determined from multiple measuring of tracks, was smaller, but this method does not measure deviations from the true direction but records the consistency with which the human eye can 'fit' a straight line to four sparks.

The value of 45 mrad was suitable for events with good 'satisfaction of measurement' codes, but a larger tolerance was required for cases with less well defined tracks. The values of $\delta\theta_t$ for events with 'poor measurement' codes showed that a variance of 70–80 mrad should be used. For simplicity the variance in the values of θ_e and ϕ_e was taken as 80 mrad for all events.

6.4 Further tests of the reconstruction and fitting programs

About 200 events selected from the films in which there was no shower counter requirement were measured and kinematically analysed with the intention of testing the reconstruction and fitting programs. These events, which had been assumed to be predominantly due to $\pi^+ \pi^- n$ production, were tested for consistency with the hypothesis $\pi^- p \longrightarrow \pi^+ \pi^- n$. The distribution of χ^2 obtained was inconsistent with that predicted by fitting Monte Carlo events. This discrepancy could be explained either as an absence of $\pi^+ \pi^- n$ events or as an error in the reconstruction and fitting programs.

The total cross-section for $\pi^+ \pi^- n$ events in $\pi^- p$ interactions at 1.59 GeV/c is 6.45 mb.[36] The kinematic demands on the neutron in the ϕ decay restricted its momentum in the c.m.s., to $p^* \lesssim 130$ MeV/c and therefore the effective cross-section was only a fraction of the total. Fig. 6.3 shows the density of states for phase space $\pi^+\pi^-n$ events as a function of p^*,[27] which is given by

$$\frac{dR}{dp^*} = \frac{p^{*2}}{E_n^*} \left\{ 1 - \frac{4m_\pi^2}{(E_c - E_n^*)^2 - p^{*2}} \right\}^{\frac{1}{2}} \qquad \ldots 6.1$$

where $E_n^{*2} = p^{*2} + m_n^2$ and E_c is the total energy in the c.m.s.. Only 7.6×10^{-3} of the $\pi^+\pi^-n$ events generated formed potential triggers and therefore the effective cross-section was only 30.6 μb. which corresponded to about 3600 events per 10^8 pions. The efficiency for detecting these events was about 3.3% (neutron counter efficiency $\sim$15%; acceptance of chambers, 22%) and therefore $\sim$120 $2\pi n$ events were expected per 10^8 pions. This corresponded to only 10-15% of the total triggers; hence the discrepancy between the χ^2 distributions from experiment and Monte Carlo. A similar calculation for $3\pi n$ phase space events showed that although the total cross-section is lower, 3.96 mb,[36] the effective cross-section for events with $p^* < 130$ MeV/c was

Fig. 6.3 The density of final states in $\pi^- p \longrightarrow \pi^+ \pi^- n$ as a function of p^*

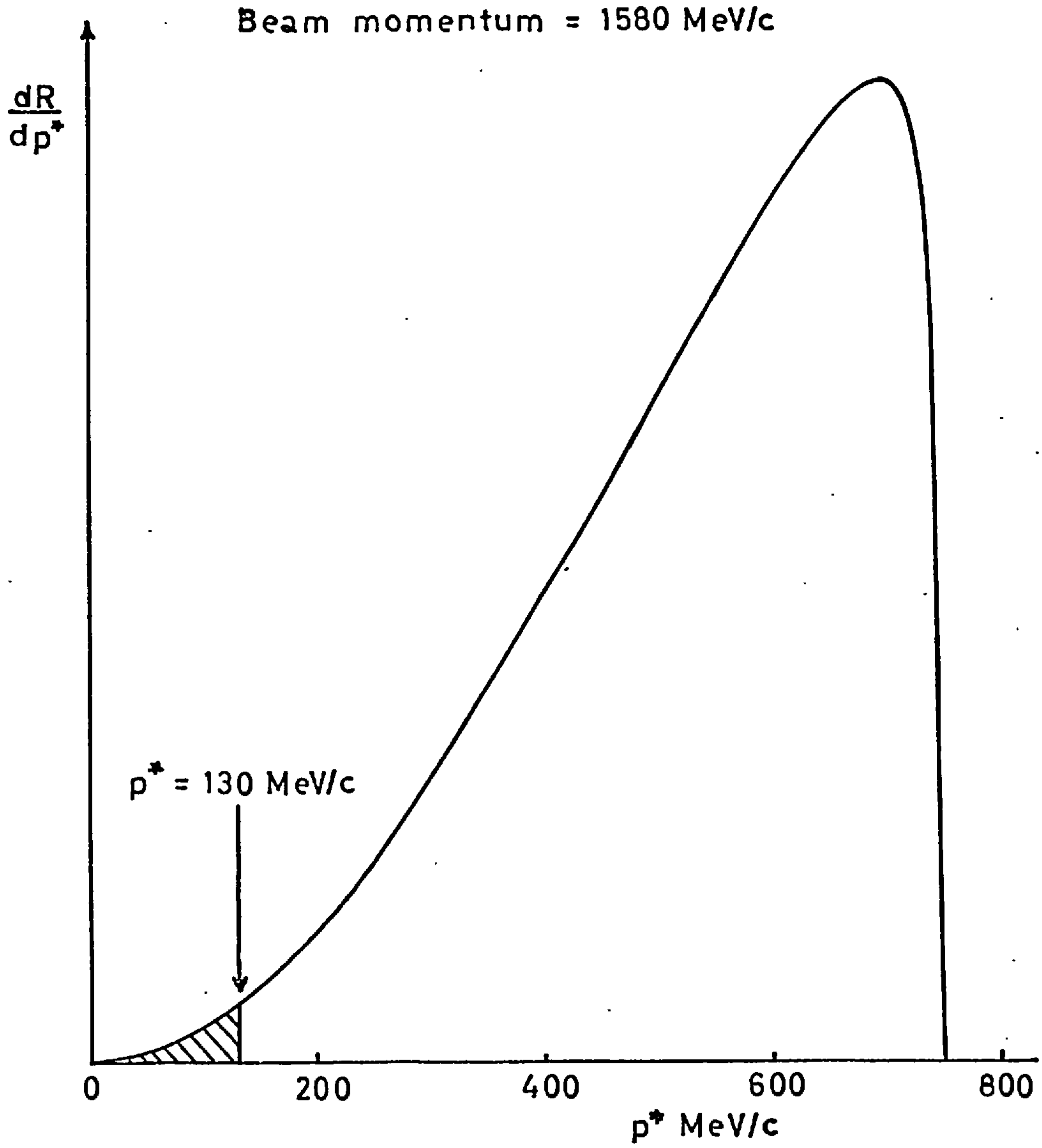

Few neutrons with $p^* > 130$ MeV/c are collected by the neutron counters. The fraction of all $\pi^+\pi^- n$ events accepted is given by

$$\approx \frac{\text{area}(p^* < 130\ \text{MeV/c})}{\text{total area}} = 7.6 \times 10^{-3}$$

higher, 93.5 μb and, allowing for the chamber acceptance for $\pi^+\pi^-$ from $3\pi n$ events, this corresponded to ~ 180 triggers/10^8 pions.

Since there were very few $2\pi n$ events, the reconstruction and fitting programs could not be tested as had been anticipated. Their satisfactory operation was deduced as follows. From the Monte Carlo tests of the fitting program (section 5.4) we concluded that any errors would be due to systematic errors in the data used for each event. The effects of various systematic errors in the ten parameters were considered in turn by modifying Monte Carlo generated events, fitting them to the $\pi^- p \longrightarrow e^+e^- n$ hypothesis, and comparing the resulting χ^2 distributions with that obtained without systematic errors.

The χ^2 distributions obtained for events in which the neutron time of flight, τ_n, was modified by -2, -1, +1, +2 nsec are shown in Fig. 6.4. In the dashed plot, τ_n is not modified. The percentage of events rejected using a χ^2 cut-off of 16 are shown also. Although the shapes of the plots change with the error, using a χ^2 cut-off of 16 the loss of events is insignificant and shows that errors as

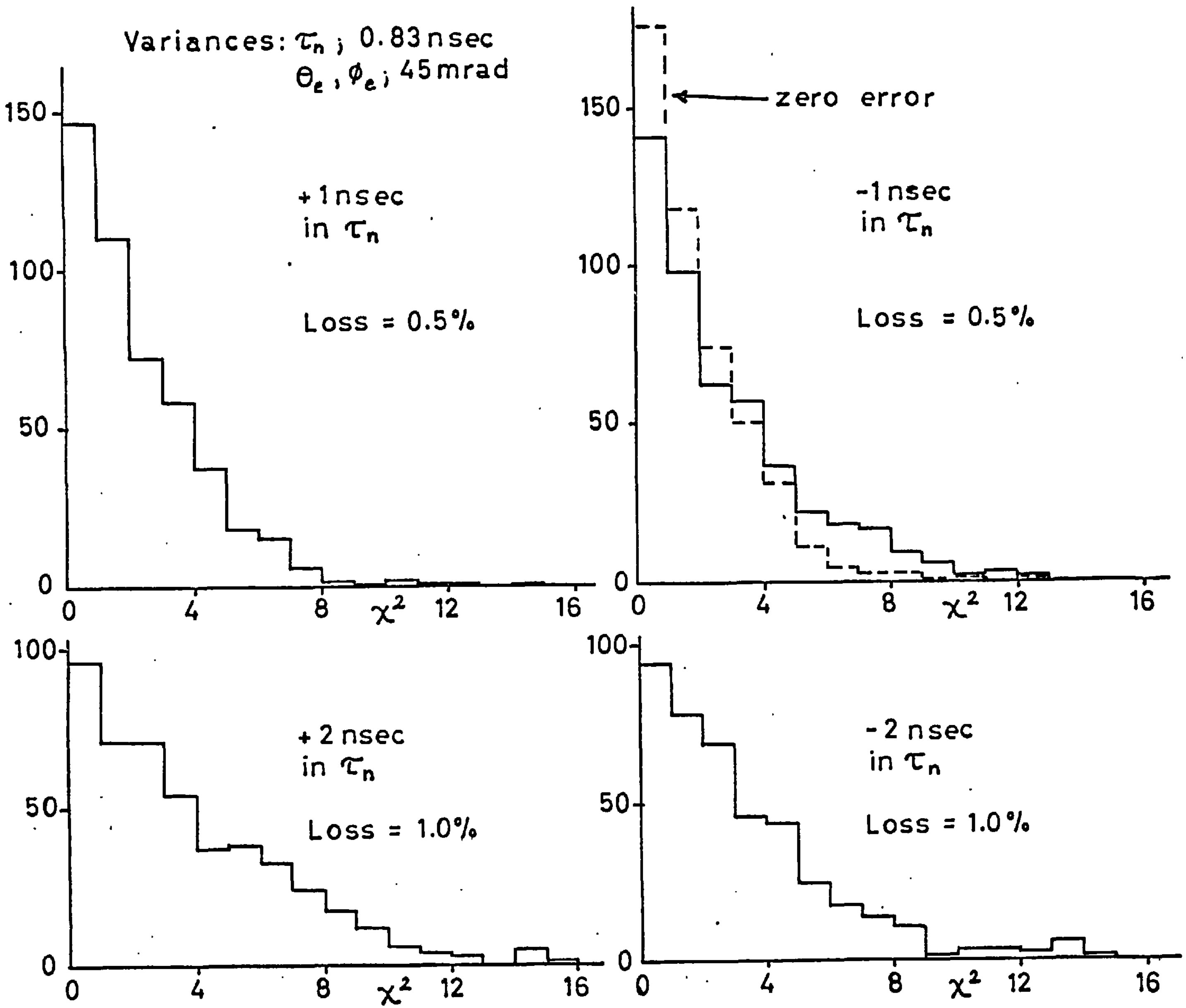

Fig.6.4 χ^2 distribution for Monte Carlo $\phi \to e^+ + e^-$ events with systematic errors in the time of flight parameter, τ_n.

large as 6.6 τ_n digits (1 ns = 3.31 digits) could be tolerated.

Similarly, distributions are shown in Fig. 6.5 for events with systematic errors of 90, 45, -45, -90 mrad added to the values of ϕ_{e_1}. The same error is subtracted from ϕ_{e_2} simultaneously so, for events in which the decay plane is near horizontal, these errors correspond roughly to closing the opening angle by 180, 90, -90, -180 mrad respectively. Again the losses are small. In the above calculations, the variance in the electron angles was 45 mrad, but, to fit the measured events, 80 mrad was used. With the larger tolerance systematic errors of the magnitudes tested would be less important. The χ^2 distributions, using 80 mrad, are shown in Fig. 6.6.

Systematic errors in the 'θ' angles of the electrons were unimportant as these merely changed the orientation of the decay plane and as the transverse momentum was small the effect on the 'fit' was insignificant. For the same reason the neutron angles were not critical but these were fixed by the locations of the counters and not subject to systematic errors. The beam momentum, set by reference to the n.m.r. frequency, could have a small error only.

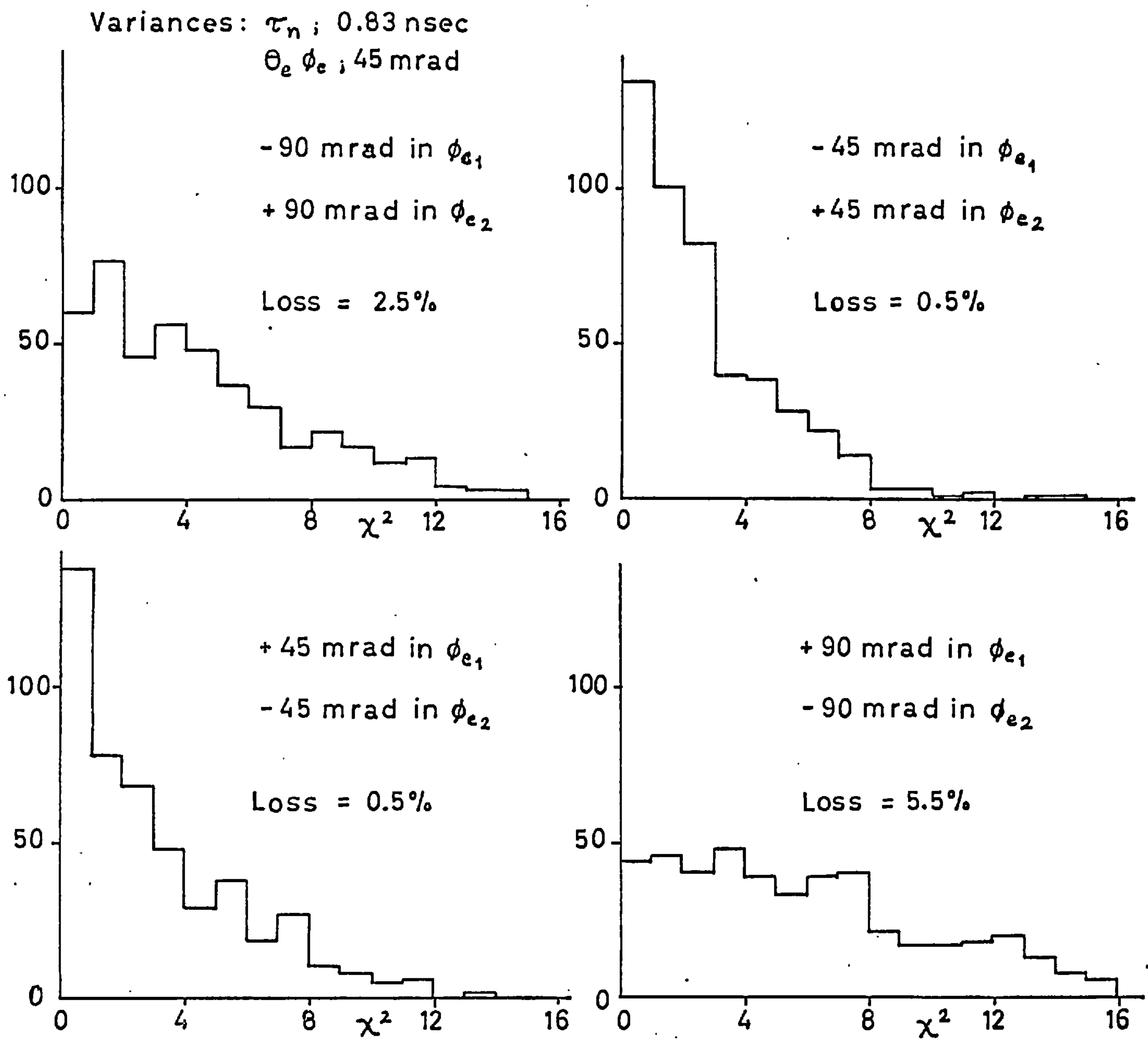

Fig. 6.5

χ^2 distributions for Monte Carlo $\phi \rightarrow e^+ + e^-$ events with systematic errors in the eletron angles, ϕ_{e_1}, ϕ_{e_2}

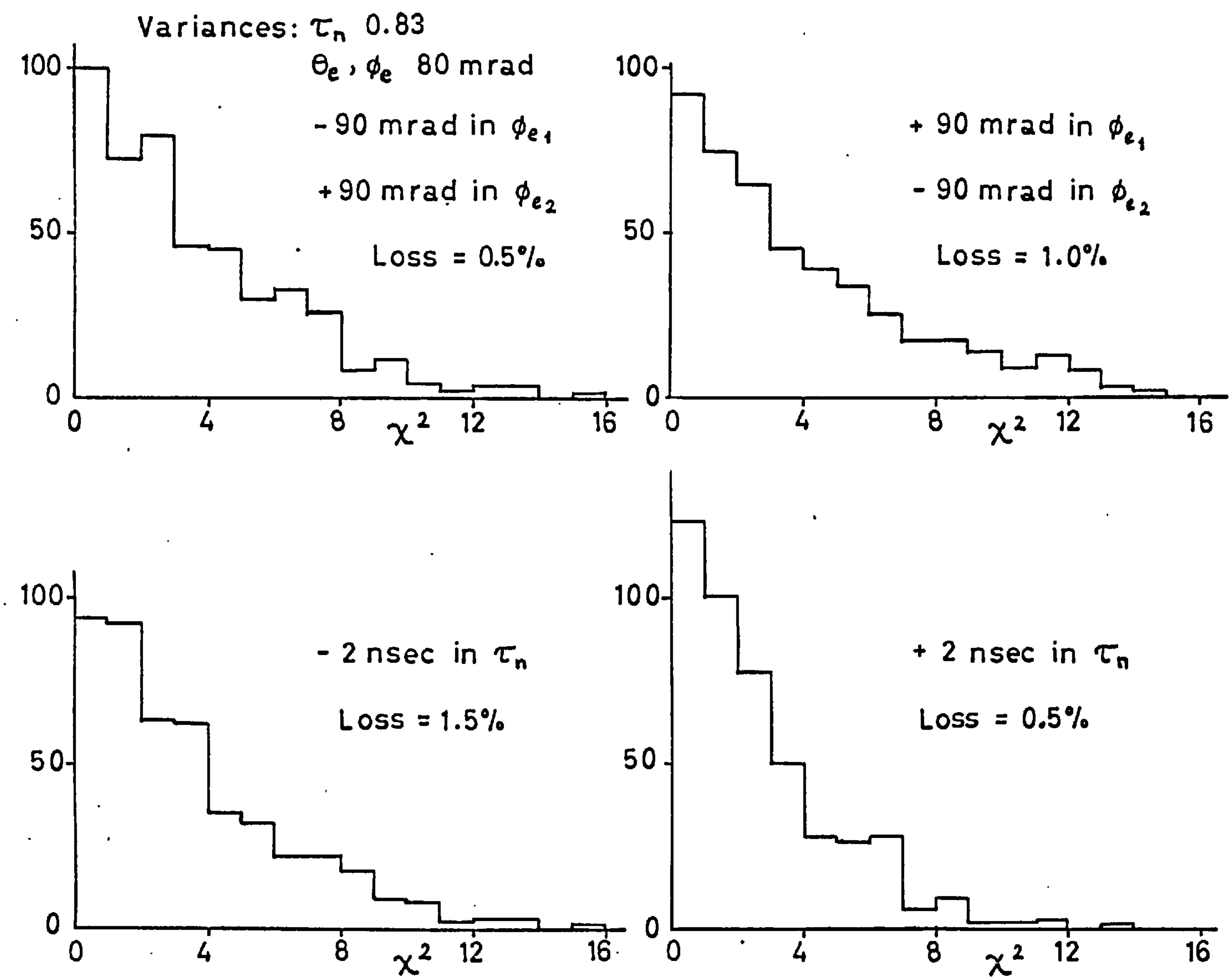

Fig. 6.6

χ^2 distributions for Monte Carlo $\phi \rightarrow e^+ + e^-$ events with systematic errors with variances of 80 mrad in θ_e and ϕ_e

τ_n had been found to drift slowly by $\pm$ 2 digits but as an error $\pm$ 6.6 digits could be tolerated, this, therefore, could not lead to a large loss of events. The vertex distributions had shown that any errors in the reconstructed values of the electron angles were less than 45 mrad and, as systematic error of $\pm$ 90 mrad was acceptable, there was no appreciable loss from this source. Since τ_n and ϕ_e were the only parameters in which systematic errors could both occur and affect the fit appreciably, and any errors present were below the level at which a significant number of events were lost, the reconstruction and fitting programs were proved to be satisfactory and measured events for which the value of χ^2 was < 16 were considered consistent with the hypothesis $\pi^- + p \longrightarrow e^+ + e^- + n$.

6.5 Data reduction using the reconstruction and fitting programs

The 349 events surviving the shower criteria were subjected to the reconstruction and fitting programs using the variances and limits discussed. In addition to the χ^2 stipulation, the events were required to satisfy a 'coplanarity' requirement. This demanded that the angle between the plane of the decay products and the ϕ direction, as computed from the known neutron parameters, should be zero within 3 standard deviations. The losses incurred by this limit are included in the losses corresponding to various systematic errors given in Figs. 6.4-6.

The results of the kinematic analysis are shown in Table 6.1.

Table 6.1

	Non-hydrogen	Non-Coplanar	Fit $\chi^2 > 16$	Fit $\chi^2 < 16$
Ø	37	32	47	50
K	35	36	84	28

Monte Carlo tests showed that the fitting program did not favour any particular range of time of flight or beam momentum and therefore was unbiased towards Ø or K.

10" x 8" prints were made of the 78 events selected by the first and second criteria and the fitting program. During the application of the first and second criteria the code letters, 'Ø' and 'K', had been visible, but the equality of the numbers had shown there had been no bias towards either class and, as the number of events was large, the probability of associating particular events with either signal or background was considered negligible. After fitting kinematically, the number of candidates was smaller and, to avoid bias towards ϕ or K, the next stage was performed by a non-physicist: the prints were checked to be the correct frames, the digital data and code letters were obliterated with black adhesive tape, the events were shuffled and finally each print was given a new number. There was no list of new/old numbers.

6.6 The third criteria

During the third measurement it was noted that many events which had been recorded as 'fits' were obviously not electron pairs and the application of further criteria was anticipated, but, as the numbers were small, further criteria designed using the 78 events would be subjective. To avoid using the 78 the criteria were derived from non-fitting events since the 'showers' in both 'non-fits' and the non-electron events in the 78 would be mainly from the same background processes. Prints were made of 47 events with values of χ^2 in the range $16 < \chi^2 < 32$. Of these 47, 17 events failed the second criteria and so only 30 were used in the third criteria design. (Not all of the 47 had been examined during the third measurement as this was unnecessary in cases where earlier measurements were consistent, hence the high second criteria failure rate at this stage). Again the demands on the criteria were that they should be objective, of small loss to electrons, and effective in reducing the background events.

Several of the 30 high-χ^2 events showed π-like tracks, i.e. connected tracks, each leading into the next, although not necessarily straight. In an attempt to reject events with such tracks the asymmetry requirement was extended to demand:

"If a shower shows 4 or more tracks that are 'connected' in both views, then some secondary track(s) must be present on both sides of this track in each view; code πA/S."

When applied to the 30 frames, this criterion rejected 8 events. Using the calibration electrons the corresponding loss was found to be 1 $\pm$ 1% at 650 MeV/c and 4 $\pm$ 1.4% at 450 MeV/c in addition to the losses incurred by the second criteria. Although this loss due to πA/S was higher than from any other criterion, no other way of objectively eliminating a large fraction of the events with obvious pions was evident.

The 'showers' on several other prints fell within another class which was characterised by a lack of tracks in the final two chambers. Inspection of the prints indicated that the rejection of events without tracks in the last two chambers would form a powerful criterion. From the calibration electron photographs the events without tracks in the 5th or 6th chambers were examined. The numbers are shown in Table 6.2 subdivided into the number of tracks in the 4th chamber.

Table 6.2

No. of tracks in 4th chamber	No. of events with no tracks in 5th and 6th chambers	
	450 MeV	650 MeV
0	2	2
1	3	0
2	3	2
3	2	1
4	2	0
5	1	1
Total no. in sample	270	200

One of the backgrounds without tracks in chambers 5 and 6 was from pions which stopped in the 3rd or 4th lead plate. As events from this source tended to have not more than one track in the 4th chamber and also, to keep the electron loss small, events with 2 or more tracks in the 4th chamber were retained. Formally the criterion required "more than one track in the fourth chamber if there was no evidence of a shower beyond that stage; coded '000' or '100' as appropriate". Events rejected under '000' or '100' were already inhibited partially as they had no track through the outer shower counter. The additional loss introduced by this criterion was 1.8 $\pm$ 0.9% at 450 MeV and 1.0 $\pm$ 0.7% at 650 MeV.

The two criteria above rejected more than half of the 30 high-χ^2 events. Other events could be rejected, but for individual reasons only. If the criteria were equally effective on the 78 events, then only $\lesssim 40$ events would remain. Were there to be (say) 20 examples of $\phi \longrightarrow e^+ + e^-$ then the difference in the numbers of ϕ and K events would be ~ 3 standard deviations; a difference of 12 events would still be just significant (2 Std. dev.).

The pion rejection efficiency of the combined criteria was found using 2000 photographs of 650 MeV/c pions. The photographs had been taken during the calibration electron experiment (see section 5.2) using the Cerenkov counter in anticoincidence to reject electrons and muons. Five examples were found which satisfied all the shower requirements and therefore simulated electrons. Allowing for both chamber banks in the ϕ decay, this indicated an overall discrimination against pions of better than 1 in 10^5.

6.7 Application of the third criteria

The third criteriawere applied to the 78 events with $\chi^2 < 16$ by four physicists working independently and, as the ϕ/K information was concealed, there was no bias towards either class. The fate of the events was decided in all but six cases which depended on whether a track was within 5.4 cm of the incident track. For these six, the original negatives were projected onto the DMAC table by a technician who ensured that the ϕ or K data remained obliterated. Using the original templates physicists concluded the fate of these events.

The result of the application of the third criteria is shown in Table 6.3.

Table 6.3

Criterion	No.	Criterion	No.
accepted	27	Dalitz pairs	7
$\pi A/S$	21	$\geq$ 8 tracks	3
000	9	2nd criteria	1
100	10	Total	78

The eleven events which had survived unjustly to this stage were from films which had shown no discrepancies between first and second measures and therefore had not been examined during the third measure. Twenty-seven candidates remained which satisfied all the shower and kinematic criteria, yet still several events in these '27' did not resemble electron pairs. To avoid bias, the decision whether or not to apply any further criteria had to be taken before the identity of the events was revealed. A surplus of 11 or more ϕ events would appear as 2 standard deviations and permit a branching ratio to be quoted. A smaller difference would establish an upper limit only.

As the loss of electron pair events would become significantly less certain if further criteria were applied, we decided to use the 27 events to quote either a branching ratio or an upper limit, depending on the significance of any difference between the numbers of ϕ and K events, but in addition, to make a further selection to search for positive evidence of the decay, $\phi \longrightarrow e^{+} + e^{-}$.

6.8 The final selection of events

Prior to identification, events which could in no way be faulted were selected from the '27'. This final selection consisted of a number of stages. First of all the 27 events were examined independently by four physicists who graded the events subjectively into four classes and ascribed points as follows:

a) 'Definitely' an electron pair - 3 points

b) 'Probably' " " " - 2 "

c) 'Possibly' " " " - 1 "

d) 'Not' " " " - 0 "

Thus from the four independent assignments, each event could receive a maximum of 12 points. Events with 4 or less points were considered unlikely to be electron pairs and were rejected.

Secondly, events suspected of being 'wide angle Dalitz pairs' were rejected. Such events could arise as follows:.

one electron from a Dalitz decay of a neutral pion assumes almost the full energy of the pion and travels close to the parent direction; the other electron of low energy does not pass beyond the first lead plate yet causes a second track which, although not close to the 'candidate', has a common vertex.

Thirdly, tighter requirements were made on the hydrogen vertex, which allowed no tolerances around the physical edges of the target and also required that the value of $\delta\theta$, the angle through which the tracks had been altered to produce a vertex, should not exceed 60 mrad.

Finally more severe demands were made on the kinematic fit. The variance allowed in the measured angles of the electrons was reduced from 80 mrad to the 45 mrad that had been indicated by the vertex distributions (see section 6.3). Also the χ^2 cut-off was lowered from 16 to 12. Neither the geometric nor the kinematic requirements could be applied until the events had been identified, and therefore the limits to be applied were specified in detail prior to unveiling the ϕ/K information.

No attempt was made to correlate the shower structures with the computed electron momenta since this would be of little practical use as the subjective selection would already have inhibited weak electron showers. The loss of genuine pairs incurred during the final selection was uncertain and no attempt was made to estimate it.

6.9 The relation between ϕ and K events

As $\phi \longrightarrow e^+ + e^-$ events, if present, were to be shown as a difference in the final numbers of ϕ and K events, it was necessary to know the relation between ϕ and K triggers. Roughly, each frame was equally likely to be an 'electron-pair' from a process other than ϕ decay, and hence the correspondence between ϕ and K was given approximately by the relative number of frames used. The 'ϕ' candidates were selected from 88,600 frames and the 'K' candidates from 105,300 frames. Hence in determining the final difference, the number of K events selected should be reduced by $\sim 88,600/105,300 = 0.84$.

As the trigger rate was a function of shower counter bias, the above method of normalisation was approximate and a more sophisticated method was used which related the total beam counts $\Sigma\pi_{\phi}$ and $\Sigma\pi_K$, in the ϕ and K runs. Had the triggers populated the time of flight gates uniformly, the relation between $\Sigma\pi_{\phi}$ and $\Sigma\pi_K$ would have been simply the ratio of the gate widths, but as the distributions were not flat the ϕ:K relation was found as follows.

The distributions of τ_n, the digital time of flight record, are shown in Fig. 6.7 for samples of both ϕ and K films (1 nsec = 3.31 digits). On the τ_n scale the fast peak corresponds to $\tau_n = 117$. As τ_n was found to be subject to drifts of $\pm$ 2 digits, the K gate τ_n distribution was positioned so that the estimated τ_n values of the fast peaks in both samples coincided. This uncertainty in the true value of τ_n had a negligible effect on the kinematic fit (see section 6.4). The error in the relative location of the ϕ and K τ_n spectra, which was found by reference to the calibration fast peak and white spectra taken during the data runs, was estimated to be $\pm$ 1 digit. To avoid effects due to the edges of the histograms, we supposed that both the ϕ and K runs had employed the same gate with infinitely sharp edges at τ_n = 80 and 95, then, ignoring the small phase space difference and statistical fluctuations, the

Fig. 6.7 The τ_n distributions of ϕ and K triggers, normalised to the same number of counts in bins 80-95 inclusive

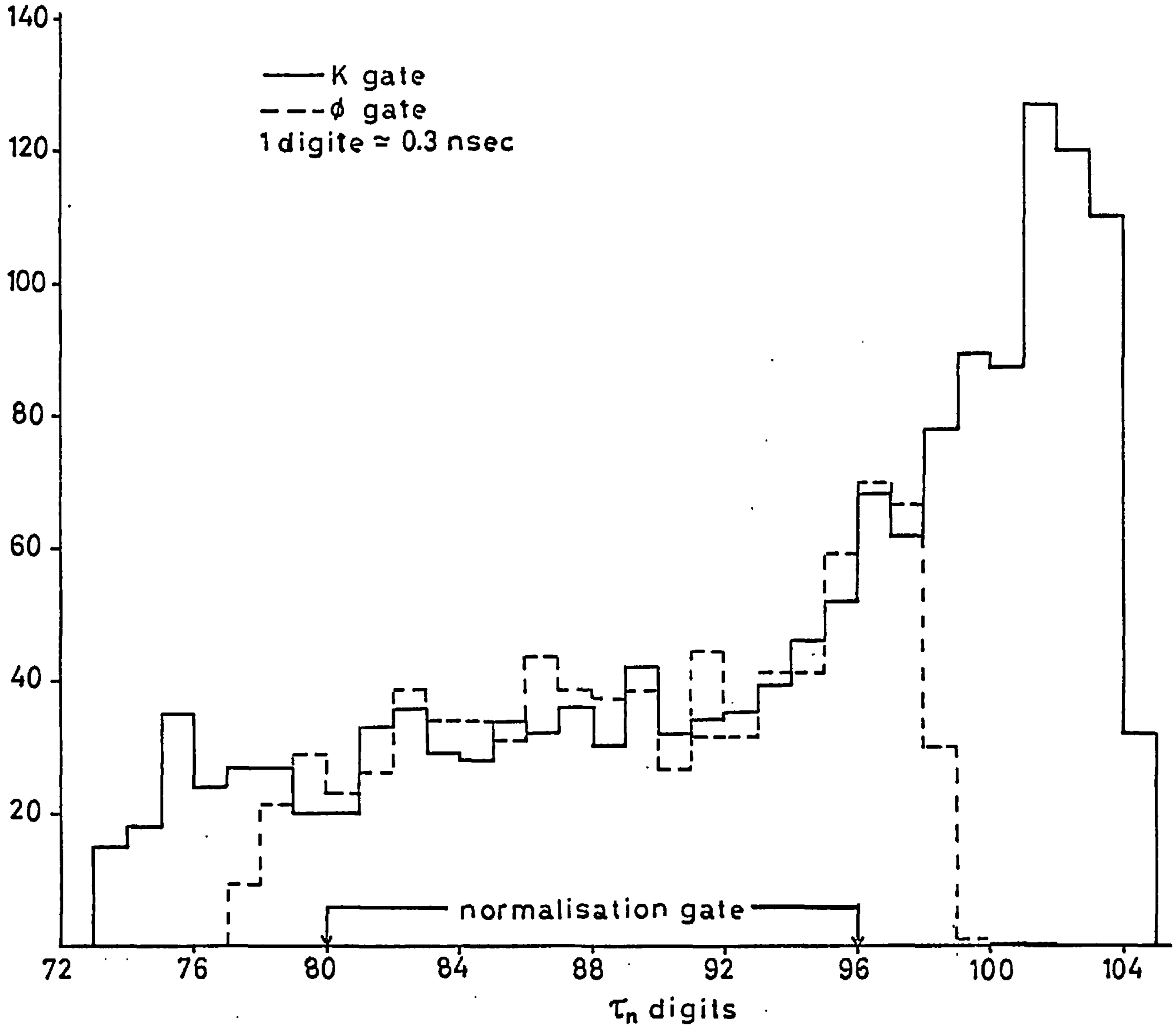

same number of beam particles would yield the identical number of events at either momentum. In Fig. 6.7 the ϕ spectrum is shown superimposed on the K spectrum after normalising to the same number of events in bins 80-95 inclusive.

Since the fitting program had a uniform response at all times of flight and beam momenta used, and as the nature of the background processes was estimated to be constant in the kinematic regions considered, the correspondence between ϕ and K events was the ratio, R_1, of the areas of the normalised ϕ and K spectra. We define: $\sum_i^j A$ = the number of events in bins i to j inclusive, ($A = \phi$ or K). The normalised number of ϕ events in the plot is given by $\sum_{all}\phi \times \sum_{80}^{95} K / \sum_{80}^{95}\phi$; and therefore,

$$R_1 = \frac{\sum_{all}\phi}{\sum_{all}K} \times \frac{\sum_{80}^{95} K}{\sum_{80}^{95}\phi} \qquad \ldots\ 6.2$$

The inverse of this ratio, $1/R_1$, was found to be $1.84 \pm 10\%$ where the error was estimated as follows.

Due to the uncertainty of one digit in the relative position of the spectra on the τ_n scale the value of $\sum_{80}^{95}\phi$ could vary from $\sum_{81}^{96}\phi$ to $\sum_{79}^{94}\phi$. To reduce statistical fluctuations in computing the error, the number of events in each bin at the edges of the '80-95' gate was estimated as the mean of the counts in the relevant bin and its adjacent bins. The error was found to be ± 6%, which, combined with the statistical error of 7.5%, gave a total error of about 10%.

The K runs took 3.54×10^{10} beam particles, but had the ∅ gate been used throughout, then 1.84 ± 10% as much beam would have been required. Thus the equivalent number of beam particles used in the runs below threshold was 6.52×10^{10} ± 10%. In the signal runs 6.03×10^{10} particles had been used and thus each K candidate was worth only 6.03/6.52 ± 10% (= 0.925 ± 10%) of a ∅ candidate. This is consistent with the ratio of the numbers of frames employed.

Analysis of the ∅ search data had shown that the change in the level of the pion background in going from 1540 to 1580 MeV/c was small and could be neglected compared to the 10% error above.

During the data taking the time of flight gate used in the signal runs had been set about 0.6 nsec closer to the fast peak than intended. From the Monte Carlo calculations, only 3% of accepted $\phi \longrightarrow e^+ + e^-$ events fell in the two channels at the edge of the gate near the fast peak. As events in these channels had only a remote chance of being $\phi \longrightarrow e^+ + e^-$, it was decided, prior to the identification of the prints, that such events would be removed from the 'ϕ' samples, treated as background events and included with the 'K' events.

The fraction of the triggers in the two channels concerned was found to be $(14 \pm 1)\%$. Allowing for the exchange of 14% of the events, the effective number of beam particles used at the two momenta becomes $(5.2 \pm 0.3) \times 10^{10}$ in the signal runs and $(7.4 \pm 0.9) \times 10^{10}$ in the runs below threshold.

6.10 The result of the identification of the events

Once the programme of the various geometric and kinematic limits pertinent to the final selection had been specified in detail, the identities of the 27 events were revealed. 20 events were found to be from the runs above threshold and 7 from the runs below threshold. Three of the 20 ϕ events had times of flight in the channels which were to be considered as background and therefore in quoting a Branching Ratio the numbers of events used were 17 events in the signal from $(5.2 \pm 0.3) \times 10^{10}$ beam particles and 10 events in the background from $(7.4 \pm 0.9) \times 10^{10}$ beam particles. After normalisation, this yielded an excess of 10.0 ± 4.8 in the signal runs.

Nine events were picked by the subjective selection discussed in section 6.8. These were found to comprise 8 events from signal and 1 from background, which, when normalised, corresponded to 8 and 0.7 respectively. Although the efficiency of this selection was unknown, it was without bias and therefore the difference between signal and background could only be explained by: a statistical fluctuation, another decay of the ϕ meson, or the existence of the decay, $\phi \longrightarrow e^{+} + e^{-}$.

A statistical explanation is ruled out as, were there to be no real effect, the probability of an asymmetry of the magnitude found is less than 0.1%. The most likely ϕ decay to simulate an $e^{+}e^{-}$ event is $\phi \longrightarrow \pi^{+} \pi^{-} \pi^{0}$ in which the charged pions satisfy the kinematics and the photons from the π^o decay lie close to the pions. Less than 0.1 event is estimated to originate from this source. We conclude, therefore, that we have observed examples of the decay $\phi \longrightarrow e^+ + e^-$. The photograph in Fig. 6.8 is one of the $\phi \longrightarrow e^+ + e^-$ candidates. The shower in the right-hand views (lower in photograph) is typical of an electron of $\sim$600 MeV. In the other pair of views, the shower is crossed by a non-interacting straight track which is characteristic of a pion or muon. In assessing the shower this track is ignored. The non-ionising link in the third chamber is also characteristic of an electron shower.

6.11 Normalisation

In order to quote a Branching Ratio it was necessary to determine the number of potential $\phi \longrightarrow e^+ + e^-$ events. This was done in two stages. First from the analysis of the ϕ search experiment, we found the number of effective ϕ's produced and then we considered the detection efficiency for the e^+e^- decay.

The curve shown in Fig. 6.9, taken from the ϕ search experiment,[4] shows, as a function of beam momentum, the

Fig. 6.8

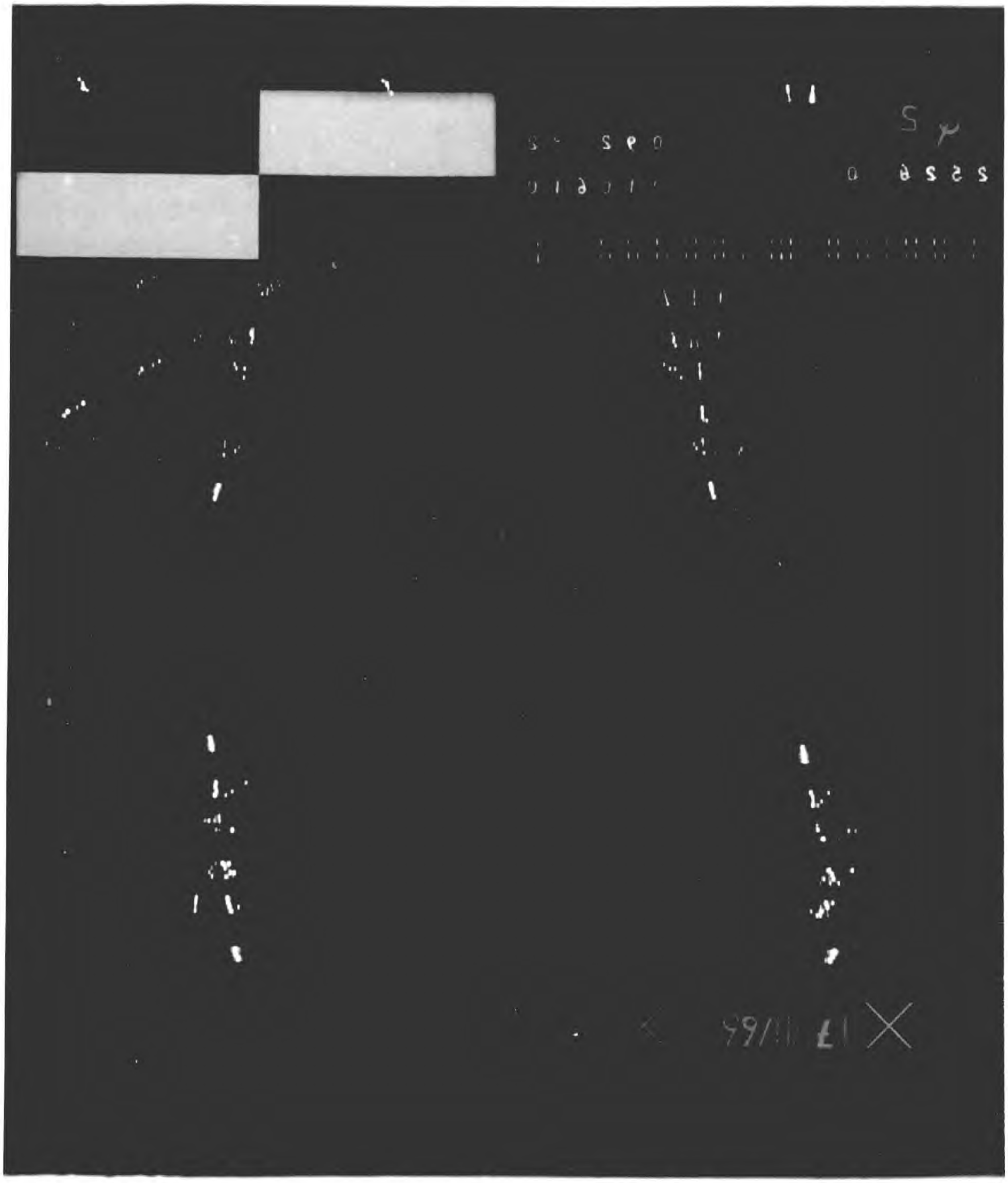

Fig. 6.9 Experimental yield of K^+K^-n events as a function of beam momentum

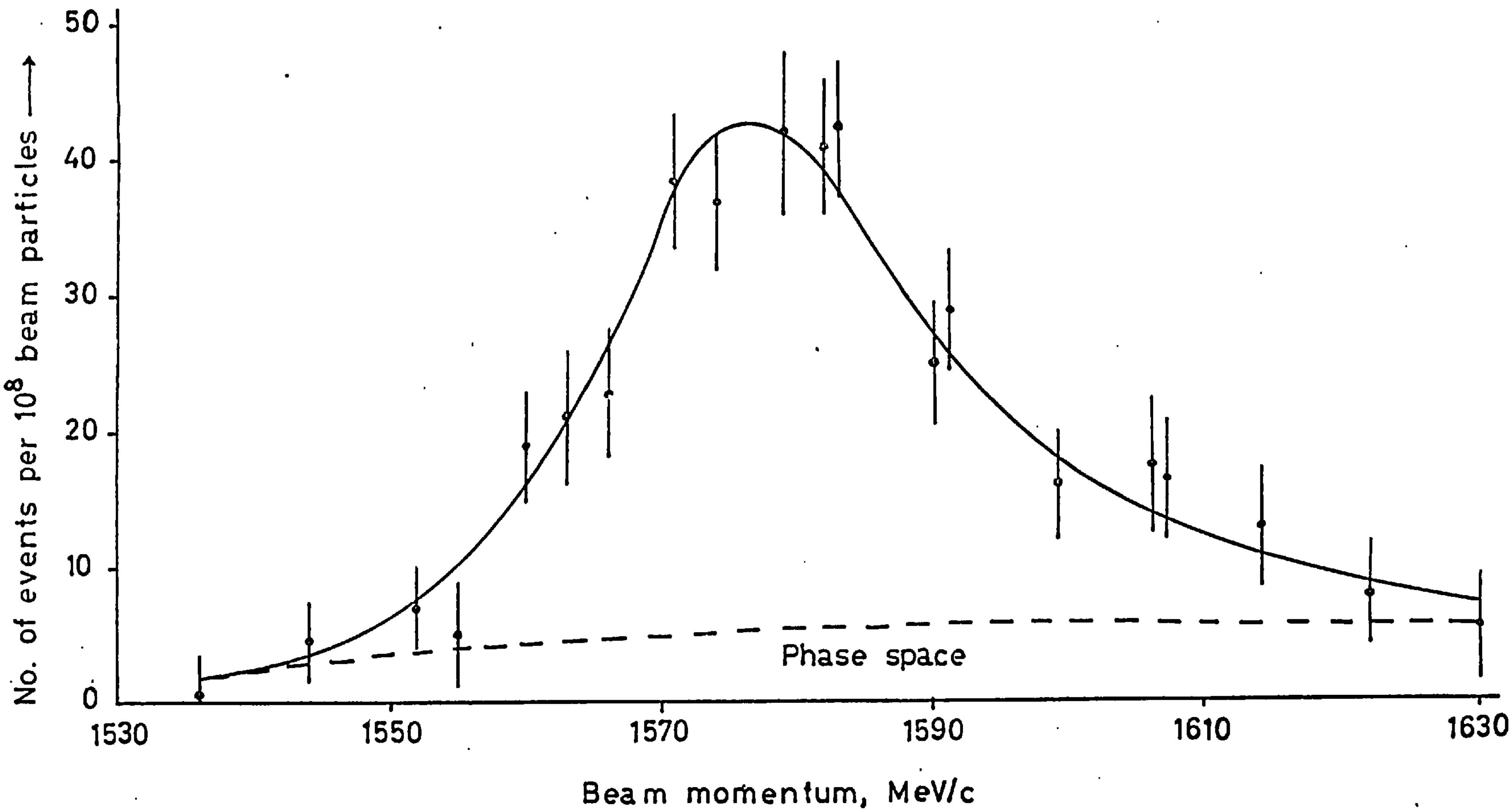

number of $\phi \longrightarrow K^+K^-$ triggers detected per 10^8 beam particles after allowing for high beam rate effects. By using the ϕ search data at this stage rather than the cross-section, the beam composition and the efficiency of the neutron counters were irrelevant. Consider the central momentum channel at p_π = 1582 MeV/c. From Fig. 6.9, the number of $\phi \longrightarrow K^+K^-$ detected per 10^8 beam particles is 33.5 ± 12%. In the ϕ decay, the time of flight gate used was narrower and had this gate been applied in the ϕ search, the Monte Carlo time of flight distribution showed the corresponding number of triggers would have been only 30.5.

The geometric efficiency of the K^+K^- detection system was only 35%. In addition there was a (3 ± 3)% loss of events due to δ-rays caused by kaons in the Cerenkov counter and therefore, had the kaon detectors been perfect and covered 4π stereradians, 88.7 triggers would have been recorded. The ratio, $\phi \longrightarrow K^+K^-/\phi$-total, is given[25] as 0.48 ± 0.03 and therefore, the ϕ decay experiment was sensitive to 184 ϕ's per 10^8 beam particles.

The curve in Fig. 6.9 had been corrected for occupancy (section 2.6) which was mainly due to casuals in the beam veto counter, A_o. In the ϕ decay the corresponding counter, A_{10}, also led to a loss of events. This loss was found from a comparison of the rate in the interactions monitor with its value at low beam intensity when the occupancy was negligible. The interaction rates are shown in Fig. 6.10 as a function of film number in chronological order. The rate with low beam is shown for comparison. The deviation from the low beam rate value gives a measure of the occupancy which was found to be 7 $\pm$ 2% and hence the number of ϕ's to which the ϕ decay experiment was sensitive was reduced by this amount. Hence, allowing for the various errors in the factors used above, the ϕ decay experiment was sensitive to 171 $\pm$ 16.5% ϕ's per 10^8 beam particles at 1582 MeV/c.

The various factors used to derive the yield of useful ϕ's per 10^8 beam from the number of $\phi \longrightarrow K^+K^-$ triggers were not significantly dependent on momentum in the range considered and thus the yield in the other channels were obtained. The yield is shown in Table 6.4 for each of the three momenta used together with the total beam counts used. The product of the two terms is the estimated

Fig. 6.10 The measured interaction rate as a function of time. The occupancy is monitored by the deviation from the rate at low beam.

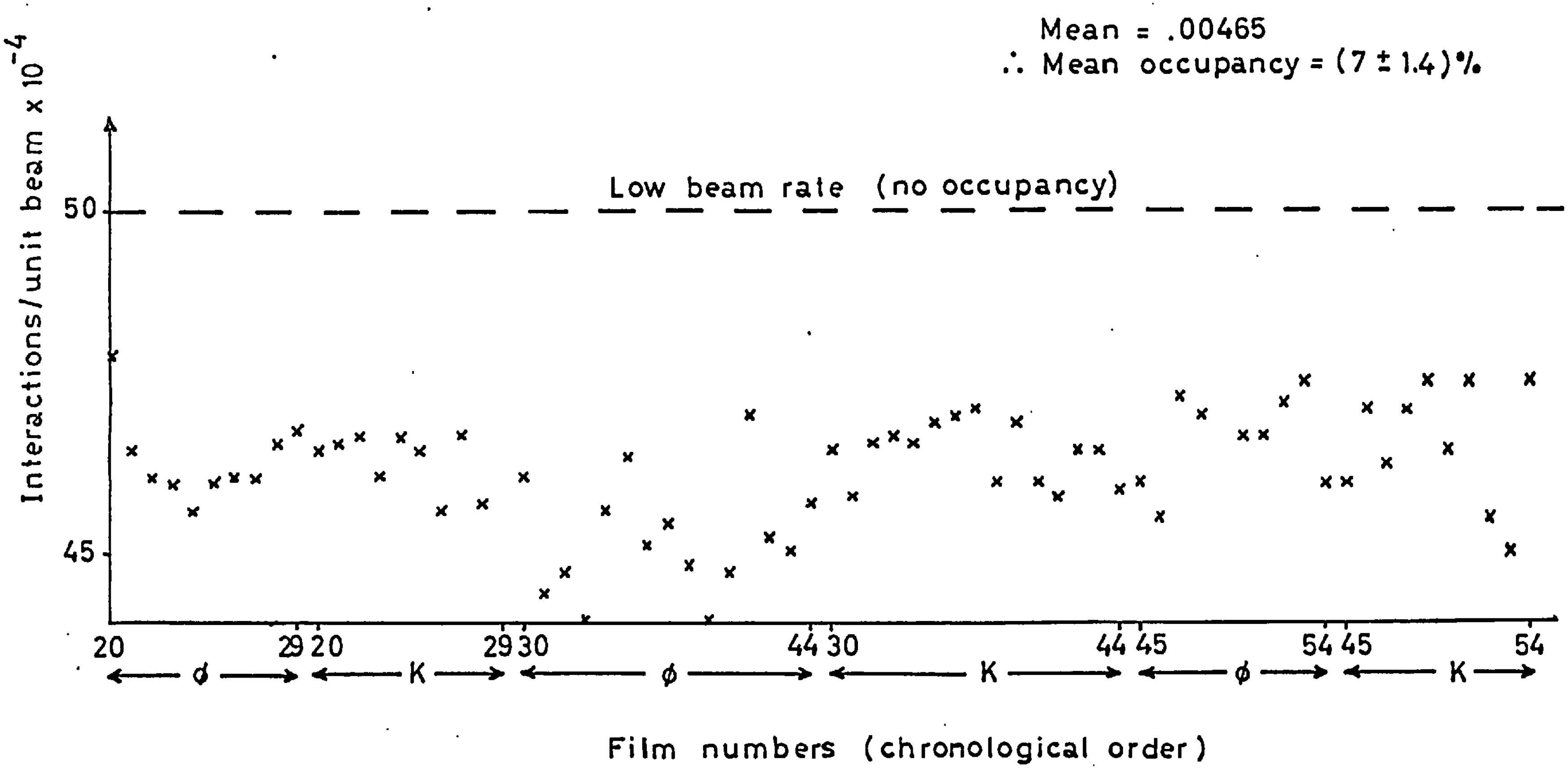

yield of ϕ's.

Table 6.4

Beam momentum	$\phi \longrightarrow K^+K^-$ detected/ 10^8 beam	Useful ϕ/ 10^8 beam	No. of beam x 10^8	No. of useful ϕ's produced
1574	37.1	189.5	185.5	35,200
1582	33.5	171.0	239.2	40,900
1590	21.9	112.0	178.8	20,000
				96,100

From the three momentum channels used, the total yield of ϕ mesons, where the corresponding neutron was detected within the time of flight gate used, was estimated to be 96,100 $\pm$ 17%.

We now proceed to determine the number of potential $\phi \longrightarrow e^+ + e^-$ candidates, i.e. the fraction of these 96,100 ϕ's which, if they all were to have decayed into e^+e^-, would have been detected by the apparatus. This fraction, f, or the detection efficiency is formed as the product of many individual efficiencies, f_i. The major factors discussed below enter at either the electronics stage or at the film analysis stage.

i) Losses due to the electronic trigger

a) The solid angle subtended by the chambers - $f_1 = 0.22$.

Using the simple S-wave model the fraction of $\phi \longrightarrow e^+e^-$ decays collected was 0.22. The justification for using the S-wave model is discussed in the next chapter.

b) The efficiency of the inner counters, S_3, S_4 - $f_2 = 0.975 \pm 0.015$

The combined inefficiency of the inner counters, due to the dead-times of the discriminators, was estimated to be $(2.5 \pm 1.5)\%$ from the known dead-times and counting rates.

c) The loss due to the shower counter biases - $f_3 = 0.88 \pm 0.045$

The losses at low and high biases were estimated to be $(9.0 \pm 3.5)\%$ and $(15.5 \pm 5.5)\%$ respectively (see section 4.6). Of the total beam used in the ϕ runs 56% was at low bias and 44% at high bias. The weighted mean loss was estimated to be $(12 \pm 4.5)\%$. Correlations between the trigger and criteria losses are considered later.

d) Losses from other sources such as an electron conversion before the inner chamber or a shower product in triggering a veto counter were negligible.

ii) Losses during the film analysis

a) Losses during the preliminary scan - $f_4 = 0.96 \pm 0.04$

The loss of electrons due to the very weak criteria of the first scan were small and are automatically included in f_5, the total criteria loss. The only loss considered in the first scan is due to the scanning efficiency.

9,000 frames were rescanned using the second criteria. One event, which failed the third criteria but should undoubtedly have been included in the candidates remaining after the second scan, was missed. The ϕ events were selected from $\sim$90,000 frames and therefore the corresponding loss to candidates selected in the second scan is 10 ± 10 events. Using the approximation that the kinematic and third criteria would reduce these ten events and the 248 second scan candidates proportionally, the loss is estimated to be $(4 \pm 4)\%$. Since the likelihood of overlooking an electron shower is less than for missing a candidate which satisfied the criteria for some technical reason, a 4% loss is probably an overestimate.

b) Losses incurred by the criteria - $f_5 = 0.92 \pm 0.08$

The loss due to the first and second criteria was estimated to be $7.5 \pm 3.5\%$ (see section 5.6). In addition there was the effect of the third criteria. For single electrons the loss additional to that of the former criteria was shown to be $(2 \pm 1.4)\%$ at 650 MeV/c and 5.8 ± 1.6 at 450 MeV/c (see section 6.6). To determine losses at other momenta, a linear dependence on momentum was assumed above 450 MeV/c. Thus the loss of $\phi \longrightarrow e^+ + e^-$ events was estimated to range from $(4 \pm 2.4)\%$ for a symmetric event with two 650 MeV/c electrons to $(5.8 \pm 1.6)\%$ for events with one 450 and one 850 MeV/c electron. As few events with greater asymmetry were encountered, the third criteria loss was taken as $(5 \pm 3)\%$ over the momentum range used. To find the overall loss due to the criteria this value was combined with the $(7.5 \pm 3.5)\%$ loss from the earlier criteria to give $(12.5 \pm 4.5)\%$.

There was some correlation between this loss and that introduced by the shower counter bias. An event with a weak shower was unlikely to cause a trigger; this same event, had there been no ΣM bias and a photograph been taken, would probably have failed on criteria grounds.

Thus, as many events which would fail the criteria were not photographed, the loss due to the criteria was less than the estimated $(12.5 \pm 4.5)\%$. As insufficient data were available, only a crude estimate of the overlap between the two losses was possible. To estimate the overlap, we considered events symmetric in momentum and one of the 650 MeV/c electrons to be 'average' and thus produce a pulse height of ~ 6.3 min I. in the relevant counters. To initiate a trigger, the second electron would need to supply the balance to reach the ΣM threshold. Inspection of the eight 650 MeV/c calibration electrons which failed the criteria indicated the correlation was $\sim 30\%$ and hence the effective loss due to the criteria was $\sim 8\%$ and not $12.5 \pm 4.5\%$. In view of the gross uncertainty in this estimate the value used was $(8 \pm 8)\%$.

c) Loss due to casual Dalitz pairs - $f_6 = 0.99 \pm 0.01$

This loss was found to vary from $(0.5 \pm 0.5)\%$ to $(1.3 \pm 0.7)\%$ (see section 5.7) depending on the beam rate. As this loss is small compared to others, the value used was $(1.0 \pm 1.0)\%$.

d) Loss due to rejection of events with ≥ 8 tracks in the inner chambers - $f_7 = 0.95 \pm 0.01$.

See section 5.7 for the estimation of this loss.

e) Loss due to spark chamber inefficiency - $f_8 = 0.96 \pm 0.03$.

Chamber efficiency is a function of the number of tracks supported, therefore in calculating the overall efficiency we considered the sum, $\sum_i g_i \eta_i$, where g_i is the fraction of events with i tracks in one of the inner chambers and η_i is the chamber efficiency when supporting i tracks. The distribution of g_i was averaged over several samples of film and, by combining with the values of η_i deduced from Fig. 5.2, the value of $\sum_i g_i \eta_i$ was found to be $(2.1 \pm 1.7)\%$ for events with only one spark in the chamber and $\sim 8\%$ for events with only two sparks. The former class constituted a direct loss which, allowing for both sides, was $(4.2 \pm 3.4)\%$. In 50% of the latter class the two sparks were adjacent and, allowing for both sides, the resulting poor measurement led to a possible loss of events of up to $\sim 8\%$, but as a variance of 80 mrad was used in the electron angles the actual loss was considered negligible.

f) <u>Loss due to limits in the reconstruction and fitting programs</u> - $f_9 = 0.99 \pm 0.01$.

In the absence of large systematic errors these losses were estimated to be $\sim 1\%$.

All events, once accepted by the first scan, were checked at least twice and therefore the possibility of erroneous rejection was considered negligible.

The value of f $(= \prod_i f_i)$ was found to be $0.15 \pm 10.5\%$. Thus, from the $96{,}100 \pm 17\%$ useful ϕ mesons produced in the signal runs, we derived the number of potential $\phi \longrightarrow e^+ + e^-$ events to be $14{,}300 \pm 19.5\%$.

CHAPTER 7

RESULTS AND COMPARATIVE DISCUSSION

7.1 The branching ratio and partial width, discussion

After subtraction of the background, only 10.0 ± 4.8 events from the 88,000 photographs taken above the ϕ threshold were found to be consistent with the hypothesis

$$\pi^- + p \longrightarrow n + \phi, \quad \phi \longrightarrow e^+ + e^- \qquad \ldots\ 7.1$$

The number of potential $\phi \longrightarrow e^+ + e^-$ events was estimated to be 14,300 ± 2,800 and therefore we estimate the branching ratio to be

$$BR = \frac{10.0 \pm 4.8}{14,300 \pm 2,800}$$

$$\frac{\Gamma(\phi \longrightarrow e^+ + e^-)}{\Gamma(\phi \longrightarrow \text{total})} = (7.0 \pm 3.6) \times 10^{-4} \qquad \ldots\ 7.2$$

From the current estimate[25] of 3.4 ± 0.8 MeV/c^2 for $\Gamma\phi$ we deduce a partial width of $\phi \longrightarrow e^+ + e^-$ of 2.4 ± 1.4 KeV/c^2.

The value for the photon - ϕ meson coupling constant, γ_ϕ, was determined using equation 1.12; thus

$$\frac{\gamma_\phi^2}{4\pi} = 1.9^{+2.6}_{-0.7} \qquad \dots 7.3$$

Our value for the branching ratio is subject to certain assumptions. First the value used for the ratio,[25] $(\phi \longrightarrow K^+K^-)/(\phi \longrightarrow \text{all known modes}) = 0.48 \pm 0.04$, may be revised as further decay modes are detected. Secondly, no allowance has been made for radiative corrections, but these have been estimated[37] and in our case are negligible ($\sim 4\%$). Finally in determining the acceptance of the electron detection system, S-wave production and decay were assumed. The assumption of S-wave production can be justified from the ϕ search results and since the ϕ mesons were produced close to threshold. The effect of anisotropic decay is considered below.

Angular distributions are defined such that

$$\int W(\theta^*, \phi^*)\, d\Omega = 1 \qquad \dots 7.4$$

where θ^* and ϕ^* are defined in Fig. 7.1 and are measured in the centre of mass of the e^+e^- pair.

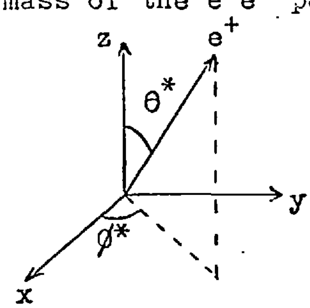

Fig. 7.1 The beam direction is taken along the z-axis and the normal to the production plane along the y-axis.

It follows from equation 7.4 that for isotropic decay $W(\theta^*, \phi^*) = 1/4\pi$.

We define $W_{KK}(\theta^*, \phi^*)$ to be the angular distribution for the decay of a vector meson into two spinless particles, e.g. $\phi \longrightarrow K^+K^-$, and $W_{ee}(\theta^*, \phi^*)$ to be the corresponding distribution for the leptonic decay mode. The two are related via:[38,39]

$$W_{ee}(\theta^*, \phi^*) = \frac{3}{8\pi}\left\{1 - \frac{W_{KK}(\theta^*\phi^*)}{N}\right\} \qquad \dots 7.5$$

where N is a constant which can be derived from the normalisation condition (7.4) and is found to be $3/4\pi$. From equation 7.5 it follows that if the K^+K^- decay is isotropic, then the same is true for the electron-positron decay. However to treat anisotropy, we consider the effect of a $K\bar{K}$ angular distribution of the form

$$W_{KK}(\theta^*, \phi^*) = A(1 + a\cos^2\theta^*) \qquad \dots 7.6$$

where A is a normalisation constant which can be found from equation 7.4 and yields

$$W_{KK}(\theta^*, \phi^*) = \frac{1}{4\pi(1 + a/3)}\left\{1 + ax^2\right\} \qquad \dots 7.7$$

where $x = \cos\theta^*$.

From Monte Carlo calculations, the range of $\cos\theta^*$

accepted was found to be $-0.55 < \cos\theta^* < 0.55$, and, assuming complete azimuthal coverage, the fraction of events accepted, is estimated to be given by

$$\eta = \int_0^{2\pi} d\phi^* \int_{-0.55}^{0.55} \frac{3}{8\pi} \left\{ 1 - \frac{4\pi}{3} \cdot \frac{(1 + ax^2)}{4\pi\,(1 + a/3)} \right\} dx \qquad \ldots 7.8$$

which leads to

$$\eta = \frac{1}{2} \cdot \frac{1}{1 + a/3} \left[(2 + a)x - \frac{ax^3}{3} \right]_0^{0.55} \qquad \ldots 7.9$$

From the analysis of the KK angular distributions in the ϕ search the best fit to the data was found to be of the form given by equation 7.6 with a value for a of 0.7 ± 0.8.[40]

Using this value in equation 7.9 we find

$$\eta = 0.585^{+0.025}_{-0.035} \qquad \ldots 7.10$$

The value of η in the isotropic case, $a = 0$, as had been used in the Monte Carlo calculation of the chamber acceptance, is $\eta = 0.55$. Since the azimuthal loss is almost independent of the value of a we conclude that the effect of anisotropy is only $\sim (7 \pm 7)\%$ and can be neglected in comparison with the statistical error of our result.

7.2 Comparison with other experiments

The branching ratio found is consistent with the estimate of between (1.8 and 7.0) x 10^{-4} of Wehmann et al.[41] who examined muon pairs produced by a K^- beam at 12 GeV/c incident upon a carbon target. Twelve events were found in which the di-muon invariant mass was consistent with the decay $\phi \longrightarrow \mu^+ + \mu^-$. The main uncertainty arises from the lack of knowledge of the ϕ production cross-section. Our result is also consistent with the result of Astvakaturov et al.[42] who find $(6.6^{+4.4}_{-2.8}) \times 10^{-4}$. In this experiment using a pion beam at 4 GeV/c, electron pairs were detected using spark chambers and scintillation and Cerenkov counters. Five events were found with an invariant e^+e^- mass consistent with a $\phi \longrightarrow e^+ + e^-$ decay. The error quoted is purely statistical and no account is taken of the substantial uncertainty in the ϕ production cross-section. The data used are that of Hess et al.[28] who, on the basis of one event, quote a cross-section of 15 $\pm$ 20 μb.

Subsequent to the publication of our result[43] three further values for the branching ratio have been reported.

Zichichi et al.[44] found BR = $(4.5 \pm 1.7) \times 10^{-4}$. They used a pion beam at 1.93 GeV/c to produce ϕ mesons which were selected preferentially using neutron angular and time of flight information. The electrons were detected using a system of optical spark chambers, lead plates and scintillation counters. The showers were selected both on individual and total pulse heights from counters in the detection system. No mention is made of errors in the estimated detection efficiency. They find ten events in the mass range 1000-1040 MeV/c^2 compared to an average of 1 event in the adjacent mass bins. For normalisation, the data of Hess et al.[28] are used, who quote $\sigma(\pi^- p \longrightarrow n\phi)$ at 2.0 GeV/c = $30 \pm 8\ \mu b$. Two other measurements of the ϕ production cross-section are given, but ignored, namely their own measurement[44] of $21 \pm 7\ \mu b$ at 2.1 GeV/c and the value of Boyd et al.[45] of $19^{+9}_{-8}\ \mu b$ also at 2.1 GeV/c.

The value of BR quoted by Zichichi et al. at the 1968 Vienna conference was revised and is now quoted[46] as BR = $(6.0 \pm 2.7) \times 10^{-4}$ using the same value for the ϕ production cross-section.

Asbury et al.[39] give $(2.7 \pm 0.8) \times 10^{-4}$ as their value of the branching ratio. To produce the ϕ mesons they used a photon beam incident upon a carbon target and detected both e^+e^- and K^+K^- pairs using the same apparatus. In all they obtain about 100 e^+e^- events[47] but have to allow for the Bethe Heitler contribution to the process. To minimise this background which varies rapidly with the opening angle ($\sim \theta^{-6}$) wide angle pairs only were measured. The BH contribution under the ϕ peak is then $< \frac{1}{2}$ of the total yield. Their result is based on 40 events and is also subject to the uncertainty in the $\phi \longrightarrow K^+K^-$ branching ratio.

The most significant result to date is that of the Orsay colliding beam group.[48] Electron and positron beams each of 510 MeV/c^2 collide and produce ϕ's at rest. Since the K meson mass is almost $\frac{m_\phi}{2}$, the Q value is very small and the charged K pairs do not escape the walls of the vacuum vessel. This experiment is done both by detecting the $\pi^+\pi^-$ pairs from $K^o_s \longrightarrow 2\pi$ and the $\pi^+\pi^-\pi^o$ decay of the ϕ directly. The angle between the two pions is close to 180^o and also the range of these pions is short and thus gives a good signature of a ϕ event. The result of this part of the experiment, based on 150 events and using the branching ratio[25] of $\phi \longrightarrow K^o_1K^o_2 = 0.389 \pm 0.031$, is BR = $(3.10 \pm 0.5) \times 10^{-4}$.

Using the 3π decay mode, for which the detection efficiency is estimated to be 4%, and the $\phi \longrightarrow 3\pi$ branching ratio of 0.138 ± 0.043,[25] on the basis of about 50 events they find $BR = (5.8 \pm 1.4) \times 10^{-4}$. The disagreement with their other value may be due in part to an error in the $\phi \longrightarrow 3\pi$ branching ratio. In addition they have measured the branching ratio for $\phi \longrightarrow K_1^o K_2^o$ to be 0.312 ± 0.016 and, using this value instead of that given in the Rosenfeld tables, give as their best estimate of the branching ratio a value of $(3.9 \pm 0.62) \times 10^{-4}$.

The significant results to date are summarised in Table 7.1 below.

Table 7.1

Group	B.R. $\times 10^{-4}$
This experiment	7.0 ± 3.6
CERN	6.1 ± 2.6
DESY - M.I.T.	2.7 ± 0.8
ORSAY	3.9 ± 0.62

The average value for the Branching Ratio is found to be

$$BR\ (\phi \longrightarrow e^+ + e^-)_{av} = (3.60 \pm 0.48) \times 10^{-4} \qquad \ldots\ 7.11$$

which, using a total ϕ width of 3.4 ± 0.8 MeV/c^2, gives a partial width of $\Gamma(\phi \longrightarrow e^+ + e^-)_{av} = 1.22 \pm 0.33$ KeV/c^2.

If we use the world data for $\Gamma\phi$, namely 3.4 ± 0.8 MeV/c^2, and the Orsay value[48] of 4.2 ± 0.9 MeV/c^2, which give a mean of

$$\Gamma\phi_{av} = 3.8 \pm 0.6 \text{ MeV}/c^2 \qquad \ldots\ 7.12$$

we find the partial decay width is

$$\Gamma(\phi \longrightarrow e^+ + e^-)_{av} = 1.37 \pm 0.28 \text{ KeV}/c^2 \qquad \ldots\ 7.13$$

and using equation 1.12 we find

$$\left.\frac{\gamma_\phi^2}{4\pi}\right)_{av} = 3.30^{+0.85}_{-0.56} \qquad \ldots\ 7.14$$

7.3 <u>Leptonic decay modes of the ω and ρ mesons</u>

a) <u>The ω meson</u>

Until recently the only experimental measurement of the branching ratio, BR ($\omega \longrightarrow e^+ + e^-$) was that of Binnie et al.[2] who found $5.10^{-5} <$ BR ($\omega \longrightarrow e^+ + e^-$) $< 6.10^{-4}$, on the basis of three events. Other values have been reported,[49,50] but these are deduced from measurements on the ρ using SU_3.

An experiment was carried out at CERN by Zichichi et al.[51] using the same techniques as in their $\phi \longrightarrow e^+ + e^-$ experiment.

Assuming the $\omega-\rho$ interference to be zero and using the known production angular distributions they obtained a branching ratio of $(0.40 \pm 0.15) \times 10^{-4}$.

The ratio has also been measured using colliding beams at Orsay[52] by detecting the charged pions in the reaction

$$e^+ + e^- \longrightarrow \omega \longrightarrow \pi^+ + \pi^- + \pi^o \qquad \text{... 7.15}$$

using the same apparatus as in their ϕ measurement.

The three body events were identified and separated from the two body ones and background by selecting events with non-colinear tracks with a common origin on the beam axis. They found a branching ratio of $(0.85 \pm 0.16) \times 10^{-4}$ and a best fit of $\Gamma(\omega \longrightarrow e^+ + e^-) = 1.04 + 0.19$ KeV/c^2.

The average of the two gives a branching ratio of $BR_{av} = (0.61 \pm 0.11) \times 10^{-4}$ which, using $\Gamma\omega = 12.2 \pm 1.3$ MeV/c^2,[25] gives

$$\Gamma(\omega \longrightarrow e^+ + e^-)_{av} = 0.744 \pm 0.156 \text{ KeV/c}^2 \qquad \text{... 7.16}$$

or using equation 1.12

$$\gamma_\omega^2/4\pi)_{av} = 4.69^{+1.24}_{-0.81} \qquad \text{... 7.17}$$

Substitution of the world averages for $\Gamma(\omega \longrightarrow e^+e^-)$ and $\Gamma(\phi \longrightarrow e^+e^-)$ in equation 1.13 leads to a generalised mixing angle given by

$$\tan^2\theta_{av} = \frac{m_\omega}{m_\phi}\,\frac{\Gamma(\omega \longrightarrow e^+e^-)_{av}}{\Gamma(\phi \longrightarrow e^+e^-)_{av}} \qquad \ldots\ 7.17$$

which gives

$$\theta_{av} = 32.8^{\circ}\,{}^{+3.6^{\circ}}_{-4.4^{\circ}} \qquad \ldots\ 7.18$$

b) The ρ meson

The leptonic branching ratio for the ρ meson has been measured by several groups. The more significant evaluations are summarised below.

At D.E.S.Y., Asbury et al.[53] used a precision spectrometer with a mass resolution of $\pm$ 15 MeV/c^2. To reduce systematic errors both ρ^{o} production and the $\rho \longrightarrow e^+ + e^-$ decay were measured using the same apparatus. The experiment used a low energy photon beam, 2.7 GeV, as then the ω contamination was expected to be small. They found a branching ratio of $(6.4 \pm 1.5) \times 10^{-5}$.

The experiment of Wehmann et al.[54] from Harvard used the muonic decay. They found a branching ratio of $(5.8 \pm 1.2) \times 10^{-5}$ which is in good agreement with the result of Asbury et al. above and therefore gives no evidence of a departure from equation 1.22.

The colliding beam groups at Novosibirsk[55] and Orsay[56] measured the e^+e^- annihilation into $\pi^+\pi^-$ using similar apparatus. They used thin plate spark chambers to measure the angles of the particles, range and shower spark chambers to distinguish pions from electrons, coincidence counter arrangements triggered in phase with the beam bunches and additional veto counters to reduce cosmic ray background. They find a branching ratio of $(5.0 \pm 1.0) \times 10^{-5}$ and $(6.54 \pm 0.72) \times 10^{-5}$ respectively. Other less accurate results[57] are consistent with the above.

The data on $\rho \longrightarrow \ell^+ + \ell^-$ are summarised in Table 7.2.

Table 7.2

Group	$\Gamma\rho$ MeV/c^2	B.R. x 10^{-5}
Novosibirsk	105 ± 20	5.0 ± 1.0
Harvard	97 ± 20	5.8 ± 1.2
Orsay	112 ± 12	6.54 ± 0.72
DESY/MIT		6.4 ± 1.5
Average	108 ± 9	6.04 ± 0.50

These results yield an average branching ratio of $(6.04 \pm 0.50) \times 10^{-5}$ which, using a ρ width of 108 ± 9 MeV/c^2, gives a partial width of

$$\Gamma(\rho \longrightarrow \ell^+ + \ell^-)_{av} = 6.52 \pm 0.75 \text{ KeV}/c^2 \qquad \ldots 7.19$$

or using equation 1.12

$$\left.\frac{\gamma_\rho^2}{4\pi}\right)_{av} = 0.52^{+0.07}_{-0.06} \qquad \ldots 7.20$$

7.4 Comparison of the world data on the leptonic decay modes with theoretical predictions

The average experimental results are summarised in Table 7.2.

Table 7.2

Decay	BR x 10^{-5}	$\Gamma(V \to e^+e^-)$ KeV/c^2	$\frac{\gamma_V^2}{4\pi}$	γ_V^{-2}
$\rho \to e^+e^-$	0.604 ± 0.05	6.52 ± 0.75	$0.52^{+0.07}_{-0.06}$	9
$\omega \to e^+e^-$	6.1 ± 1.1	0.744 ± 0.156	$4.69^{+1.24}_{-0.81}$	1.0 ± 0.24
$\phi \to e^+e^-$	3.60 ± 0.48	1.37 ± 0.28	$3.30^{+0.85}_{-0.56}$	1.4 ± 0.34

First we consider the current state of '9:1:2' ratio. The average experimental values are compared with theoretical predictions in Table 7.3.

Table 7.3

	SU_3 + ideal mixing	SU_3 + mass mixing	Oakes and Sakurai	Das Mathur Okubo	Experimental averages
ρ	9	9	9	9	9
ω	1	1.2	0.65	1.21	1.0 ± 0.24
ϕ	2	1.8	1.33	1.34	1.4 ± 0.34
No. of std. dev.	1.75	1.45	0.95	0.89	

The best agreement is with the prediction of Das, Mathur and Okubo but the experimental data are not sufficiently precise to exclude other predictions.

As a test of the current mixing model we consider Weinberg's first sum rule (equation 1.14) which, using equation 1.12 can be re-written in the form

$$\frac{m_\rho \, \Gamma(\rho \longrightarrow e^+e^-)}{3} = m_\omega \, \Gamma(\omega \longrightarrow e^+e^-) + m_\phi \, \Gamma(\phi \longrightarrow e^+e^-) \qquad \ldots \; 7.21$$

This sum can be represented by a triangle as indicated in Fig. 7.2. The shaded region corresponds to the sum rule (7.21) being satisfied within the experimental errors.

The world average value for the generalised mixing angle, θ_{av}, obtained using equation 7.17 follows directly from Fig. 7.2. The predicted mixing angles of $\theta = 28.2^\circ$ and

Fig. 7.2 Comparison of the average experimental values for the partial widths, $\Gamma(V \rightarrow e^+e^-)$ with Weinburg's first sum rule.

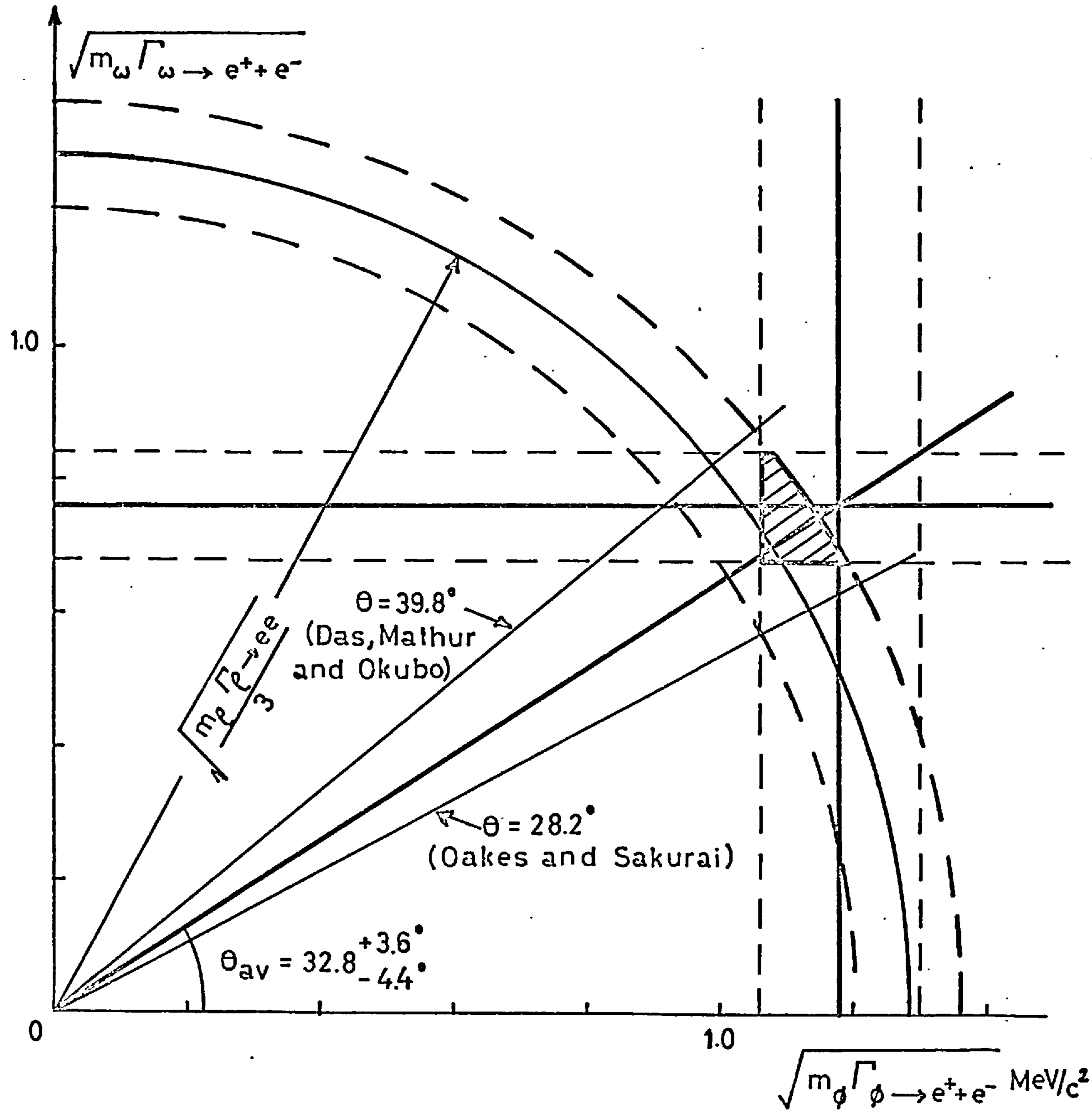

$\theta = 39.8^{o}$ by the Cakes and Sakurai model,[10] and Das, Mathur and Okubo[18] model respectively are shown for comparison. Both values are within two standard deviations of the experimental results.

7.5 Conclusions

The original intention[58] of our series of experiments was to test the hypothesis of ω-ϕ mixing as required by SU_3. By showing that both the ω and ϕ mesons have leptonic decay modes, we are able to conclude that neither ω nor ϕ is a pure unitary singlet and that the general concept of ω-ϕ mixing is correct. In order to test the various theoretical models which have been proposed in the last few years it is necessary to turn to the later more accurate experiments.

The most significant determinations of the branching ratio for the decay $\omega \longrightarrow e^{+} + e^{-}$, namely the CERN and Orsay results of $(0.40 \pm 0.15) \times 10^{-4}$ and $(0.85 \pm 0.16) \times 10^{-4}$ respectively, are not in good agreement, and the true error in the weighted mean may be larger than is calculated.

The determination of the $\phi \longrightarrow e^{+} + e^{-}$ branching ratio by the Orsay group uses their own value of the $K_1^oK_2^o$ branching ratio which differs from the previously accepted value by

$\sim 25\%$. The decay rate of $\phi \longrightarrow 3\pi$ is also in dispute. In addition the value for the ϕ width measured by the Orsay group is also $\sim 25\%$ different from the value found in the Rosenfeld tables. In part, the current data on $\phi \longrightarrow e^+ + e^-$ are limited by the uncertainties in the width and the main decay rates and further evaluations of these quantities are needed.

The average values of the data on the leptonic decays agree well with the predictions of Weinberg's first sum rule based on the current mixing model. However, due to the uncertainties above, the average values of the data are not sufficiently accurate to exclude any of the theoretical models discussed in Chapter One.

It is clear that further theoretical and experimental studies of the leptonic decays of the neutral vector mesons are necessary.

ACKNOWLEDGEMENTS

I wish to thank Professor C.C. Butler for the opportunity of carrying out research as a member of the High Energy Physics group at Imperial College.

I am most grateful to my supervisor, Dr. D.M. Binnie, for his guidance and encouragement throughout. A great debt is also due to the late Mr. J.A. Newth for his interest in the early stages of my research.

Many thanks are due to my colleagues: Mr. A. Duane, Dr. A.R. Faruqi, Dr. W.G. Jones, Mr. M.E. Kay, Dr. D.C. Mason, Mr. P.J. Nicholson, Dr. I.U. Rahman, Dr. J. Walters and Mr. J.G. Wilson at Imperial College, and Dr. P. Palit at the Rutherford Laboratory. Their extensive contribution to the experiment cannot be over-emphasised. I wish to thank Dr. D.A. Garbutt and Dr. K.J. Barnes for many useful discussions.

Thanks are also due to Mr. R.F. Hobbs and Mr. D.J. Scholes for their careful construction of much of the apparatus, to Mr. D. Miller and Mr. R.J. Gray, and to the Staff of the Rutherford Laboratory for their continued assistance.

For financial support during the period 1964-1967 I have to thank the Science Research Council.

Finally I am indebted to Miss D. Koch for her technical help in the analysis of the data and preparation of this thesis.

REFERENCES

1. M.R. Jane. Ph.D. Thesis (1965).

2. D.M. Binnie <u>et al</u>. Phys.Lett., 18, 348 (1965).

3. D.C. Mason. Ph.D. Thesis (1968).

4. I.U. Rahman. Ph.D. Thesis (1968).

5. M. Gell-Mann and Y. Ne'eman. The Eightfold Way. (1964).

6. S. Okubo. Prog.Theor.Phys.(Kyoto), 27, 949 (1962).

7. S.L. Glashow. Phys.Rev.Lett., 11, 48 (1963).

   S. Okubo. Phys.Lett., 5, 165 (1963).

   R.H. Dalitz. Proceedings of the Sienna Int.Conf.on Elem.Part. (1963).

   J.J. Sakurai. Phys.Rev., 132, 434 (1963).

8. R.F. Dashen and D.H. Sharp. Phys.Rev., 133, B1585 (1964).

9. S.C.C. Ting. Proc.of 1967 Int.Symposium on Electron & Photon Interactions at High Energies. Stanford.

10. R.J. Oakes and J.J. Sakurai. Phys.Rev.Lett. 19, 1266 (1967).

11. N.M. Kroll, T.D. Lee and B. Zumino. Phys.Rev., 157, 1376 (1967).

12. S. Coleman and H.J. Schnitzer. Phys.Rev., 134, B863 (1964).

13. S. Weinberg. Phys.Rev.Lett., 18, 507 (1967).

14. R. Van Royen and V.F. Weisskopf. Nuovo Cimento, 50A, 617 (1967).

    A. Dar and V.F. Weisskopf. Phys.Lett., 26B, 670 (1968).

15. R.H. Dalitz. Proc.Int.Conf.on Elem.Part., Oxford (1965).

16. P.G.O. Freund. Nuovo Cimento, 44A, 411 (1966).

17. C.A. Levinson, H.J. Lipkin, S. Meshkov. Phys.Lett., 7, 81 (1963).

H. Hararai. Phys.Rev. 155, 1565 (1967).

H. Hararai. Proc.of 1967 Int.Symposium on Electron & Photon Interactions at High Energies. Stanford.

18. T. Das, V.S. Mathur, S. Okubo. Phys.Rev.Lett., 19, 470 (1967).

19. F.M. Pipkin. Proc.Int.Conf.on Elem.Part., Oxford (1965).

S.M. Berman and S.D. Drell. Phys.Rev. 133, B791 (1964).

M. Gell-Mann and F. Zachariasen. Phys.Rev. 124, 953 (1961).

M. Gell-Mann, D. Sharp and W.G. Wagner. Phys.Rev.Lett. 8, 261 (1962).

20. G.L. Kane and R.A. Zdanis. Phys.Rev. 151, 1239 (1966).

21. J.J. Sakurai. Proc.of 'Enrico Ferm:' School at Varenna (1963).

22. E.D. Zhizkin and V.V. Solovev. Soviet Physics. JETP, 16, 192 (1963).

23. L. Bertanza et al. Phys.Rev.Lett., 9, 180 (1962).

24. P.L. Connolly et al. Phys.Rev.Lett. 10, 371 (1963).

P. Schlein et al. Phys.Rev.Lett., 10, 368 (1963).

25. A.H. Rosenfeld et al. UCRL-8030 (Aug. 1968).

26. W.G. Jones. Ph.D. Thesis (1966).

27. High Energy and Nuclear Physics Data Handbook. Rutherford Laboratory (1962).

28. R.I. Hess et al. Phys.Rev.Lett., 17, 1109 (1966).

R.I. Hess et al. Phys.Rev. 163, 1377 (1967).

29. C.A. Heusch and C.Y. Prescott. Phys.Rev. 135, B772 (1964).

30. D.F. Crawford and H. Messel. Phys.Rev. 128, 2352 (1962).

31. D.G. Crabb et al. Nuc.Inst.& Methods, 45, 301 (1966).

32. R.F. Wilkins. 'A Fast Camera for Spark Chamber Photography'. Physics Dept., Imperial College, London.

33. W.G. Jones et al. Phys.Lett., 23, 597 (1966).

34. R. Böck. CERN Report 60-30 (1960).

B. Ronne. Proc. of 1964 CERN School for Physicists.

35. R.H. Dalitz. Proc.Phys.Soc.(London) A64, 667 (1951).

D.W. Joseph. Nuovo Cimento, 16, 997 (1960).

H. Kobrak. Nuovo Cimento, 20, 1115 (1961).

36. J. Alitti et al. Nuovo Cimento, 29, 515 (1963).

37. F. Ehlotzky and H. Mitter. Nuovo Cimento, 45A, 181 (1968).

38. K. Gottfried and J.D. Jackson. Nuovo Cimento, 33, 309 (1964).

R.J. Oakes. Nuovo Cimento, 44A, 440 (1966).

D.S. Beder. Cal.Tech.Report, CALT-68-43 (1965).

39. S.C.C. Ting. Proc.of XIV Int.Conf.on High Energy Physics, Vienna (1968), & Internal Report DESY F31/4 (Sept.1968).

40. D.C. Mason. Private Communication.

41. A.A. Wehmann et al. Phys.Rev.Lett., 20, 748 (1968).

42. R.G. Astvacaturov et al. Phys.Lett., 27B, 45 (1968).

43. D.M. Binnie et al. Phys.Lett. 27B, 106 (1968), & Rutherford Laboratory Report RPP/H/41.

44. A. Zichichi et al. Preprint CERN (1968).

45. J.H. Boyd et al. Phys.Rev. 166, 1458 (1968).

46. A. Zichichi et al. Nuovo Cimento, 56, 1173 (1968).

47. R. Marshall. Private Communication.

48. J.E. Augustin et al. See ref. 39.

49. K.A. Azimov et al. Phys.Lett. 24B, 349 (1967).

50. R.A. Zdanis et al. Phys.Rev.Lett., 14, 721 (1965).
& Phys. Rev. 155, 1461 (1967).

51. A. Zichichi et al. Nuovo Cimento, 57, 404 (1968).

52. J.E. Augustin et al. ω^o production by e^+e^- annihilation – Orsay preprint, see also ref.39.

53. J.G. Asbury et al. Phys.Rev.Lett., 19, 869 (1967).

54. R.A. Wehmann et al. Phys.Rev.Lett., 17, 1113 (1966).
& Proc.of XIV Int.Conf.on High Energy Physics, Vienna (1968).

55. V.L. Auslander et al. Phys.Lett., 25B, 433 (1967).
& Proc.of XIV Int.Conf.on High Energy Physics, Vienna (1968).

56. J.E. Augustin et al. Phys.Rev.Lett., 20, 126 (1968).

57. J.K. de Pagter et al. Phys.Rev.Lett., 16, 35 (1966).

B.D. Hyams et al. Phys.Lett., 24B, 634 (1967).

58. Nimrod proposal, January 1965.